ENGINEERING MORE POTENT VACCINES FOR THE TREATMENT OF CANCER AND AUTOIMMUNITY

by

Naveen K. Mehta

B.S. Biomedical Engineering and Biochemistry

University of Texas, Austin, 2013

SUBMITTED TO THE DEPARTMENT OF BIOLOGICAL ENGINEERING IN PARTIAL FULFILLMENT OF THE REQUIREMENTS FOR THE

DEGREE OF

DOCTOR OF PHILOSOPHY IN BIOLOGICAL ENGINEERING

AT THE

MASSACHUSETTS INSTITUTE OF TECHNOLOGY

~~MAY 2019~~ [June 2019]

Signature redacted

Signature of Author: _____

Naveen K.Mehta

Department of Biological Engineering

May 28, 2019

Signature redacted

Certified by: _____

Darrell J. Irvine, PhD

Professor of Materials Science & Engineering and Biological Engineering, MIT

Thesis Supervisor

Signature redacted

and by: _____

K. Dane Wittrup, PhD

Carbon P. Dubbs Professor of Chemical Engineering and Biological Engineering

Thesis Supervisor

Signature redacted

Accepted by: _____

Forest M. White, PhD

Professor of Biological Engineering and Graduate Program Chair

Thesis committee:

Darrell J. Irvine, PhD; Professor of Materials Science & Electrical and Biological Engineering, MIT (Thesis Supervisor)

K. Dane Wittrup, PhD; Carbon P. Dubbs Professor of Chemical Engineering and Biological Engineering (Thesis Supervisor)

Michael E. Birnbaum, PhD; Assistant Professor of Biological Engineering (Thesis Chair)

Glenn Dranoff, MD; Global Head of Exploratory Immuno-oncology at Novartis

ENGINEERING MORE POTENT VACCINES FOR THE TREATMENT OF CANCER AND AUTOIMMUNITY

by
Naveen K. Mehta

Submitted to the Department of Biological Engineering
on May 28, 2019 in Partial Fulfillment of the
Requirements for the Degree of Doctor of Philosophy in
Biological Engineering

ABSTRACT

Vaccination against infectious diseases has long been heralded as one of the greatest advancements in public health, yet its application to other clinical indications has fallen short of expectations. In this thesis, we apply engineering principles to develop more potent vaccines in the treatment of cancer and autoimmunity. Both major components of molecular vaccines, antigen and adjuvant, are independently explored as a part of this work.

Our antigen studies sought to improve the delivery of peptide epitopes to lymphoid organs by fusing epitopes to inert protein carriers with defined pharmacokinetic properties. To promote anti-tumor immunity, we found that antigen carriers should 1) protect peptide cargo from proteolytic degradation, 2) be appropriately bulky to drain into the lymphatics, and 3) be rapidly cleared once in the blood to prevent tolerization at distal poorly inflamed organs. Applying these principles, we identified transthyretin as an optimal delivery protein, and demonstrated efficacy against a number of clinically relevant antigens. Because our protein-epitope fusion approach is fully recombinant in nature, we were able to convert our protein vaccines into nucleic acid modalities, including plasmid DNA and self-replicating RNA, which are significantly easier and cheaper to manufacture at scale. Finally, we applied our learnings to purposefully induce tolerization in the treatment of autoimmunity, and found that albumin is a particularly efficacious antigen carrier protein for this application due to its extended half-life.

On the adjuvant front, we attempted to engineer novel Toll-like receptor 3 (TLR3) agonists via yeast surface display. Although we successfully developed high affinity TLR3 binders, all tested clones failed to agonize TLR3 despite the utilization of several multimerization strategies. Separately, in an effort to better understand adjuvant biology, we conducted a detailed mechanistic study of lipo-CpG, a particularly potent amphiphilic CpG variant previously developed by the Irvine lab. We uncovered a cascade of inflammatory signals originating from monocytes that facilitates the induction of high magnitude T cell responses, largely by acting in trans rather than directly on the antigen-presenting cell.

Overall, these studies have elucidated a number of design principles that should aid in the engineering of next generation vaccines to better treat cancer and autoimmunity.

Thesis Supervisors: Darrell J. Irvine, PhD and K. Dane Wittrup, PhD

TABLE OF CONTENTS

ACKNOWLEDGMENTS

An over-used phrase that graduate students hear repeatedly is that the PhD is not a sprint, but a marathon. As I reflect at the end of the almost six-year journey, I definitely agree with the sentiment – the process stretches on seemingly forever, and is some combination of rewarding and grueling throughout. But it is by no means a journey on a lonely road. Throughout the course of my graduate school career, I have been incredibly lucky to have been surrounded by so many fantastic people that made the process a thoroughly fulfilling one. I have so much to be grateful for.

When I first arrived at MIT and began the process of selecting advisors, I was consistently warned not to be co-advised. Common wisdom is that you are either the victim of a tug-of-war between two advisors unable to work together, or that you are forgotten by both, without any sense of direction or guidance. Darrell Irvine and Dane Wittrup not only proved this dogma wrong, but they proactively provided me with one of the most dynamic, cutting-edge, and stimulating PhD experiences I could have asked for. I will forever be grateful to both advisors for taking a chance on me to have me join their groups in a year that was particularly competitive. I never quite knew what they saw in me, but I knew exactly what I saw in them. I have been consistently amazed by how much time and focus they are able to provide each and every trainee in their labs, a trait that commonly dwindles as professors become as established as Dane and Darrell. Not only were Dane and Darrell consistent sources of clever scientific ideas and ingenious insights, but they went the extra mile to think about how each step along the way contributed to my overall growth. They didn't hesitate to let me pursue a total of three different internships/fellowships because they recognized how important it was to my education, and they never pushed their agenda onto me, instead giving me the freedom and flexibility to explore my project quite independently. As I reflect on the PhD process, it astounds me how much was shaped by the extremely positive work environment promoted by both advisors, and both will serve as a source of inspiration as I move into the real world post-grad school.

I am also fortunate to have landed a fantastic committee. Thanks to Michael Birnbaum for joining as my committee chair before he even officially started his appointment at MIT. It was a lot to ask of someone just a few years out from the PhD process himself, but Michael was consistently generous with his time and ideas, and did a fantastic job navigating the science while being mindful of my personal goals and timelines. Thanks, also, to Glenn Dranoff, who had recently shifted from academia to the head of Immuno-Oncology at Novartis, but was still more than willing to be a part of my thesis committee. The amount of time and attention Glenn puts into everything he touches is an inspiration, and he was the most consistent member of the committee to thoroughly review every document I ever sent and to follow up with insightful questions and comments. During the last year, in particular, both Michael and Glenn were able to help me re-shape and re-frame some of my disparate projects in a way that truly tightened the story and potentially improved its impact. It is so meaningful to me that both Michael and Glenn really put the effort into their spots on my committee to significantly improve my work rather than treating it as just a formality without consequence.

Dane and Darrell have also put together an amazing set of individuals in their labs. Both labs ultimately felt more like a second and third family rather than just a set of colleagues. Brimming with talent and with a strong culture of collaboration and cooperation, both labs gave me all I could have hoped for during graduate school. I learned so much just be being a part of such a stellar crowd, and I can point to so many specific comments during group meetings or discussions on the side after a long day in lab that meaningfully impacted my work. Scientific progress truly is the product of a whole ecosystem of ideas, and I was fortunate enough to be immersed in one without even having to make an effort of it.

To the original Wittrup lab crowd, Alessandro Angelini, Tiffany Chen, Michael Traxlmayr, Jim Van Deventer, Monique Kauke, Ryan Kelly, Eric Zhu, Alice Tzeng, Byron Kwan, Katie Mass, Nicole Yang, Cary Opel, Seymour de Picciotto, and Adrienne Rothschilds, I'm glad at least some people remember the pool party era. Special shout-out to Michael, who introduced me to the workings of the lab early on and taught me practically everything I know about yeast display. Michael is one of the most thorough scientists I have ever worked with, and one of the most patient teachers I have ever been lucky enough to train under. Big thanks to Adrienne for not only being my partner as a newbie in the early years in the lab, but also for being such a great friend both in and out of the lab. I seriously wasn't sure whether to thank Adrienne here or later on with out-of-MIT friends, because she really did serve both roles glowingly. From troubleshooting frustrating experiments in the lab to tasting a ridiculous spread of margarita and tiki flights, Adrienne has been such a positive force during my PhD and I can't thank her enough for making the experience such an enjoyable one. I still find our number of shared experiences for the past six years pretty hilarious, and there is honestly no one else who quite understands what the journey has been like as much as Adrienne does. To all the Wittrup lab students who have joined since, Alison Tisdale, Noor Momin, Byong Kang, Emi Lutz, Yash Agarwal, Allison Sheen, Joseph Palmeri, Sarah Cowles, Keith Kun, and Bri Lax, I have thoroughly enjoyed watching you all blossom into capable and independent researchers. Special thanks to Noor, who has been following me since middle school years, through high school, college, and now in the same lab at MIT in graduate school. It has been such a joy getting closer to Noor for the last four years, both in and out of the lab, and I know our friendship will continue to grow even as my PhD comes to a close. Maybe she can get rid of that pesky middle initial now that I am gone. It has also been great getting to help train Yash for the past 1.5 years or so, and I am confident he will continue to do a great job navigating the joint Irvine-Wittrup lab adventure throughout the course of his PhD. Huge thanks as well to my UROP, Roma Pradhan, who worked with me for two years on several different projects. Her can-do attitude and independent work ethic made my job training her easy, and I know she will go on to be a fantastic physician one day.

To everyone who originally welcomed me into the Irvine lab, Kavya Rakhra, Sudha Kumari, Kelly Moynihan, Andrew Zmolek, Anasuya Mandal, Sabrina Yang, Yiran Zheng, Melissa Hanson, Talar Tokatlian, Yuang Zhang, Greg Szeto , Li Tang, Brad Jones, Wuhbet Abrahan, Mariane Melo, and Mark Miller, thank you all for being so friendly even though I physically lived over on the Wittrup side. I was seriously concerned early on that I would just be in a single-lab silo, but it was really thanks to your kindness and collegiality that I truly gained two families instead of just one during my time at MIT. Special thanks to Kelly Moynihan, who is not only one of the most intelligent, hard-working, purpose-driven, and capable scientists I have ever met, but who is also brimming with so much enthusiasm and optimism that it is infectious. She was incredibly generous with her time and attention, never hesitating to help me out or train me no matter how busy her own schedule. Huge thanks to Wuhbet Abraham as well, who has never found a mouse technique she can't master. To the new folks that joined the lab after I did, Aereas Aung, Brittany Hartwell, Chensu Wang, Coralie Backlund, Eric Dane, Hannah Watkins, Jacob Martin, Jason Chang, Leyuan Ma, Michael Fichter, Murillo Silva, Nitasha Bennett, Tyson Moyer, Yingzhong Li, Angela Zhang, Ben Read, Bingxu Liu, Lauren Milling, and Archana Boopathy, thanks for continuing to enrich the lab, even though many of them were able to beat me out of here.

I have also had the good fortune of collaborating with lots of talented scientists outside of either lab. Major thanks to Ava Soleimany, who may be one of the most intellectually curious people I have ever met. For the final nine months or so of my PhD, she joined me in various exploratory experiments related to tolerization and autoimmunity, just because of her general interest in the field and not because it directly related to her project. She never shied away from 6 am start times or full Sundays of work, and I

am really grateful for all the help she provided. Additionally, big thanks to all the single cell RNA seq expertise available just in my backyard: Andy Tu from the Love lab and Ang Cui from the Hacohen group were both extremely generous with their time and resources during these collaborations. To the Pfizer team that helped round out the tolerization vaccine work, Aaron Winkler, Michael Look, Kellie Kravarik, Xiao Chen, and Andre Mueller, I honestly could not have proceeded with a project completely outside of my wheelhouse without their help. A sincere thanks as well to all the advisors I worked with at my various internships, including Stefan Vitorovic and Arjun Goyal at Vida Ventures and Dominik Barthelme at Neon Therapeutics, for teaching me so much and helping me figure out future career decisions. Finally, to my new family at Cullinan Oncology, particularly Jen Michaelson, thanks for giving me a chance, and I can't wait to get started full-time after the thesis work officially wraps up.

When I originally applied and interviewed at MIT, I visited primarily as a means to convince myself that I shouldn't come here; I thought that as good as MIT sounds on paper, surely it is filled with some of the most miserable cutthroat personalities that would be the opposite of fun to hang out with. On the contrary, some of the people I met during that very first exposure to MIT have become lifelong friends. Huge thanks to the BE class of 2013 for helping with the original transition from undergraduate to graduate life, and for becoming a truly special set of friends. I wish we all saw each other more frequently, but whenever we do, it's like no time has passed at all. Special thanks to the Otis crew, Jaideep Dudani, Bo Qing, Andrew Chen, and Ben Mead. Extra shout-out to Jaideep, who was not only my roommate for three years, but who also remains a close friend long after we moved out, and who proactively helped get me involved with Vida Ventures, in a field I never would have felt capable or qualified for without his guidance and support. I know his goal is to get back out to the west coast, but we'll miss him here in the frigid northeast.

It is also so vitally important to stay grounded with a life outside of MIT, and for that I am incredibly thankful to Bhargav Srinivasan and Mitchell Wong for being the best friends I could ask for. From road trips to truly valuable heart-to-hearts over Google Hangouts, we have really grown together and experienced each other's pain and joys collectively since freshman year of college. As a business guy much more financially savvy than I am, Bhargav has also been invaluable as my career trajectory took a shift towards venture; and as a physician with a strong commitment to overall patient wellbeing, Mitchell has reminded me why I am so moved by medical research in the first place. Together, both Bhargav and Mitchell have been my rock through the good and the bad, and I know my graduate years have been thoroughly enriched thanks to their presence in my life. To Bhargav, I honestly can't believe that we were able to experience our fifth year as roommates in graduate school, and I hope we are similarly surprised to be in the same city as each other in the near future. Bhargav honestly knows me probably better than anyone else at this point, sometimes better than I know myself, and always has my back, no matter what. It's hard to get through the marathon of the PhD without a friend like that.

Most importantly, this thesis is dedicated to my family, Abhay, Seema, and Nishu, without whom I would have never made it here. I somehow got to this point in my academic career without any unwanted pressure from home and instead with nothing but love and encouragement from the whole family. I often joke that I was tricked into loving science just because my father, Abhay, made it seem so cool and interesting. My mother, Seema, instilled in me the importance of pursuing passions that are impactful and meaningful at a deeper level than any surface concerns like money or fame. Collectively, the values that were instilled in me from a young age made me determined to use whatever skills I gain for the good of humanity, and that continues to be the driving force in my career decisions to this day. Nishu has moved beyond just the realm of the genetic family and has become a part of my academic

family as well, with his PhD efforts in Jennifer Cochran's lab resonating closely with the work in the Wittrup group. It has been amazing actually having someone back home who can understand my scientific gibberish, and I can't wait until we both become Dr. Mehta's together. I am so fortunate to call everyone in the Mehta household not just family, but close friends as well, as I'm sure they can attest to after having to listen to all my rants, both frustrated and excited, over the years. Not many people can truly confide in their family regarding all things big and small, and I consider myself extremely fortunate to have won the lottery in that regard. Big thanks to my grandparents, Nani and Nanaji. Our family trips to visit them throughout my childhood shaped who I am today. Nanaji was the first PhD of the family and was the one who really inspired an academic trajectory from a young age. To everyone else in the family, including aunts, uncles, and cousins, I am so lucky to have been raised by such a caring "village" that has fostered me every step of the way, and I wouldn't be here without that love and support.

LIST OF FIGURES AND TABLES

CHAPTER 1. INTRODUCTION

1.1 Motivation

Vaccines have been heralded as among the greatest achievements in the field of public health, responsible for the eradication of smallpox[1] and a dramatic reduction in worldwide instances of polio[2] and measles[3]. Despite its already profound legacy, however, the field of vaccinology still has a number of frontiers that demand continued innovation and growth. For example, vaccines have yet to make a lasting impact in battling cancer, despite large strides made with the use of other immunomodulators[4]. Furthermore, clinically-approved vaccines thus far have primarily sought to generate neutralizing antibodies, but few have generated robust cytotoxic T lymphocyte (CTL) mediated immunity[5]. The field has also struggled to make vaccines without the use of live attenuated vaccines, and the centuries-old Pasteur paradigm of "inoculate, inactivate, inject" remains the standard. Subunit vaccines, which replace whole bacteria and/or viruses with their specific immunogenic antigens, have been manufactured, but typically with reduced immunogenicity[6]. Additionally, the clinical implementation of vaccines has focused almost exclusively on the induction of activating immunity rather than regulatory immunity, and the ability of vaccines to induce antigen-specific tolerance has been underexplored. The motivation behind the work described in this thesis is thus to engineer more potent T cell subunit vaccines for the treatment of cancer and autoimmune diseases.

1.2 Vaccines in the treatment of cancer

A brief overview of cancer immunotherapy

The field of cancer immunotherapy was born in the late 19th century, when Dr. William Coley injected patient's sarcomas with bacteria or bacterial derivatives to induce a localized immune response[7]. Despite encouraging clinical results from over a thousand patients, skepticism and doubt prevented cancer immunotherapy from becoming mainstream in oncology.

Fast-forward over a century into the future, and naysayers were presented with indisputable evidence of the curative potential of harnessing the immune system with the approval of ipilimumab in 2011 for the treatment of melanoma[8]. Ipilimumab belongs to a family of drugs called checkpoint inhibitors, which interfere with inhibitory receptors on T cells, such as programmed cell death protein 1 (PD-1) or cytotoxic T-lymphocyte-associated protein 4 (CTLA-4) or their associated ligands. In doing so, these drugs "inhibit the inhibitors" of the immune response, thereby taking the foot off the brakes to allow for re-invigoration of the immune system that may be naturally suppressed by the tumor. Since the approval of ipilimumab, a number of other checkpoint inhibitors have been approved as well, and the number of clinically explored immunomodulatory modalities has only expanded further, such that over 3000 agents were in development as of the fall of 2018, collectively seeking to drug over 400 biological targets of interest[9]. The data suggest that not only is immuno-oncology here to stay, but that it has evolved from the fringe in clinical oncology to the mainstream.

In recent years, the burgeoning field of cancer immunotherapy has spawned several exciting "firsts" in clinical oncology. While the vast majority of experimental new drugs are saved for patients that have failed to respond to more mainstream treatment options, in 2017 a drug named nivolumab, which targets PD-1, was approved by the FDA as a first-line therapy for a subset of lung cancer patients[10], an exciting first step in expanding adoption of immunotherapy, that might foretell a future in which an increasing number of patients may be able to replace or delay toxic strategies like chemotherapy in the post-checkpoint inhibitor era. Similarly, clinical oncologists have long decried our archaic strategy of treating patients by the anatomical location of their tumors rather than by their underlying genetic features. Here, too, cancer immunotherapy has helped move the field into the future, with the approval of pembrolizumab, also an anti-PD-1 antibody, in all patients whose solid tumors demonstrate microsatellite instability, regardless of anatomical location[11]. Additionally, the emergence of immunotherapy led to the development of the first clinically approved gene therapy, whereby a patient's own T cells are genetically modified to target their cancer cells before reinfusion into the patient[12,13].

Cancer immunotherapy has the potential to significantly improve patient outcomes. Many of the approved drugs against cancer from the 20th century, including chemotherapy and targeted inhibitors, tend to impart short-term clinical benefit until the patient ultimately relapses due to the evolution of drug resistance by the tumor[14]. In this context, the engagement of the immune system is particularly exciting, as the immune system is by its very nature a co-evolving weapon. As viruses mutate in a patient, for example, the patient's immune system

responds accordingly. As an infection progresses, patients develop an adaptive immune response that triggers the development of antibodies and T cell-mediated immunity against the specific signature elements of the infectious pathogen, or antigens. Additionally, over time the adaptive immune response develops memory to significantly decrease the risk of a repeat infection. If similar biological processes are directed against a tumor, the exquisite specificity of the immune system could impart significantly more clinical benefit over the relatively crude approach of trying to traditionally drug general targets over-expressed by the tumor.

Consistent with these theoretical ideas, the survival trends between patients treated with targeted therapies and patients treated with immunotherapy tend to differ considerably. While nearly all patients respond to targeted therapy, and respond quickly, they often ultimately succumb to disease burden as tumors develop resistance against the drug[15]. Patients treated with immunotherapy, on the other hand, may be slow to respond due to the timeframe required to generate an immune response, and a relatively small fraction may respond due to the difficulties in mounting an immune response against a tumor, but those that do respond will often have long-term, durable tumor control (**Fig. 1.1**)[15].

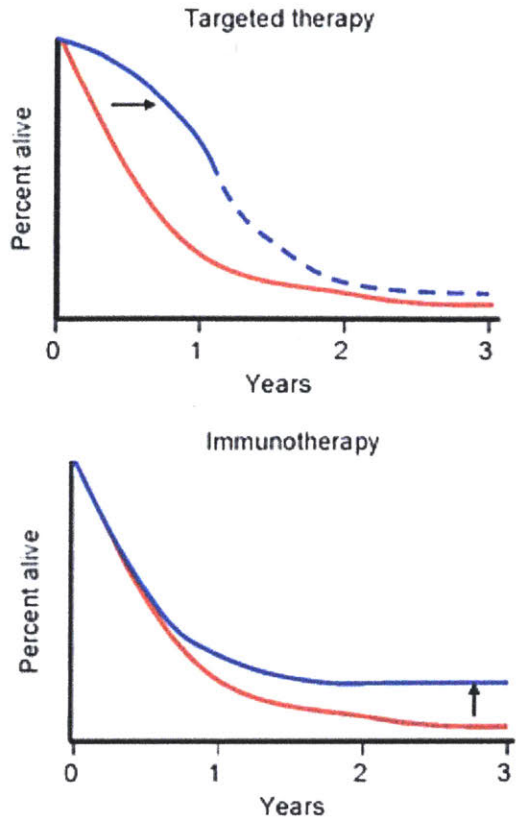

Figure 1.1. Schematic summary of the survival advantage imparted by immunotherapy[15]

An important consideration in the evolution of immunotherapy in the future is how to increase the fraction of patients that respond to treatment. Data to date suggests that patients with an ongoing immune response are the most likely to respond to checkpoint inhibitors[16–18]. Therefore, vaccines, due to their ability to generate endogenous responses against the tumor, may have a critical role to play, especially in combination with checkpoint inhibitors.

The role of vaccines in cancer immunotherapy

Unlike the vaccines we are given as children, or the vaccines we are seasonally administered, cancer vaccines are not prophylactic in nature, meaning they do not seek to

prevent cancer. Rather, they are administered after a patient already presents with cancer, and thereby the vaccine seeks to invigorate an appropriately strong immune response to control a pre-existing lesion.

The only FDA-approved therapeutic cancer vaccine to date is Provenge, an autologous cell-based therapeutic vaccine against castration-resistant metastatic prostate cancer developed by Dendreon[19]. In this vaccination scheme, patient peripheral blood is collected, shipped to a preparation facility, pulsed with prostate-specific antigen *ex vivo*, shipped back to the clinical site, and subsequently reinfused into the patient. Although this treatment extends survival for an median of 4.1 months for castration-resistant prostate cancer patients, its implementation is complex and costly. To avoid these issues, defined subunit vaccines that target tumor-specific antigens are preferable.

Subunit vaccines boil down a pathogen to its core immunological components. For example, a vaccine against influenza may seek to generate antibody responses against purified hemagluttinin—a glycoprotein antigen on the surface of the influenza viral capsid—rather than against the whole live virus. However, an antigen on its own is not sufficient to mount an immune response. To activate the adaptive immune system (generating the antigen-specific response), the innate immune system (a more non-specific response) must first be triggered. Antigen-presenting cells (APCs) express pathogen recognition receptors (PRRs) that recognize pathogen-associated molecular patterns (PAMPs). PAMPs are typically conserved and repetitive microbial components that are rarely found in mammalian organisms, including lipopolysaccharide (LPS), a glycolipid common in the outer membrane of Gram-negative

bacteria, unmethylated CpG DNA characteristic of bacterial genomes, and double-stranded RNA. PRRs come in several varieties, including Toll-like receptors (TLRs), membrane-bound receptors either embedded in the cell surface or in the endosome; RIG-I-like receptors (RLRs) that detect viral RNA species in the cytoplasm; NOD-like receptors (NLRs) that respond to diverse ligands via a large inflammasome structure; and STING, a cytosolic DNA sensor[20,21]. Agents that activate the immune system to potentiate subunit vaccination are called "adjuvants." The two core elements of a subunit vaccine are thus antigen and adjuvant.

While cancer vaccines have historically had poor success in the clinic, there are at least three reasons why cancer vaccines should see renewed interest as part of the cancer immunotherapy armamentarium, based on recent rapid advances in the field: First, the vast majority of the history of cancer vaccine development occurred before the clinical approval of checkpoint blockade therapies or other immunomodulatory agents that are now coming online[22–24]. Without combination with these agents, however, T cells activated by vaccines may simply become exhausted, dysfunctional, or immunosuppressed, failing to impart benefits on patient outcomes. Secondly, the availability of an ever-growing array of targeted drugs that can dramatically (but transiently) lower tumor burden provides a window of opportunity for vaccines to act in a setting of minimal disease, and some of these drugs may act synergistically with the immune response[25]. Lastly, powerful genomic sequencing capabilities are enabling the possibility of patient-specific vaccines targeting defined neoantigens, which have the potential for alleviating the safety and efficacy challenges of targeting unmutated self antigens[26–28].

Altogether, these recent developments in cancer therapy strongly motivate renewed efforts to develop effective therapeutic cancer vaccine approaches.

The state of the art in cancer vaccine engineering

Before our molecular understanding of innate receptors, adjuvants were loosely defined as vaccine supplements that improved immunogenicity[29]. Between the 1920s and the turn of the century, the only adjuvant approved in the United States was aluminum[30]. In practice, aluminum salts are mixed with vaccine components to boost their potency. Adsorption of antigen to aluminum results in particulate presentation of antigen, which can improve phagocytosis by DCs[31] and may serve as a signal to the immune system to increase the scale of its response[32]. Other particulate formulations that have been tested in small animals also clearly suggest that particulate vaccination dramatically improves potency. Potency has been enhanced by packaging vaccines in liposomes[33], polymeric particles[34], and virus-like particles[35], among others. In many cases, antigen and adjuvant may be packaged in the same particle, ensuring that APCs receive both signals simultaneously[36]. Despite their clear efficacy, however, particulate vaccines suffer from difficulties in characterization and reproducibility. In an industry where the bottleneck to innovation is often process development[37], a more defined strategy to improve subunit vaccine potency is preferable.

One such strategy to improve potency involves targeting certain APCs in lymphoid organs. Because dendritic cells (DCs) are considered "professional" APCs[38], work spearheaded by the late Ralph Steinman has led to the advent of vaccines fused to DC-targeting antibodies,

ensuring that a larger fraction of injected material reaches the optimal effector cell. DC-targeting antibodies include αDEC-205 and αDC-SIGN, among others, targeting DC-specific endocytic receptors to promote internalization and vaccine processing[39,40]. This strategy has been particularly effective in the generation of CD8+ T cell responses.

Another recent trend in vaccinology has been the discovery and engineering of novel adjuvants with increased potency. For example, the discovery of the cytosolic DNA sensor STING is fairly recent one[21], and use of its ligand (cyclic dinucleotides) has rapidly gained attraction in the clinic[41]. Additionally, a group in Novartis has recently co-opted drug screening principles to discover new small molecule immune potentiators that signal via TLRs to add novel drugs to the adjuvant repertoire[42].

The Irvine lab has contributed to this field with a novel method to improve the potency of subunit vaccinations[43,44]. In this work, peptide antigen and CpG DNA adjuvant were conjugated to the diacyl lipid tail 1,2-Distearoyl-sn-glycero-3-phosphoethanolamine (DSPE), generating amphiphiles with a hydrophilic head and a hydrophobic tail. In the case of peptides, which have varying degrees of solubility depending on the antigen, a 2 kDa polyethylene glycol (PEG) polymer was inserted between lipid and peptide (**Fig. 1.2**). These amphiphilic vaccine components were named amph-peptide and lipo-CpG. In solution, both amph-peptide and lipo-CpG formed micelles that could be disrupted by the presence of serum albumin due to the several lipid-binding pockets present in the globular protein[45,46]. Binding of lipo-CpG to bovine serum albumin (BSA) had an apparent Kd of 125 nM. In serum or in the interstitial space, albumin concentration is maintained at roughly 500 μM via a recycling system mediated by the

neonatal Fc receptor (FcRn) and by relatively high molecular weight[47]. Upon subcutaneous injection, therefore, nearly all lipid-conjugated vaccine bound serum albumin. Lipid-mediated albumin binding was found to have a direct correlation with lymph node (LN) uptake upon subcutaneous injection, as measured by whole organ *in vivo* imaging systems (IVIS). Lipo-CpG adjuvanted OVA vaccination resulted in tremendous increases in potency of protein antigens, generating 32-fold higher numbers of OVA-specific CD8+ T cells in the blood compared to CpG. Over 30% of the CD8+ T cells in the blood were OVA-specific, a high frequency rivaling that seen during natural infection[48]. Similarly potent responses were seen when lipo-CpG and amph-peptide were co-injected in vaccination.

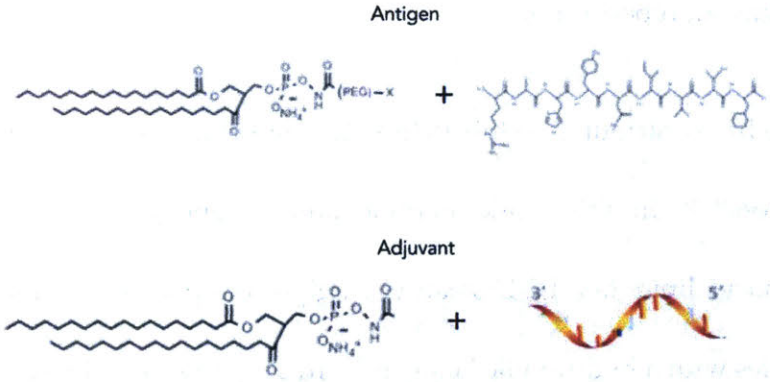

Figure 1.2. The amphiphile vaccine system

Both peptide antigen and CpG adjuvant were conjugated to DSPE, either with a PEG spacer in the case of antigen or no spacer for CpG. Lipid conjugation facilitated serum albumin complexation in situ upon injection, leading to improved lymph node uptake and vaccine responses.

Future directions in cancer vaccine engineering

Cancer vaccines have now progressed beyond the academic lab into mainstream biotech industry. As industry proceeds with the development of this exciting therapeutic modality, however, a number of challenges remain to be addressed. First, and likely of greatest

importance, is appropriate selection of tumor neoantigens. Vaccines that target too few antigens or antigens that are not truly drivers of tumorigenicity may simply lead to the generation of escape mutants. To address this challenge, the two most advanced public cancer vaccine companies, Neon Therapeutics and Gritstone Oncology, have largely competed against each other in developing the most sophisticated neoantigen prediction strategy. This is no easy feat, as mutations must first be identified following exome sequencing and then assessed for appropriate processing and HLA loading[49]. While the loading criteria for the most common HLA alleles is well-characterized, many alleles remain poorly understood, and both companies have put considerable effort into expanding the existing training set to develop better predictive models. Second, feasible and scalable antigen delivery strategies must be optimized to enhance antigen bioavailability in the secondary lymphoid organs, where immune responses are ultimately orchestrated. Third, whichever delivery strategy is utilized, vaccines must be easily and reliably manufactured. When patient-specific neoantigen vaccines are manufactured, production techniques cannot be exquisitely optimized on a case-by-case basis. Instead, manufacturing strategies must be generalizable to a large variety of antigens, and synthesis must be appropriately rapid such that patients do not succumb to disease prior to vaccine availability.

1.3 Vaccines in the treatment of autoimmunity

A brief overview of antigen-specific immunotherapy

Autoimmune disorders occur when a patient's immune system recognizes a self-antigen as foreign, thereby initiating a toxic response against healthy tissue. Because these diseases are chronic in nature, they have a staggering cost on the healthcare system. It is estimated that 50 million Americans suffer from autoimmune related diseases, leading to annual costs of $100 billion annually[50]. Some of the most common autoimmune disorders include rheumatoid arthritis (RA), characterized by the inflammatory degradation of cartilage, with 1.3 million patients; type 1 diabetes, whose disease etiology consists of autoimmune destruction of pancreatic beta cells, with 1.25 million patients; and multiple sclerosis (MS), in which the immune system attacks the myelin sheath, with 400 thousand patients. Systemic autoimmune disorders are typically characterized by autoantibodies, while organ-specific diseases are often T-cell mediated.

What mechanisms lead to the initiation of autoimmunity? Genome-wide association studies (GWAS) have so far failed to find strong predictors of autoimmunity. Thus far, particular HLA alleles have been the most implicated in the risk of autoimmune initiation, although precisely why remains controversial[51]. One proposed mechanism of action in RA is the conversion of arginine to citrulline by peptidyl arginine deiminases (PADs) during increased inflammation and stress[52,53]. In two RA-associated HLA alleles (DRB01*04:01 and DRB01*04:04), particular segments of the peptide-binding cleft are positively charged, thereby excluding

cationic arginine but accommodating citrulline. RA-resistant HLA alleles, on the other hand, tend to accommodate both arginine and citrulline[54]. In this manner, citrullination may lead to a neoantigen-like response in some patients but not others based on their HLA makeup.

When considering why autoimmune disorders occur at all, it is important to recognize that during T cell development in the thymus, self-reactive cells are only deleted if they are of sufficiently high avidity[55], leading to a reliance on peripheral tolerance to prevent aberrant autoimmunity. One mechanism of peripheral tolerance is the physical exclusion of T cells from tissues where their self-associated cognate antigen may be expressed. T cells follow CCR7 and S1P gradients from blood to secondary lymphoid organs and back, thus failing to infiltrate tissue prior to antigen exposure[56]. Additionally, the development of T_{reg} cells and the induction of checkpoint expression actively terminates the proliferation of self-reactive effector cells, promoting anergy[57]. Finally, the maturation status of antigen presenting cells during T cell priming is an additional mechanism of maintaining peripheral tolerance. If DCs present antigen from apoptotic cells, they fail to be activated by NFκB due to interactions with a family of receptors called TAM receptors (Tyro, Axl, Myr)[58]; and a dearth of TLR ligands can similarly maintain DCs in an inactive state during antigen presentation, leading to T cell anergy[59]. While these mechanisms of preserving peripheral tolerance have typically gone awry during the initiation of autoimmunity, they are important to consider as potential strategies to induce antigen-specific tolerance.

Currently, autoimmune diseases are treated with a variety of anti-inflammatory agents that broadly suppress the immune system in a non-antigen-specific manner. As a result,

patients remain at risk of infection in a chronic manner, necessitating the development of antigen-specific tolerization strategies instead. Beyond the typical prescription of anti-inflammatory steroids, other FDA-approved drugs include Orencia, a CTLA4-IgG fusion[60]; Humira, an anti-TNFα antibody[61]; Xeljanz, a JAK/STAT inhibitor[62]; Actemra, an anti-IL6R antibody[63]; and methotrexate, a chemotherapeutic that can be used to dampen the immune response[64]. Next generation therapeutics should a) be antigen-specific, obviating the need for broad immunosuppression, and b) lead to long-lasting memory, reducing the need for frequent, lifelong drug administration[65].

The state of the art in tolerizing vaccines

While no tolerizing vaccines have yet been FDA approved, a number of preclinical studies show promise and best capture the current state of the art. Jeff Hubbell's group has focused on fusing or conjugating antigen to scFv's that target red blood cells (RBCs), thereby extending the half-life of antigen and shunting antigen into regions of erythroptosis, or the apoptosis or RBCs, ensuring that antigen is presented in the immunosuppressive apoptotic context[66,67]. A similar goal but alternative approach was developed by Harvey Lodish and Hidde Ploegh, where genetically engineered RBCs were covalently conjugated with peptide antigen using sortase to induce antigen-specific tolerance[68]. In addition to cellular delivery strategies, a number of groups have been engineering biomaterial-based approaches to induce tolerization in an antigen-specific manner. Stephen Miller has designed poly(lactide-*co*-glycolide) (PLG) nanoparticles conjugated to peptide antigen, which if injected intravenously can prevent and/or treat the onset of experimental autoimmune encephalomyelitis (EAE)[69].

Chris Jewell has instead opted to develop large microparticles that co-deliver antigen and rapamycin; microparticles are injected directly into lymph nodes, where they persist for several days, and can induce systemic induction of T_{reg} cells that are effective at treating even distal inflammatory sites[70]. Perhaps one of the most intriguing approaches has been developed by Pere Santamaria, who has engineered pMHC-decorated iron oxide nanoparticles. The high density of pMHC induces the differentiation of T_h1 cells (that typically secrete IFNγ) into T_r1 cells (that instead secrete IL-10). By directing the differentiation of disease-mediating effector cells into ameliorative regulator-type cells, this approach is specifically effective in the therapeutic context during active, ongoing disease[71].

The current state of preclinical research in tolerizing vaccines remains heterogeneous, however, without clear consensus on which preclinical models are most predictive of clinical outcomes. In future development, studies should be prioritized that a) are based on spontaneous models of autoimmunity that reliably capture the polyclonality of human disease, rather than single-antigen directed models; b) are therapeutically treated rather than simply prophylactically treated; c) demonstrate evidence of long-term efficacy without rapid dosing; and d) show tissue-specific effects rather than broad immunosuppression. Criticism based on these criteria will help ensure that only the most promising tolerizing vaccine candidates progress to clinical validation.

1.4 Thesis Overview

As I joined the lab(s) in January 2014, the Irvine lab had recently published on the lymph node targeting amphiphile vaccine approach[43], and already both labs were pursuing a fruitful four-part therapy leveraging these highly potent vaccines combined with cytokine- and antibody-based immunotherapy[72]. It was clear that these vaccines were going to have staying power in both the Irvine and the Wittrup labs, but that there was much about their mechanism of action that remained poorly understood. I thus defined as my major goal during the PhD to better understand how the amphiphile vaccines worked to the point that we could manipulate and improve upon them.

To further investigate the mechanism of action of peptide amphiphiles, we fused peptide antigens to mouse serum albumin, as peptide amphiphiles were thought to traffic to the lymph node by hitchhiking off serum albumin *in situ* (Chapter 2). In doing so, we freed ourselves from the dependence on *in situ* albumin, and could instead swap out various well-defined proteins to better understand what protein carriers work versus which fail. This strategy turned out to be highly informative, as we found that all protein carriers of sufficient mass could appropriately traffic to the draining lymph node, but that the optimal protein carriers ought to have rapid clearance rates from blood to minimize bioavailability in distal lymphoid organs that have not been inflamed by adjuvant. In other words, the broad organ-level pharmacokinetics of the antigen delivery vehicle seemed to dominate the response, as opposed to specific molecular interactions between albumin and the immune system, as we originally conjectured. At this point, a hypothesis-driven scientific inquiry morphed into an

engineering exercise, as we honed in on transthyretin as an ideal protein carrier, and we pushed the protein-antigen fusion system into still further applications, including DNA/RNA vaccines (Chapter 3) and in pursuit of tolerization applications for autoimmunity (Chapter 4).

Our conclusions regarding mechanism of action of CpG amphiphiles (lipo-CpG) proved to be quite different, unexpected by Occam's razor (Chapter 5). Rather than lipo-CpG gaining its advantage over CpG by virtue of lymphoid organ bioavailability, we instead found that lipo-CpG preferentially segments into different cell types than CpG (particularly, monocytes), even if CpG is dosed such that it accumulates in lymph nodes to the same extent as lipo-CpG. The strong propensity of lipo-CpG to be uptaken by monocytes triggers an IL-12 driven cascade that is significantly stronger than that induced by CpG, ultimately driving highly proliferative T cell responses. We hoped to apply these lessons in adjuvant delivery to a new synthetically produced adjuvant that we attempted to engineer using yeast surface display (Chapter 6). While this part of the project never fully panned out, we overall uncovered useful design principles in adjuvant delivery that can be applied to next-generation vaccines.

CHAPTER 2. PHARMACOKINETIC TUNING OF PROTEIN-ANTIGEN FUSIONS TO ENHANCE THE POTENCY OF THERAPEUTIC T CELL VACCINES

Abstract

Recent advances in immuno-oncology have generated renewed optimism for therapeutic anti-tumor vaccination, and peptide vaccines in particular are being extensively employed in clinical studies. However, peptide vaccines generally suffer from poor immunogenicity. Here, we pharmacokinetically tune vaccine responses via fusion of peptide epitopes to carrier proteins to optimize vaccine potency. Antigen-carrier fusions enable 3 factors to be optimized: a) efficient uptake in draining lymphatics from the site of injection, b) protection of epitope payloads from proteolytic degradation, and c) reduction of antigen presentation in uninflamed distal lymphoid organs. We find that peptides expressed as fusions with protein carriers like transthyretin can solve all three pharmacokinetic challenges, enhancing peptide vaccine immunogenicity up to 90-fold in mice. We demonstrate the utility of this approach with several clinically relevant antigens, including viral antigens, tumor-associated antigens, oncofetal antigens, and shared neoantigens. Protein-epitope fusions represent a facile and generalizable approach to enhance T cell responses elicited by subunit vaccines.

2.1 Introduction

In recent years, immunotherapies have transformed clinical oncology, including checkpoint blockade antibodies[73–75], chimeric antigen receptor T cells[12,13], bispecific T cell engagers[76], and oncolytic viruses[77]. However, therapeutic cancer vaccines, the oldest and most-studied form of immunological intervention, have had only modest clinical success, with a single FDA approval to date[19], despite their theoretical potential to enhance the response rates of checkpoint inhibitors[16–18]. Peptide vaccines in particular have been a focus in many recent cancer therapy trials, due in part to their safety, modest cost, and capacity to be rapidly manufactured, enabling patient-specific neoantigen vaccines[78,79]. However, the potency of peptide vaccines remains poor, especially in humans.

A number of pharmacokinetic (PK) shortcomings of peptide vaccines have been well characterized, including inefficient antigen transport to local draining lymph nodes (dLNs)[43,80] and proteolytic instability[44,81]. Delivery strategies have been developed to address these limitations, including the formulation of peptide antigens in synthetic particles[34,82,83], antibody-mediated targeting of antigen to dendritic cells[84,85], or direct intra-nodal injections[70,86] to obviate the need for antigenic trafficking altogether. These approaches, while effective, are complex in terms of manufacturing and/or administration, motivating the development of additional solutions.

Here, we studied the role of vaccine antigen pharmacokinetics (PK) in controlling the potency of subunit vaccines, and define strategies to optimize vaccine potency via PK tuning of

antigen delivery. To control antigen degradation rates and PK, we fused tumor-associated epitopes to inert protein carriers. By varying the identity of the carrier protein, we systematically altered the PK and biodistribution characteristics of the fusions to define key factors controlling vaccine potency. We find that immunogenicity is maximized by employing carrier proteins that exhibit prolonged residence time in local adjuvant-inflamed draining lymph nodes but short half-lives in systemic circulation, to minimize uptake in distal non-inflamed lymphoid organs. Collectively, these conclusions help identify a set of simple pharmacokinetic design criteria to aid in the engineering of molecular vaccines.

2.2 Results and Discussion

Tuning k_{abs} and proteolytic stability of peptide antigens by fusion to albumin enhances delivery to draining lymph nodes

Upon parenteral injection, antigens can be: absorbed into systemic circulation; degraded in tissue; traffic into lymph; or, preferably, captured by antigen presenting cells (APCs) locally. We hypothesized that fusion of peptide antigens to a bulky protein carrier could limit these first two potential fates to promote immune priming. Antigen levels in the blood following subcutaneous injection are a function of the systemic absorption rate (k_{abs}) and the rate of clearance from circulation (k_{clear}). These rate constants influence the antigen bioavailability in both the dLNs and distal lymphoid organs (**Fig. 2.1a**). Previous work has shown that parenterally-administered molecules < 40 kDa are rapidly absorbed through capillary endothelial cell junctions into systemic circulation, while larger molecules are size-excluded

from entering the blood vasculature and instead drain to lymphatic vessels[80]. To determine the hydrodynamic threshold for efficient lymphatic uptake in mice, we first assessed lymph node accumulation of dextrans of varying molecular weight. While 4 kDa dextran (hydrodynamic radius 1.2 nm) did not access the dLN above background, 20 kDa dextran (radius 2.4 nm) did so effectively (**Fig. 2.2a,b**).

Based on these data, we hypothesized that peptide epitopes (~2 kDa) would have low lymphatic uptake and high k_{abs} rates that could be greatly reduced upon fusion to mouse serum albumin (MSA, 69 kDa), with a hydrodynamic radius of 3.3 nm (**Fig. 2.2a**). To test this idea, we fused a long peptide from human papillomavirus (HPV) $E7_{38-57}$, containing the immunodominant H-2D^b-restricted CD8$^+$ T cell epitope $E7_{49-57}$, to the C terminus of MSA, including a His tag for purification[87] (**Fig. 2.1b**). Following expression and purification of MSA-$E7_{38-57}$ in human embryonic (HEK) cells, size exclusion chromatography (SEC) confirmed that the protein preparation was pure and monomeric (**Fig. 2.3a**). To determine k_{abs} for this antigen fusion, we injected FITC-labeled MSA-$E7_{38-57}$ or $E7_{38-57}$ peptide subcutaneously in mice and measured concentrations in serum over time (**Fig. 2.1c**). These measurements revealed that k_{abs} was greatly reduced for MSA-$E7_{38-57}$ compared to the free peptide (0.14 hr^{-1} vs. 1.37 hr^{-1}, respectively) (**Fig. 2.1d**). Thus, fusion to albumin enables the systemic absorption rate constant of peptides to be reduced by ~10-fold.

In addition to rapid systemic absorption, peptides suffer from poor dLN bioavailability due to proteolytic instability[44,81]. To assess the impact of MSA fusion on the stability of peptide antigens, we re-stimulated $E7_{38-57}$-vaccinated splenocytes *ex vivo* with varying concentrations of

either fresh or serum-treated $E7_{38-57}$ antigens and measured their IFN-γ production by intracellular cytokine staining (ICS). *Ex vivo* splenocyte recall in response to free $E7_{38-57}$ peptide was substantially reduced following serum treatment ($EC_{50,serum}/EC_{50,fresh}$ = 47.9), while stimulation by MSA-$E7_{38-57}$ was minimally affected by pre-treatment of the antigen fusion with serum ($EC_{50,serum}/EC_{50,fresh}$ = 0.95) (**Fig. 2.1e**). As a more direct measure of proteolysis, $E7_{38-57}$ peptides and MSA fusions were prepared with His_6 and FLAG tags flanking the N- and C-terminal ends of the epitope, respectively. These tagged antigens were incubated in 20% mouse plasma, followed by a sandwich ELISA with FLAG capture and His_6 detection, to detect cleavage of the $E7_{38-57}$ epitope (**Fig. 2.4a**). This assay detected cleavage of 34% of $E7_{38-57}$ in 4 hr, while MSA-$E7_{38-57}$ remained fully intact over this time course (**Fig. 2.4b**).

Although protection from extracellular proteases is desirable, intracellular epitope cleavage is an important step in antigen processing by antigen presenting cells. We found that not only are MSA-fused epitopes bioactive, but they are more readily processed than epitopes buried in the primary structure of protein antigens. OTI splenocytes with T cells specific for H-$2K^b$/$Ova_{257-264}$ were pulsed for 24 hours *ex vivo* with $Ova_{251-270}$ peptide (20mer that requires processing), MSA-$Ova_{251-270}$, or whole Ova protein, using CD69 MFI expression on $CD8^+$ T cells as a read-out of priming. While $Ova_{251-270}$ peptide was most effectively processed and presented to OTI cells, MSA-$Ova_{251-270}$ was more immunogenic than whole protein Ova (**Fig. 2.5**). These results demonstrate that displaying epitopes on the terminal end of MSA simultaneously protects epitopes from serum degradation while preserving bioactivity in APCs.

Due to its appropriate size and improved proteolytic stability, FITC-labeled MSA-$E7_{38-57}$ effectively trafficked to the dLN following subcutaneous administration, while labeled $E7_{38-57}$ peptide failed to accumulate above background as measured by IVIS imaging (**Fig. 2.1f**). Surprisingly, even ten-fold higher molar doses of labeled $E7_{38-57}$ peptide were not detectable in the dLN. Notably, administering the peptide instead in the commonly used Montanide water-in-oil emulsion adjuvant also failed to improve peptide bioavailability in the dLN (**Fig. 2.6a**) and instead led to retention at the injection site (**Fig. 2.6b**), a phenomenon previously demonstrated to lead to aberrant trafficking of antigen-specific T cells to the injection site and subsequent anergy/deletion[88]. Collectively, we conclude that expression as a fusion to MSA substantially improves delivery to draining lymph nodes by improving a peptide epitope's bioavailability.

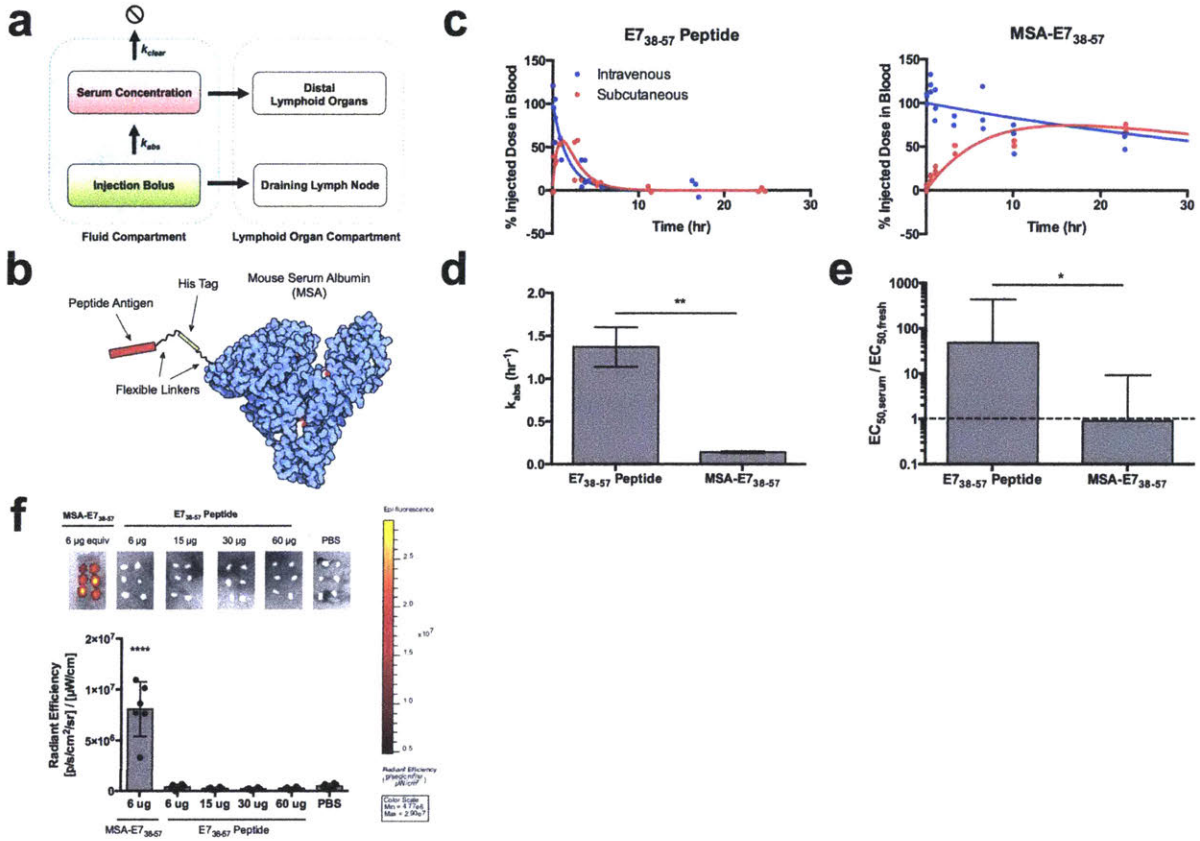

Figure 2.1. Albumin fusion enhances the bioavailability of antigen in the dLN

(a) Schematic of pharmacokinetic model describing absorbance rate (k_{abs}) and clearance rate (k_{clea}which determine bioavailability in lymphoid organs. **(b)** Schematic of MSA-$E7_{38-57}$ protein design. **(c)** FITC labeled $E7_{38-57}$ or MSA-$E7_{38-57}$ was injected either subcutaneously or intravenously in mice (n = 3 mice per group). <10 µl blood draws were used to quantify antigen concentration in serum over the course of 24 hours following injection. **(d)** Calculated k_{abs} rates for $E7_{38-57}$ peptide and MSA-$E7_{38-57}$ (data ± SE). **(e)** Splenocytes from $E7_{38-57}$-vaccinated mice were restimulated in the presence of brefeldin A with indicated antigen either fresh or treated with 10% mouse serum for 24 hours. Shown is the fold EC_{50} increase following serum treatment (data + SE). **(f)** FITC-labeled $E7_{38-57}$ or MSA-$E7_{38-57}$ was injected subcutaneously in mice at the indicated doses. 8 hours after injection, inguinal lymph nodes were excised and imaged on IVIS (n = 6 lymph nodes per group). Data are representative of two independent experiments. * $P < 0.05$; ** $P < 0.01$; **** $P < 0.0001$ by one-tailed t test **(d,e)** or one-way ANOVA with Tukey's multiple comparisons test **(f)**.

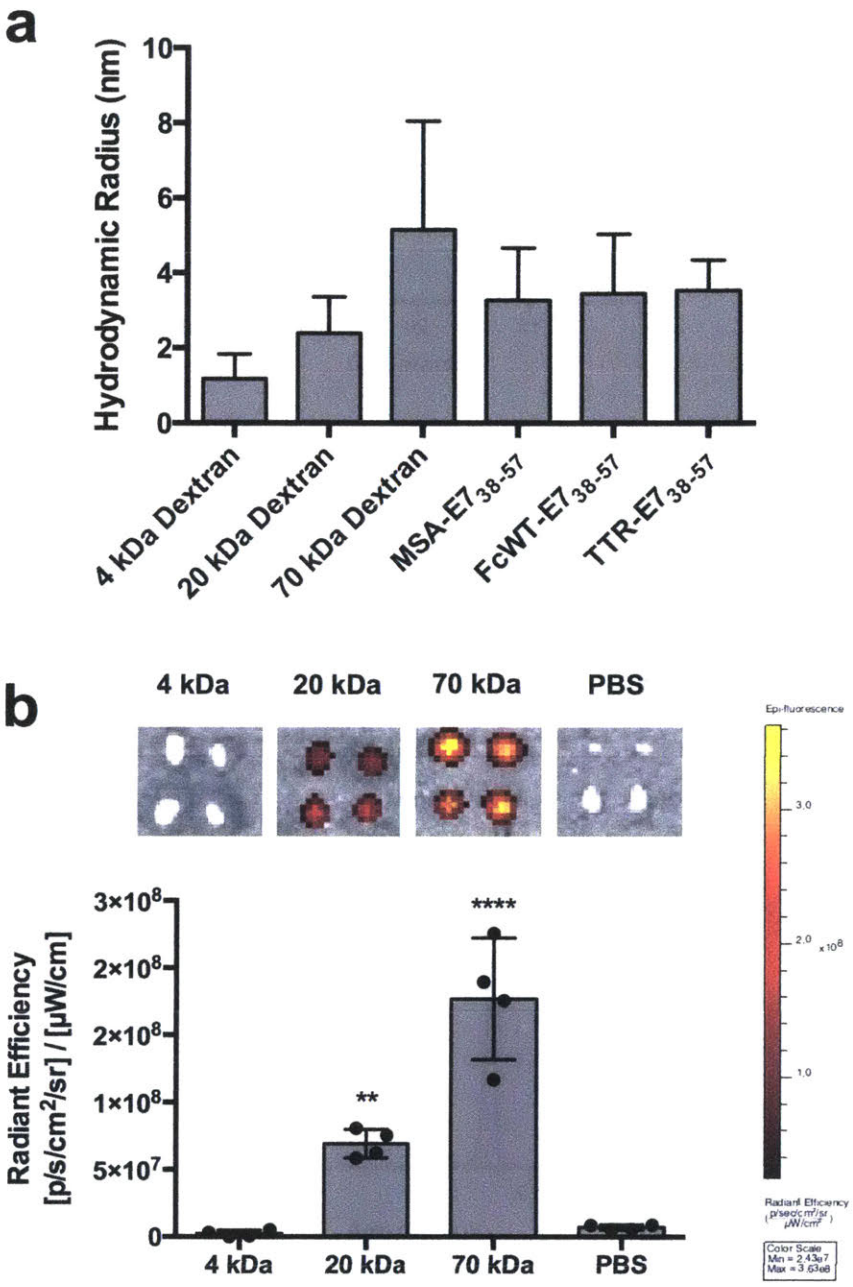

Figure 2.2. Lymph node uptake is directly related to molecular weight

(a) Shown are hydrodynamic radii of dextran and the indicated protein fusions were quantified on DLS. **(b)** Equimolar doses of FITC-dextran with the indicated molecular weight were injected subcutaneously in mice. 8 hours later, inguinal lymph nodes were excised and imaged on IVIS (n = 4 lymph nodes per group). ** $P < 0.01$; **** $P < 0.0001$ by one-way ANOVA with Tukey's multiple comparisons test against PBS **(a)**.

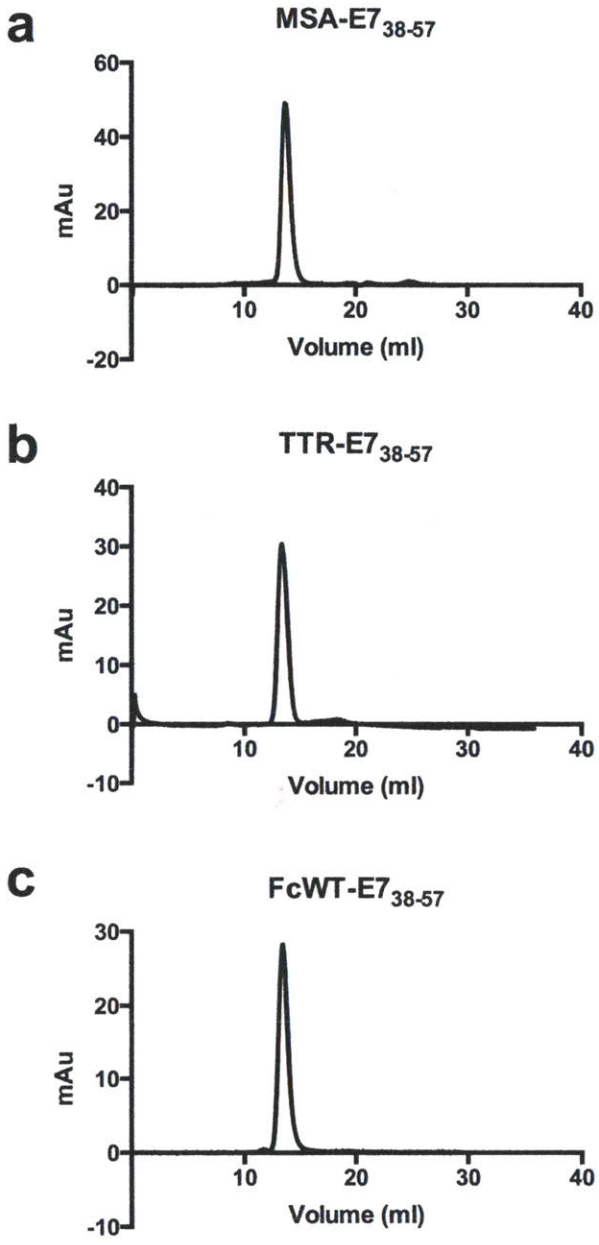

Figure 2.3. Protein-antigen fusion constructs run as single peaks in size exclusion chromatography

(a-c) SEC plots of the indicated protein-antigen fusion. 50 µg of protein were run in PBS on an analytical Superdex 200 Increase column.

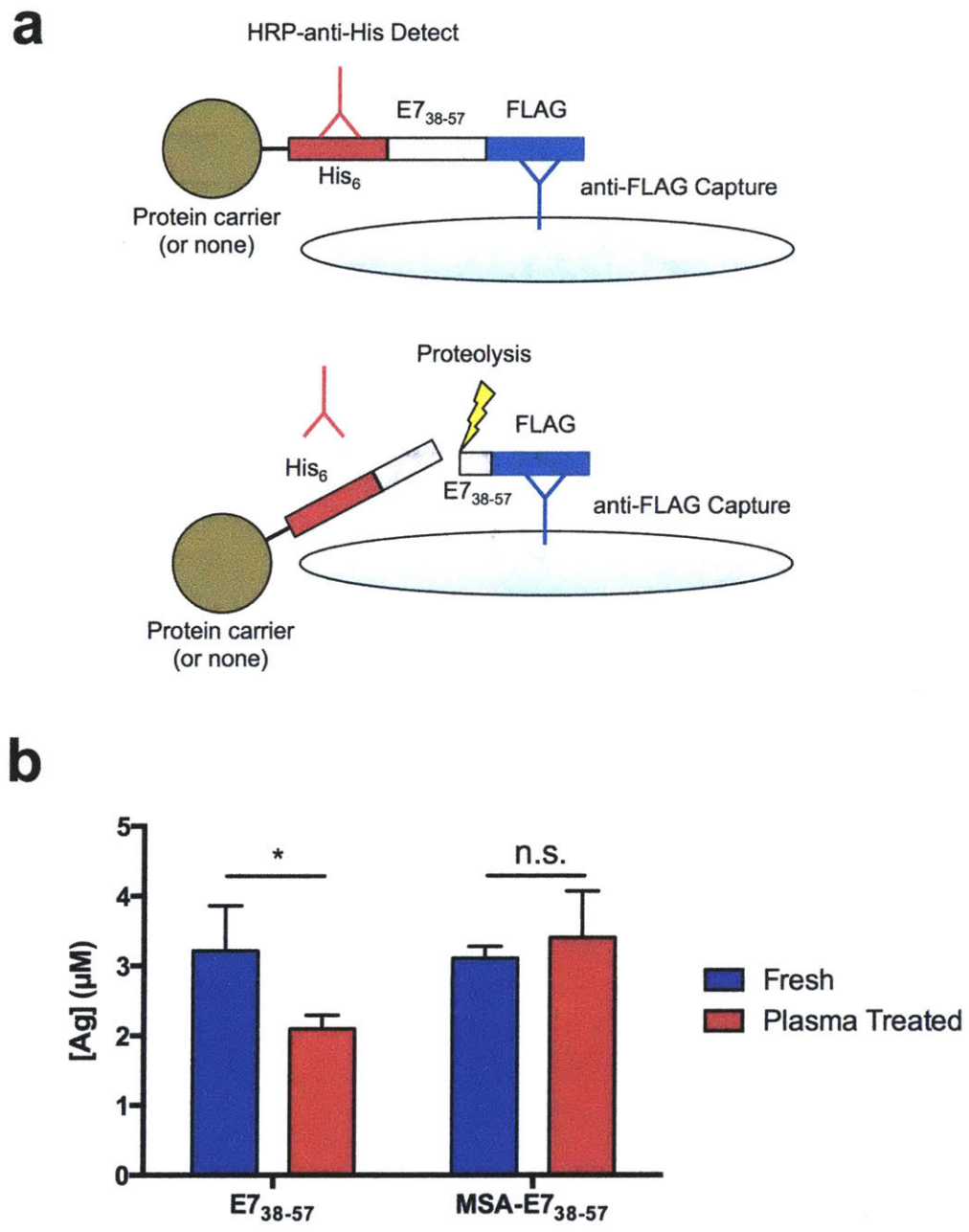

Figure 2.4. Direct test of proteolytic stability

(a) Schematic of the sandwich ELISA used to assess proteolytic stability. Following plasma incubation, mixed reaction was incubated with ELISA plates coated with anti-FLAG capture antibody. Detection was performed with an HRP-conjugated anti-His antibody. **(b)** His-$E7_{38-57}$-FLAG or MSA-His-$E7_{38-57}$-FLAG was incubated in fresh 20% mouse plasma for 4 hours. Intact antigen concentration was quantified via sandwich ELISA with FLAG capture and His detection (n = 3 technical replicates). Data are representative of two independent experiments. * $P < 0.05$ by two-tailed t tests within each group on the x axis **(b)**.

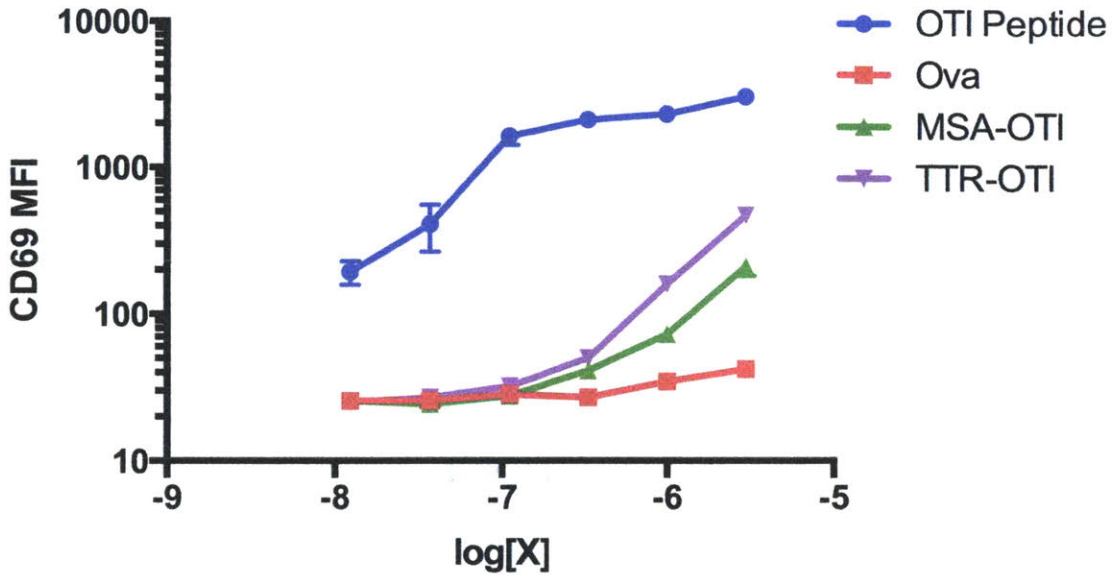

Figure 2.5. MSA- and TTR-epitope fusions are better processed than whole protein antigen

Splenocytes from OTI mice were cultured with the indicated antigenic constructs for 24 hours. After incubation, CD8+ T cells were assessed for CD69 expression by flow cytometry.

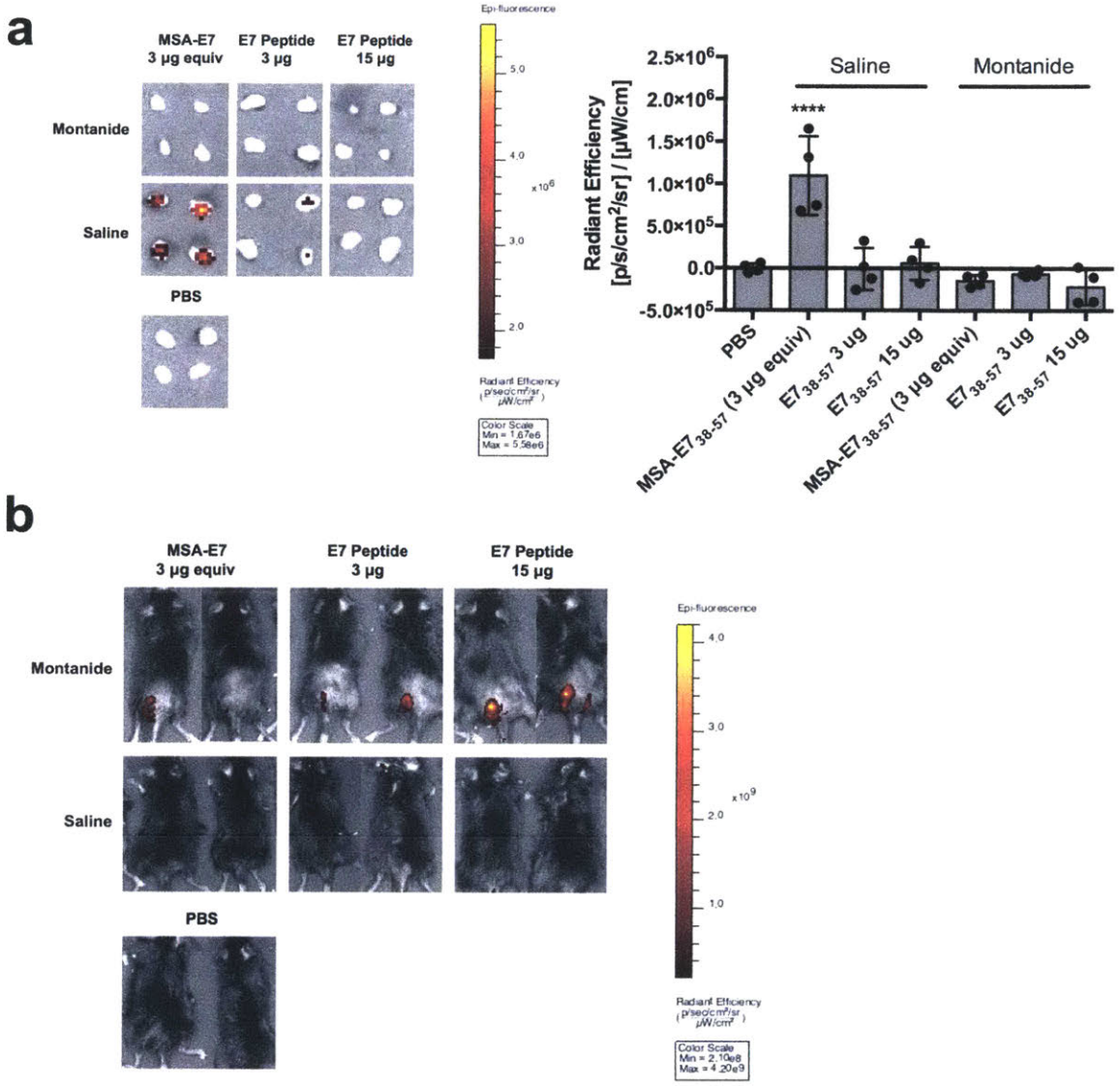

Figure 2.6. Montanide formulation fails to enhance dLN bioavailability

(a,b) FITC-labeled $E7_{38-57}$ or MSA-$E7_{38-57}$, formulated either in saline or Montanide, was injected subcutaneously in mice at the indicated doses. 8 hours after injection, inguinal lymph nodes (n = 4 lymph nodes per group) **(a)** and injection sites (n = 2 mice per group) **(b)** were imaged on IVIS. **** $P < 0.0001$ by one-way ANOVA with Tukey's multiple comparisons test versus PBS control **(a)**.

Albumin-antigen fusions effectively prime functional CD8⁺ T cell responses

To test the immunogenicity of MSA-E7$_{38-57}$ relative to free E7$_{38-57}$ peptides, mice were subcutaneously primed and boosted with E7$_{38-57}$ or equimolar doses of MSA-E7$_{38-57}$ mixed with cyclic-di-GMP, a cyclic dinucleotide (CDN) STING agonist[21], as an adjuvant. H2-D^b/E7$_{49-57}$ tetramer staining revealed that MSA fusions elicited 49-fold greater frequencies of E7$_{49-57}$-specific CD8⁺ T cells in blood compared to E7$_{38-57}$ peptide vaccination (**Fig. 2.7a**). Even tenfold higher doses of E7$_{38-57}$ peptide failed to replicate the immunogenicity of the albumin-antigen fusion protein (**Fig. 2.7b**), likely due to the poor dLN accumulation of even high peptide doses. Importantly, antibodies were not raised against MSA (**Fig. 2.8a,b**), and induction of protective memory responses was confirmed in MSA-E7$_{38-57}$-vaccinated animals, which rejected challenge with E7⁺ TC-1 tumor cells two months after boost (**Fig. 2.9**).

We next assessed whether vaccination with MSA-E7$_{38-57}$ fusions could elicit therapeutically effective T cell responses against established subcutaneous E7⁺ TC-1 tumors. Mice bearing TC-1 tumors were treated weekly with equimolar doses of E7$_{38-57}$ or MSA-E7$_{38-57}$ and CDNs. Mice treated with MSA-E7$_{38-57}$ had a statistically significant improvement in tumor control relative to PBS-treated mice, leading to substantially prolonged survival and a 40% cure rate, while the median survival of E7$_{38-57}$-treated mice was unchanged relative to untreated animals and only 10% of mice were cured (**Fig. 2.7c**).

The generalizability of the MSA delivery strategy was assessed by testing alternative adjuvants, attaching other tumor-associated epitopes, and utilizing alternative albumin-binding agents. To confirm that vaccine potentiation was not restricted to the use of CDN as an adjuvant, MSA-E7$_{38-57}$ was compared against E7$_{38-57}$ with a panel of adjuvants; including CpG, a TLR9 agonist; poly(I:C), a TLR3 agonist; and lipo-CpG, a potent lymph-node targeting variant of CpG[43]. In all cases, MSA-E7$_{38-57}$ vaccinated animals primed at least ten-fold stronger anti-E7$_{49-57}$ responses than E7$_{38-59}$ vaccinated animals (**Fig. 2.7d**).

In anti-tumor vaccine design, altered peptide ligands (APLs) are engineered to promote stronger affinity for MHC molecules without modifying specificity against the wild-type epitope, thus generating more potent responses against the tumor[89]. We tested MSA fusion vaccines targeting melanoma-associated Trp1$_{1455-63}$ APL[90], gp100$_{20-39}$ APL[91], and oncofetal antigen CEA$_{567-84}$. Following prime and boost vaccination, peripheral blood mononuclear cells (PBMCs) were re-stimulated with the appropriate CD8$^+$ T cell optimal peptide, and IFN-γ and TNF-α expression were assessed via ICS. As measured by IFNγ^+CD8$^+$ T cells, MSA-epitope fusion vaccines outperformed their peptide counterparts by 18-fold for Trp1$_{1455-63}$ APL, 39-fold for gp100$_{20-39}$ APL, and 61-fold for CEA$_{567-84}$ (**Fig. 2.7e**). MSA-fusion vaccines also generated polyfunctional CD8$^+$ T cell responses that secreted both IFN-γ and TNF-α while peptide-based vaccines failed to do so.

We next asked whether immunogenicity potentiation was dependent on direct covalent linkage of epitope to MSA. First, we fused E7$_{38-57}$ to a small 7 kDa protein (sso7d) recently characterized as a non-antibody protein engineering scaffold[92,93]. While an irrelevant sso7d

fusion (Irr sso7d-E7$_{38-57}$) failed to prime CD8+ T cell responses relative to naïve animals (**Fig. 2.7f**), an engineered variant of sso7d that bound MSA with a K_d of 8 nM fused to E7$_{38-57}$ (M18.2.5-E7$_{38-57}$) successfully primed anti-E7$_{49-57}$ responses equivalently to MSA-E7$_{38-57}$ (**Fig. 2.7g**). Additionally, when MSA-E7$_{49-57}$ was directly compared against amph-E7$_{49-57}$ with lipo-CpG as the adjuvant, both the recombinant fusion and the amphiphile performed equivalently (**Fig. 2.10**). Collectively, these data suggest that 1) fusion to a small protein carrier is insufficient to potentiate immunogenicity, and 2) that both reversible and irreversible linkages to MSA can enhance vaccination potency.

Immunogenicity of MSA-E7$_{38-57}$ was dependent on cross-presenting Batf3$^+$ cells *in vivo* (**Fig. 2.11a**). Because albumin as an antigen carrier does not direct antigen uptake to particular APCs, we evaluated the impact of including a targeting moiety for cross-presenting DC subsets in the MSA-antigen fusion design. Using yeast surface display, we engineered a fibronectin clone (DEC1) that bound DEC-205 with a K_d of 0.66 nM (**Fig. 2.11b**), and fused it to the N-terminal end of MSA-E7$_{38-57}$ (DEC1-MSA-E7$_{38-57}$). Immunization with DEC1-MSA-E7$_{38-57}$ increased lymph node-resident CD8$^+$ DC uptake of antigen by 39-fold compared to MSA-E7$_{38-57}$ (**Fig. 2.11c**); interestingly, though, it did not improve total dLN accumulation as measured by IVIS (**Fig. 2.11d**). As an immunogen, DEC1-MSA-E7$_{38-57}$ elicited T cell responses that were not statistically different from MSA-E7$_{38-57}$ for antigen doses ranging from 0.3-3 μg peptide equivalence (**Fig. 2.11e**). Thus, enhanced lymphatic delivery and protection of peptides from premature degradation are sufficient for protein carriers to substantially enhance peptide

vaccine immunogenicity, and specific APC targeting does not further improve T cell responses, at least for albumin fusions.

The use of protein carriers as a concept is not new: peptides are routinely conjugated to immunogenic protein carriers like keyhole limpet hemocyanin (KLH) to increase B cell receptor crosslinking and co-deliver antigen with CD4+ T cell epitopes, boosting humoral immunity[94]. However, T cell responses are exclusively detected against KLH, not against the antigen of interest[95]; and the impacts of KLH on biodistribution have been understudied. Here, we utilize immunologically inert protein carriers to direct cellular responses against fused epitope payloads, and we tune immunogenicity by the modulation of pharmacokinetics.

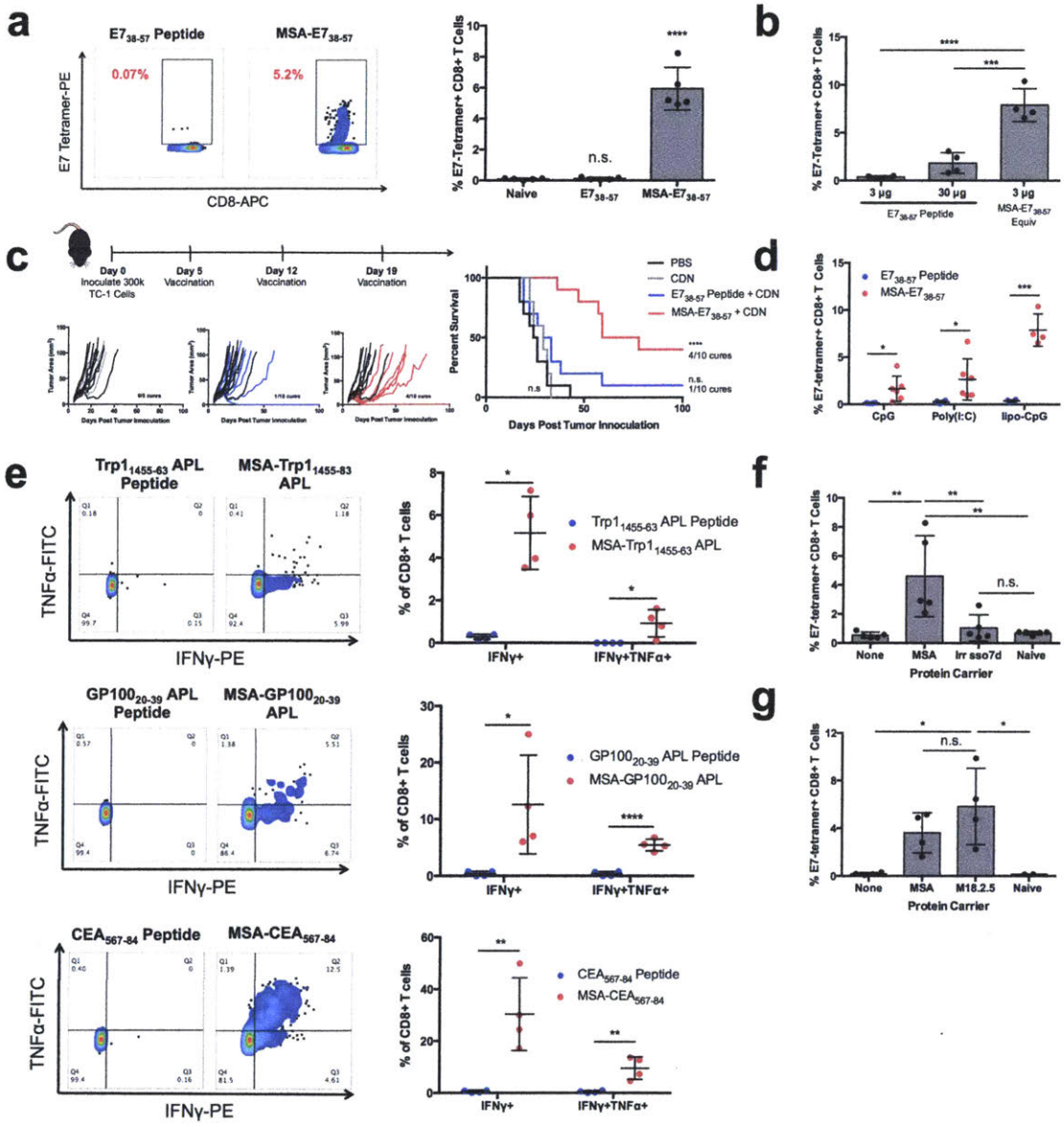

Figure 2.7. Albumin delivery of epitopes is a generalizable immunogenicity enhancement strategy

(a) Mice were primed and boosted with $E7_{38-57}$ or MSA-$E7_{38-57}$ plus CDN subcutaneously. Shown are representative tetramer stain flow plots among CD8+ T cells 6 days after boost, and quantification (n = 5 mice per group). Data are representative of over five independent experiments. **(b)** Mice were primed and boosted with $E7_{38-57}$ or MSA-$E7_{38-57}$ as in **(a)** at the indicated doses. Shown are tetramer stain data among CD8+ T cells 6 days after boost (n = 4 mice per group). **(c)** Timeline and treatment schematic of TC-1 tumor study, along with tumor growth plots and survival curves (n = 5 - 10 mice per group). Data are compiled from two independent experiments. **(d)** Mice were primed and boosted with $E7_{38-57}$ or MSA-$E7_{38-57}$ plus the indicated adjuvants subcutaneously. Shown are tetramer stain data among CD8+ T cells 6 days after boost (n = 6 mice per group for CpG and poly(I:C) and n = 5 mice per group for lipo-CpG). **(e)** Mice were primed and boosted with the indicated antigens as in **(a)**. 6 days after boost, peripheral blood cells were stimulated for 6 hours with WT optimal antigenic peptides in the presence of brefeldin A. Shown are representative flow cytometry plots plots for intracellular cytokine staining among CD8+ T cells and quantification (n = 4 mice per group). **(f-g)** Mice were primed and boosted with the indicated vaccine as in **(a)**. Shown are tetramer stain data among CD8+ T cells 6 days after boost (n = 5 mice in **(f)** and n=

4 mice in **(g)**). Throughout, * P < 0.05; ** P < 0.01; *** P < 0.001; **** P < 0.0001 by one-way ANOVA with Tukey's multiple comparisons test **(a,b,f,g)**; by log-rank (Mantel-Cox) test versus PBS **(c)**; and by two-tailed t tests within each group on the x axis **(d,e)**.

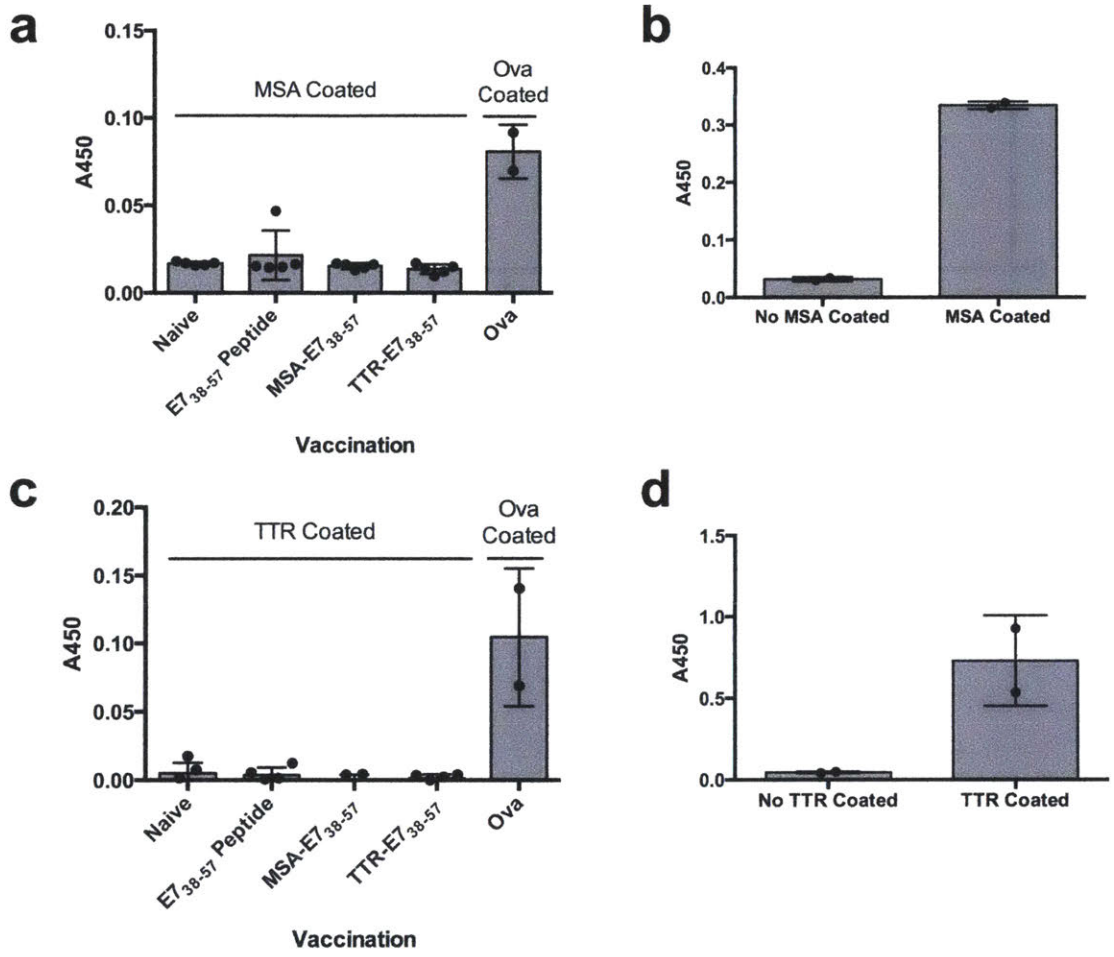

Figure 2.8. No antibody responses are detected against MSA nor TTR following vaccination

(a,c) Serum from mice primed and boosted with the indicated vaccine was collected and IgG purified with Protein A resin. The presence of anti-MSA **(a)** or anti-TTR **(c)** antibodies was measured with an ELISA plate coated with the corresponding protein of interest. Following serum incubation and washes, a chicken anti-mouse antibody was used as a detection reagent. Ova vaccinated animals and ova-coated wells were used as positive controls (n = 2 mice for Ova controls and n = 5 mice for other groups). **(b,d)** To confirm that MSA- **(b)** and TTR- **(d)** coated wells were of high quality, anti-MSA and anti-TTR antibodies were used as detection reagents (n = 2 mice per group).

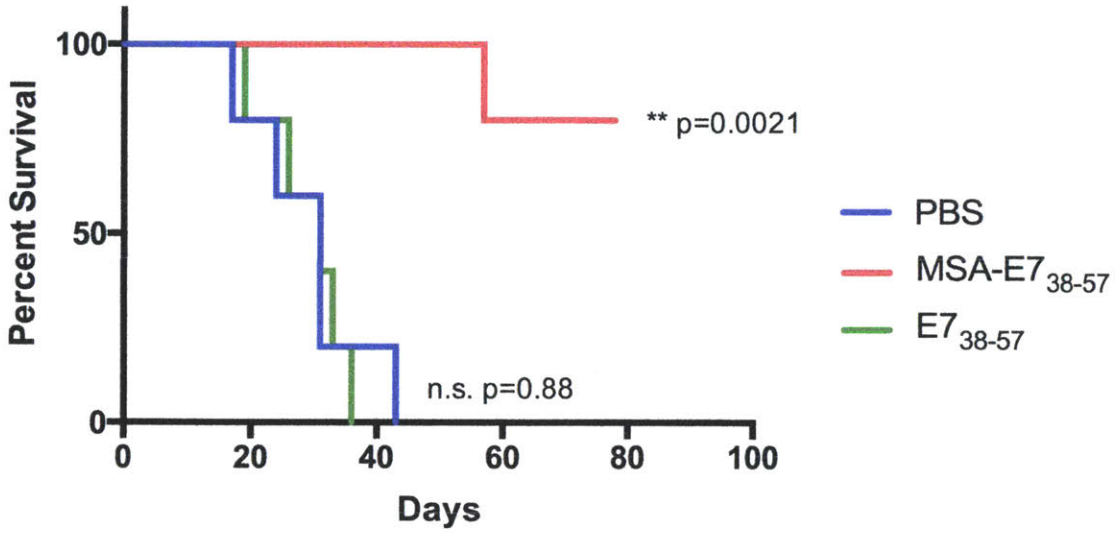

Figure 2.9. MSA-E7$_{38-57}$-vaccinated mice generate anti-E7 memory

MSA-E7$_{38-57}$-vaccinated mice generate anti-E7 memory. 66 days following boost, mice were inoculated with 300k TC-1 cells and euthanized after tumors exceeded 100 mm^2 in area (n = 5 mice per group). ** P < 0.01 by long-rank (Mantel-Cox) test versus PBS.

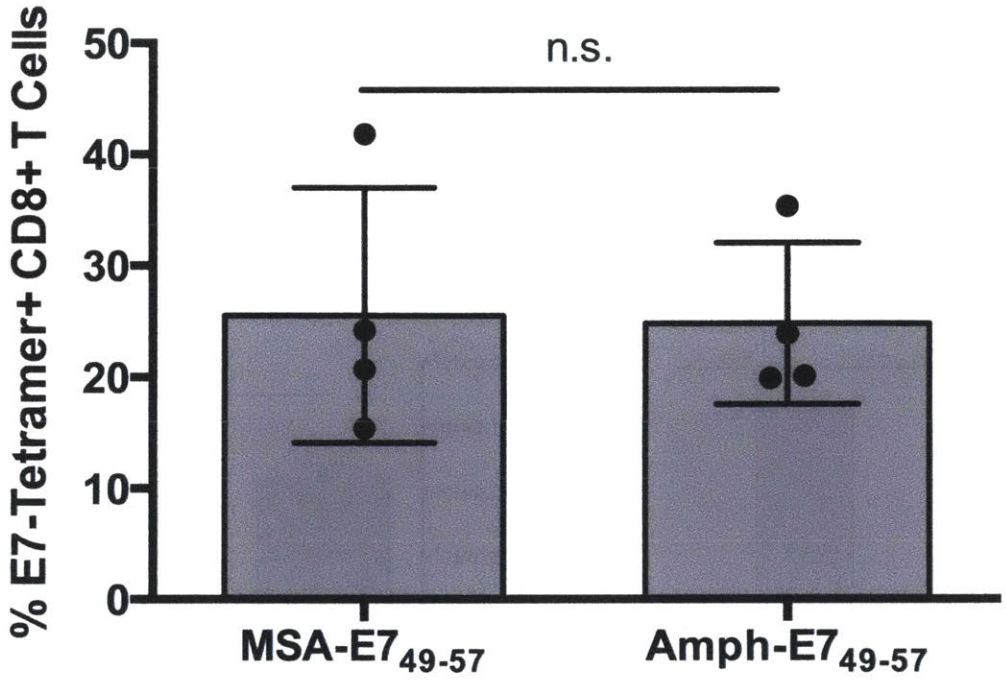

Figure 2.10. MSA-E7$_{49-57}$ performs similarly to amph-E7$_{49-57}$

Mice were primed and boosted with 5 μg amph-E7$_{49-57}$ or equimolar MSA-E7$_{49-57}$ plus lipo-CpG subcutaneously. Shown are tetramer stain data among CD8+ T cells 6 days after boost (n = 4 mice per group). Data are representative of two independent experiments. Two-tailed t test performed to assess statistical significance.

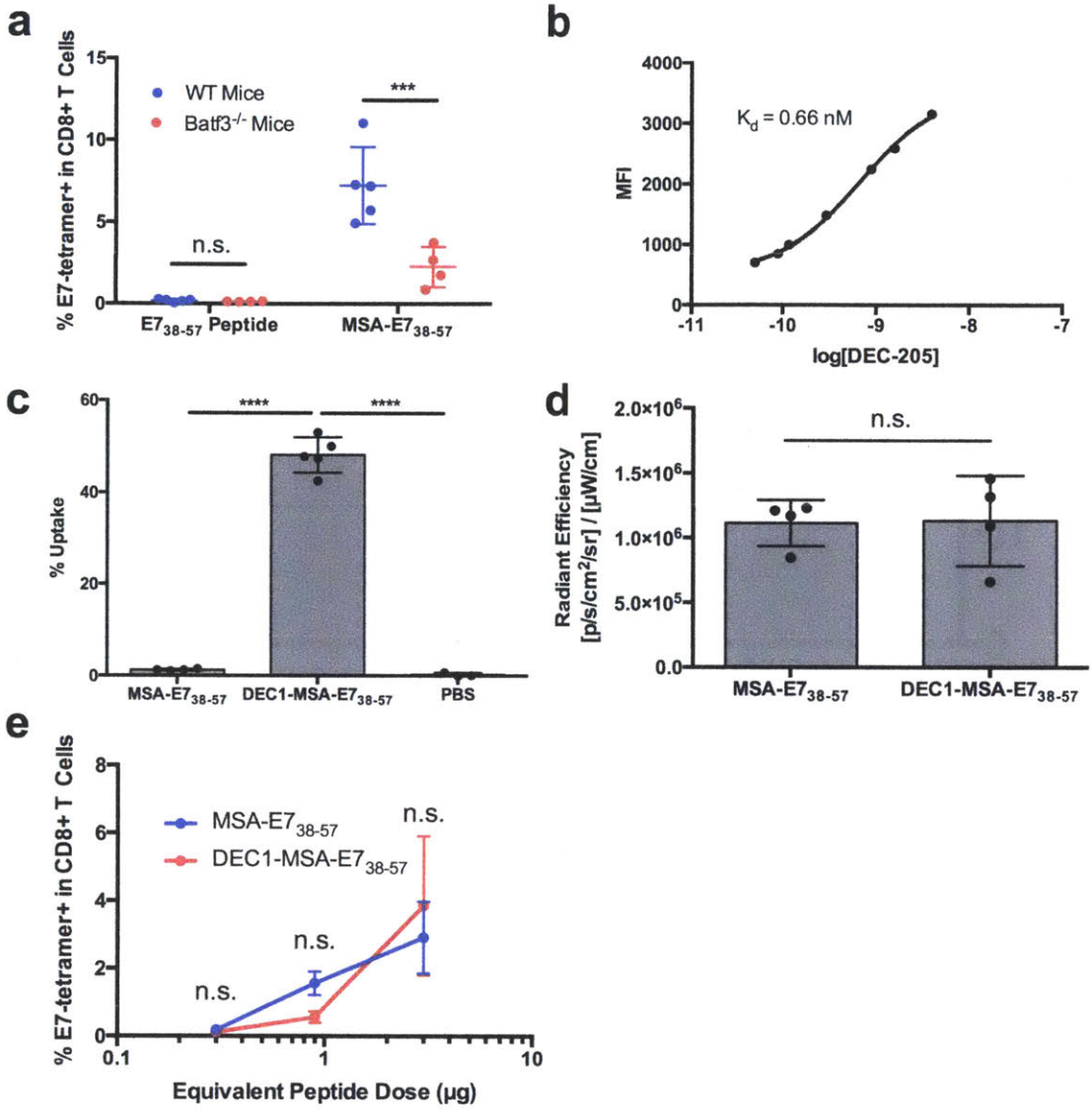

Figure 2.11. Targeting CD8+ DCs fails to enhance MSA-E7$_{38-57}$ immunogenicity.

(a) Mice (WT or Batf3$^{-/-}$) were primed and boosted with E7$_{38-57}$ or MSA-E7$_{38-57}$ plus CDN subcutaneously. Shown are tetramer stain data among CD8+ T cells 6 days after boost (n = 4-5 mice per group). **(b)** Soluble biotinylated DEC-205 was used to label yeast displaying DEC1 fibronectin, and MFI following secondary incubation was used to calculate the K_d of DEC1. **(c)** AF488-labeled MSA-E7$_{38-57}$ or DEC1-MSA-E7$_{38-57}$ was injected subcutaneously in mice. 24 hours later, the inguinal lymph node was excised and AF488 signal in CD8+ DCs was assessed by flow cytometry (n = 5 mice per group). **(d)** FITC-labeled MSA-E7$_{38-57}$ or DEC1-MSA-E7$_{38-57}$ was injected subcutaneously in mice. 8 hours later, the inguinal node was imaged by IVIS. **(e)** Mice were primed and boosted with the indicated doses of MSA-E7$_{38-57}$ or DEC1-MSA-E7$_{38-57}$ plus CDN subcutaneously. Shown are tetramer stain data among CD8+ T cells 6 days after boost (n = 5 mice). Data are representative of three independent experiments. Throughout, *** $P < 0.001$ and **** $P < 0.0001$ by two-tailed t tests within each group on the x axis **(a,d)** or at each indicated dose **(e)**; and by one-way ANOVA with Tukey's multiple comparisons test **(c)**.

Systemic antigen exposure during vaccination promotes tolerance

We hypothesized that systemic absorption distal from the injection site might blunt immune responses to vaccination, because the absence of inflammatory cues provided by adjuvant would promote tolerance rather than immune priming. Notably, we found that even when administered together with the CDN adjuvant, i.v.-administered MSA-$E7_{38-57}$ failed to prime a cellular immune response (**Fig. 2.12a**). Rather, i.v. administration induced tolerance against subsequent recall challenge with the same antigen: when mice were administered a single i.v. injection of MSA-$E7_{38-57}$ and then challenged with a s.c. prime and boost vaccination with the antigen fusion two weeks later, there was a > 85% drop in the magnitude of the T cell response to the s.c. immunization compared to animals that had received a control i.v. injection of PBS prior to challenge in lieu of the albumin fusion (**Fig. 2.12b**). Tolerance was induced by MSA-antigen fusions administered i.v. alone or co-administered with either of two different adjuvants (CDN or CpG) (**Fig. 2.12b**). Strikingly, i.v. tolerization via MSA-$E7_{38-57}$ was significantly more effective than i.v. administration of $E7_{38-57}$ peptide, the typical gold standard method of tolerization (**Fig. 2.12c**).

Persistent antigen presentation in the absence of inflammatory cues can induce T cell tolerization and dysfunction[88,96–98]. Our pharmacokinetic measurements showed the serum half-life of MSA-$E7_{38-57}$ to be 36 hours; we hypothesized that this long half-life may prolong antigen presentation and induce persistent T cell priming in distal lymphoid organs that fail to be inflamed from subcutaneous injection of the adjuvant. To test this idea, we subcutaneously vaccinated C57Bl/6 mice with 100 μg MSA-$gp100_{20-39}$ APL and CDN adjuvant. After 1, 4, or 7

days, 500k pmel Thy1.1$^+$ cells expressing TCRs specific for the gp100 epitope were adoptively transferred into vaccinated animals to serve as reporters of antigen presentation. 24 hours later, the local dLN (inguinal node) and distal lymphoid organs (mesenteric node and spleen) were excised and resident Thy1.1 cells were assessed for CD69 expression indicative of TCR triggering. At equivalent time points, CD8$^+$ DCs were analyzed for CD86 expression indicative of DC activation and exposure to inflammatory signals induced by the adjuvant. As anticipated, only the local dLN was inflamed by CDNs to induce activation in CD8$^+$ DCs. However, antigen presentation persisted for extended periods of time even in distal non-inflamed organs, with pmel T cells still showing CD69 upregulation in the mesenteric LNs when transferred 4 days after immunization or 7 days after immunization in the spleen (**Fig. 2.12d**). Collectively, these data suggest that only the local dLN likely contributes to activating immunity due to the simultaneous presence of both antigen and inflammatory cues, and persistent dysfunctional priming in distal organs serves to blunt functional immunity overall.

To more specifically query the mechanism of tolerance following systemic exposure to albumin fusions, we transferred 1 million CFSE-labeled Thy1.1$^+$ pmel cells into recipient mice and subsequently administered PBS, gp100$_{20\text{-}39}$ peptide, or MSA-gp100$_{20\text{-}39}$ i.v.; 72h later, Thy1.1$^+$ cells in the spleen were analyzed for CFSE dilution and PD1, Lag3, and Tim3 expression. MSA-gp100$_{20\text{-}39}$ administration led to significant proliferation of Thy1.1$^+$ cells (**Fig. 2.12e-g**) and the adoption of a PD1$^+$Lag3$^+$ phenotype (**Fig. 2.12g**). In the absence of adjuvant, persistent systemic distribution of MSA fusions proliferates and exhausts antigen-specific T cells.

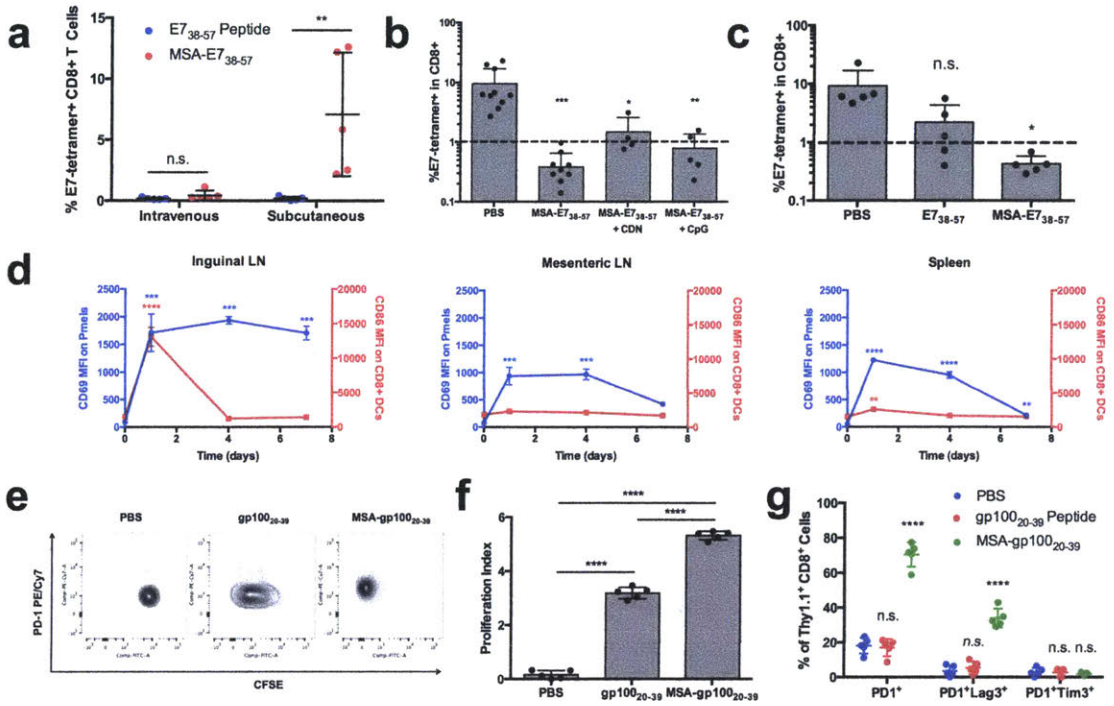

Figure 2.12. The systemic distribution of albumin fusions induces tolerance

(a) Mice were primed and boosted with $E7_{38-57}$ or MSA-$E7_{38-57}$ plus CDN either subcutaneously or intravenously. Shown are tetramer stain data among CD8+ T cells 6 days after boost (n = 5 mice per group). Data are representative of two independent experiments. **(b-c)** Mice were intravenously administered the indicated vaccine and prime/boost challenged two weeks later subcutaneously with CDN. Shown are tetramer stain data among CD8+ T cells 6 days after challenge boost (n = 4-10 mice per group in **(b)** and n = 5 mice per group in **(c)**). **(d)** Mice were subcutaneously administered MSA-$gp100_{20-39}$ APL with CDN. Following 1, 4, and 7d post-vaccination, 0.5M pmel CD8+Thy1.1+ cells were transferred into mice. 24 hours after transfer, the indicated organs were excised and CD69 MFI measured on Thy1.1+ cells by flow (blue curves). At the same time points post-vaccination, the indicated organs were excised and CD86 MFI measured on CD8+ DCs by flow cytometry (red curves) (n = 3 mice per group). **(e-g)** 1M CFSE-labeled pmel CD8+Thy1.1+ cells were transferred into WT mice and the indicated vaccines administered intravenously without adjuvant 24 hours later. After 72 hours, Thy1.1+ cells in the spleen were assessed by flow cytometry. **(e)** Shown are representative flow plots of CFSE dilution and PD1 expression. **(f)** Quantification of proliferation index via CFSE dilution. **(g)** Quantification of the frequency of expression of exhaustion-associated markers. Throughout, * $P < 0.05$; ** $P < 0.01$; *** $P < 0.001$; **** $P < 0.0001$ by two-tailed t tests within each group on the x axis **(a)**; by one-way ANOVA with Tukey's multiple comparisons test compared against PBS **(b,c,g)**; compared against the day zero time point for each measurement **(d)**; or compared between all groups **(f)**.

Increasing k_{clear} can improve the immunogenicity of protein-epitope fusions

The counterbalancing tolerizing impact of persistent systemically-distributed protein compelled us to search for an alternative protein carrier that preserved the slow k_{abs} of albumin while exhibiting a more rapid systemic k_{clear} rate constant, to increase local lymph node accumulation of antigen while decreasing systemic antigen exposure. We identified transthyretin (TTR), a ~60 KDa tetrameric endogenous hormone-trafficking serum protein as a promising candidate protein carrier, as it has a similar molecular weight as albumin but a significantly shorter systemic half life ($t_{1/2}$ of ~2 days for TTR[99] versus $t_{1/2}$ of ~3 weeks for albumin[100]). To confirm TTR's similarity to MSA in all characteristics except k_{clear}, we recombinantly produced and characterized TTR-$E7_{38-57}$ in similar fashion to the production of MSA-$E7_{38-57}$ (**Fig. 2.3b**). $E7_{38-57}$ peptide was processed and presented by either fusion protein with similar potency during *ex vivo* splenocyte restimulation with MSA-$E7_{38-57}$ or TTR-$E7_{38-57}$ (**Fig. 2.13a**), and like MSA-$E7_{38-57}$, TTR-$E7_{38-57}$ was proteolytically stable relative to free $E7_{38-57}$ peptide (**Fig. 2.14a**). Following s.c. administration, FITC-TTR-$E7_{38-57}$ accumulated equivalently to FITC-MSA-$E7_{38-57}$ in the inguinal dLN (**Fig. 2.13b**). To rule out differences in APC uptake, MSA-$E7_{38-57}$ and TTR-$E7_{38-57}$ were labeled with Alexa Fluor 647, injected subcutaneously, and the inguinal node was excised, digested, and assessed by flow cytometry 24 hours later. Equivalent uptake was detected in all analyzed DC and macrophage populations (**Fig. 2.13c**).

By contrast, analysis of blood concentrations of MSA-$E7_{38-57}$ and TTR-$E7_{38-57}$ following s.c. administration (**Fig. 2.13d**, **Fig. 2.14b**) revealed distinct systemic pharmacokinetics. While k_{abs} was similar between MSA-$E7_{38-57}$ and TTR-$E7_{38-57}$ (0.14 ± 0.03 hr^{-1} and 0.16 ± 0.03 hr^{-1}

respectively), k_{clear} was over three-fold faster for TTR-E7$_{38-57}$ relative to MSA-E7$_{38-57}$ (MSA-E7$_{38-57}$ has a k_{clear} of 0.019 ± 0.004 hr^{-1} versus TTR-E7$_{38-57}$ with a k_{clear} of 0.059 ± 0.006 hr^{-1}) (**Fig. 2.13d**). Due to this faster clearance rate, antigen presentation in distal, uninflamed lymphoid organs was much more transient for TTR than for MSA fusions. gp100$_{20-39}$ administered as a TTR fusion s.c. with adjuvant was presented and triggered reporter pmel T cell activation in the local inflamed dLN over the course of a week, while pmel activation was only detected in the mesenteric LN and the spleen at 1 day post immunization (**Fig. 2.13e**), in contrast to the persistent antigen presentation in these distal sites following MSA-fusion immunization (**Fig. 2.12d**). While the CD69 MFI area under the curve (AUC) over the course of a week was similar between MSA and TTR fusions in the draining inguinal LN, the AUCs in the mesenteric LN and spleen were significantly reduced for TTR fusions (**Fig. 2.14f**). Correlating with these findings, s.c. immunization with TTR-E7$_{38-57}$ elicited a 3.7-fold greater CD8$^+$ T cell response than MSA-E7$_{38-57}$ when dosed with equimolar E7 antigen, suggesting that a reduced duration of antigen presentation in distal lymphoid organs increases the potency of vaccination (**Fig. 2.14g**). No antibody responses against TTR were detectable (**Fig. 2.8c,d**).

TTR also differs from MSA due to its propensity to break down from tetrameric form into component monomers in acidic conditions, the rate limiting step in documented cases of TTR amyloidosis[101,102]. To rule out the possibility that this effect might affect TTR's immunogenicity, we produced TTR-E7$_{38-57}$ L55P, a mutation that further drives instability and promotes denaturation in more mild acidic conditions[103]. As expected, we found that incubation of TTR-E7$_{38-57}$ L55P at pH 5.5 for 48 hours resulted in the formation of light-scattering fibrils that

were poorly detected with WT TTR-E7$_{38-57}$ (**Fig. 2.15a**). However, TTR-E7$_{38-57}$ L55P performed equivalently to WT TTR-E7$_{38-57}$ in a head-to-head vaccination comparison study (**Fig. 2.15b**).

Thus, we conclude that the higher k_{clear} rate of TTR-E7$_{38-57}$ explains its ability to outperform MSA-E7$_{38-57}$. To pressure-test this finding, we fused and characterized the Fc portion of an IgG2c antibody to E7$_{38-57}$ (Fc-E7$_{38-57}$) (**Fig. 2.3c**), generating a fusion construct with a k_{clear} value 10x slower than TTR-E7$_{38-57}$ and 3x lower than MSA-E7$_{38-57}$ (k_{clear} = 0.006 ± 0.002 hr^{-1}) (**Fig. 2.14d**). Following prime and boost, Fc-E7$_{38-57}$ and CDN vaccination primed a 1.7% E7$_{49-57}$-specific CD8+ T cell response, a 24-fold boost in immunogenicity compared to peptide vaccination that was nonetheless weaker than responses to MSA-E7$_{38-57}$ and TTR-E7$_{38-57}$ (**Fig. 2.16**). FcγRs played no role in Fc-E7$_{38-57}$'s immunogenicity (**Fig. 2.16**). Overall, the efficacy of TTR-E7$_{38-57}$ > MSA-E7$_{38-57}$ > Fc-E7$_{38-57}$ > E7$_{38-57}$ peptide (**Fig. 2.13h**) suggests that while lowering k_{abs} is essential to generate vaccine responses over background, increasing k_{clear} can further boost potency by restricting antigen presentation in distal poorly inflamed lymphoid tissues (**Fig. 2.13i**). Collectively, we conclude that size exclusion from systemic absorption, proteolytic stability, and avoidance of distal priming all contribute to the immunogenicity of protein vaccines, which can be tuned and optimized by the judicious selection of protein fusion partner (**Table 2.1**).

Notably, the PK determinants of immunogenicity described here can be elucidated with a low number of simple, rapid, and cost-effective experiments. Data on k_{abs} and k_{clear} can be assessed with a single pharmacokinetic study, and proteolytic stability can be reliably measured by performing restimulation assays *ex vivo* on vaccinated or transgenic splenoctyes with fresh or serum-treated antigen. We propose that these two assays can be used to rapidly screen and

optimize future protein carrier strategies and improve future efforts to prime functional anti-tumor immunity.

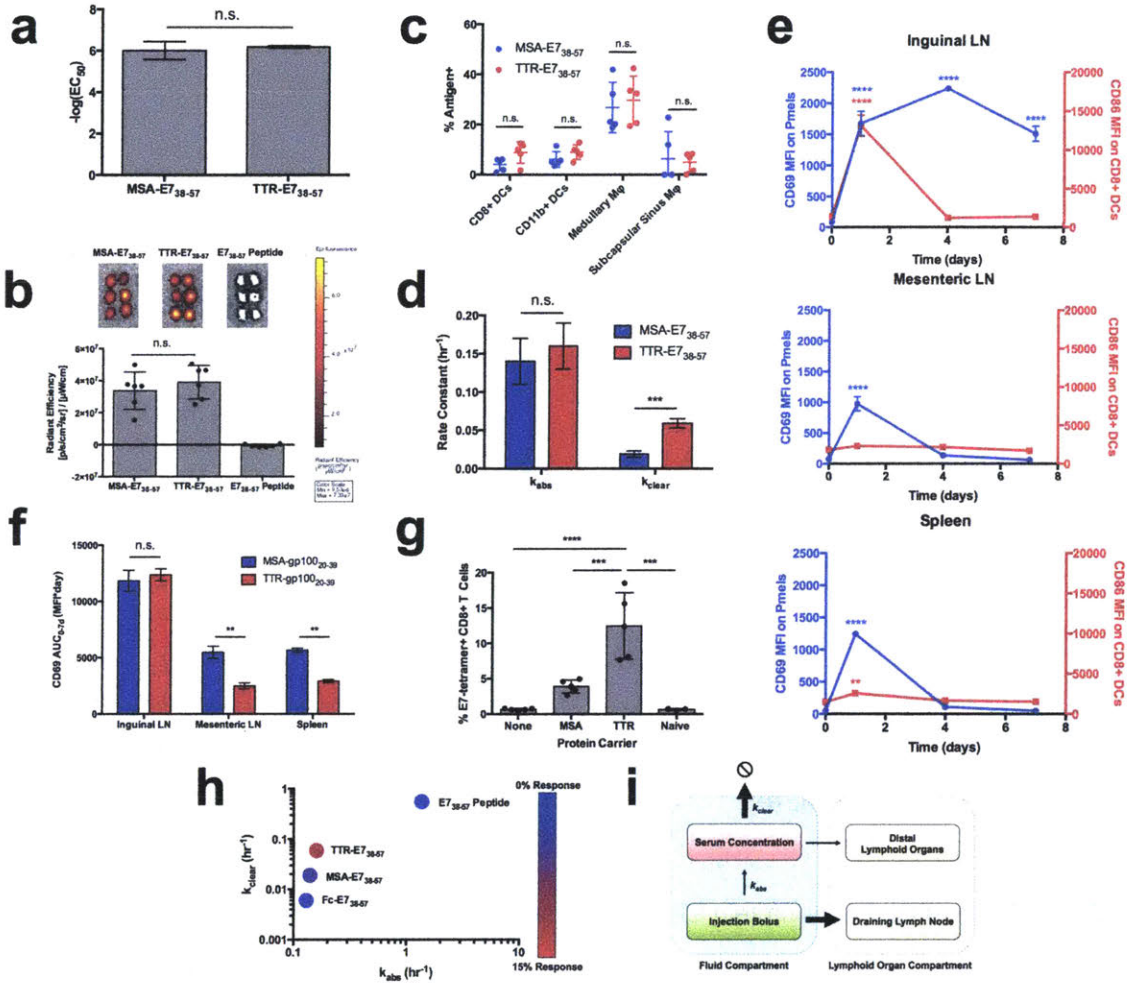

Figure 2.13. TTR fusions outperform MSA fusions due to a faster clearance rate

(a) EC_{50} values calculated from splenocyte restimulation studies with the indicated antigen (n = 3 technical replicates). **(b)** FITC-labeled antigen uptake in the dLN was measured as in **Fig. 1f** (n = 6 lymph nodes per group). **(c)** AF488-labeled MSA-$E7_{38-57}$ or TTR-$E7_{38-57}$ was injected subcutaneously in mice. 24 hours later, the inguinal lymph node was excised and AF488 signal in APCs assessed by flow cytometry (n = 5 mice per group). **(d)** Shown are k_{abs} and k_{clear} values as calculated via nonlinear regression from pharmacokinetic studies (data ± SE). **(e)** Pmel CD69 and CD8+ DC CD86 MFIs are shown. **(f)** Area under the curve calculations from CD69 MFI in **Fig. 3d** and **Fig. 4e**. **(g)** Mice were primed and boosted with the indicated vaccine plus CDN subcutaneously. Shown are tetramer stain data among CD8+ T cells 6 days after boost (n = 5 mice per group). Data are representative of over five independent experiments. **(h)** Mice were primed and boosted with the indicated vaccine plus CDN subcutaneously. Tetramer stain data are

indicated by color overlaid on a k_{abs} and k_{clear} scatterplot. **(i)** Schematic of pharmacokinetic parameters that maximize bioavailability in the inflamed dLN. Throughout, ** P < 0.01; *** P < 0.001; **** P < 0.0001; by two-tailed t test **(a)**; by one-way ANOVA with Tukey's multiple comparisons test compared between all groups **(b,g)** or compared against the day zero time point for each measure **(e)**; or by two-tailed t tests within each group on the x axis **(c,d,f)**

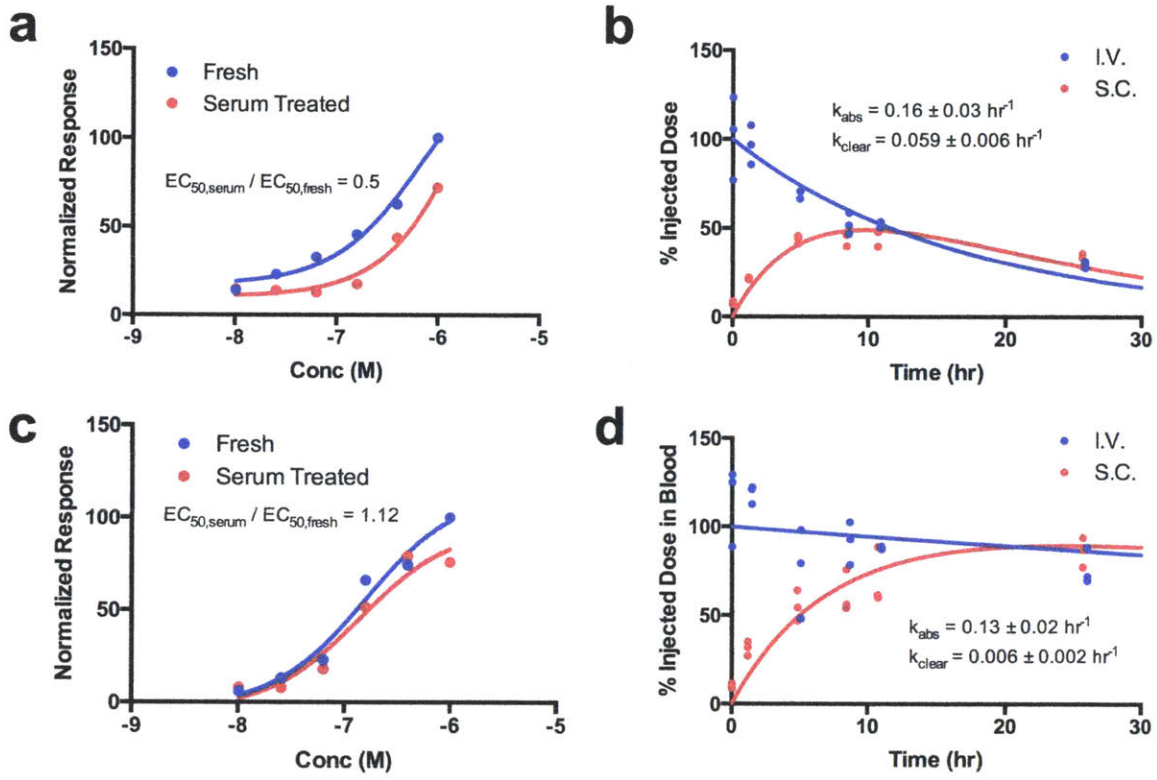

Figure 2.14. TTR- and Fc-$E7_{38-57}$ protein $E7_{38-57}$ from degradation in serum and slow systemic absorption

(a,c) Splenocytes from $E7_{38-57}$-vaccinated mice were restimulated in the presence of brefeldin A with either fresh antigen or antigen incubated in 10% mouse serum for 24 hours (n = 3 technical replicates). IFNγ production was assessed with intracellular cytokine staining. TTR-$E7_{38-57}$ shown in **(a)** and Fc-$E7_{38-57}$ shown in **(c)**. **(b,d)** FITC labeled TTR-$E7_{38-57}$ **(b)** or Fc-$E7_{38-57}$ **(d)** was injected either subcutaneously or intravenously in mice (n = 3 mice per group). 10 µl blood draws were used to quantify antigen concentration in serum over the course of 24 hours following injection.

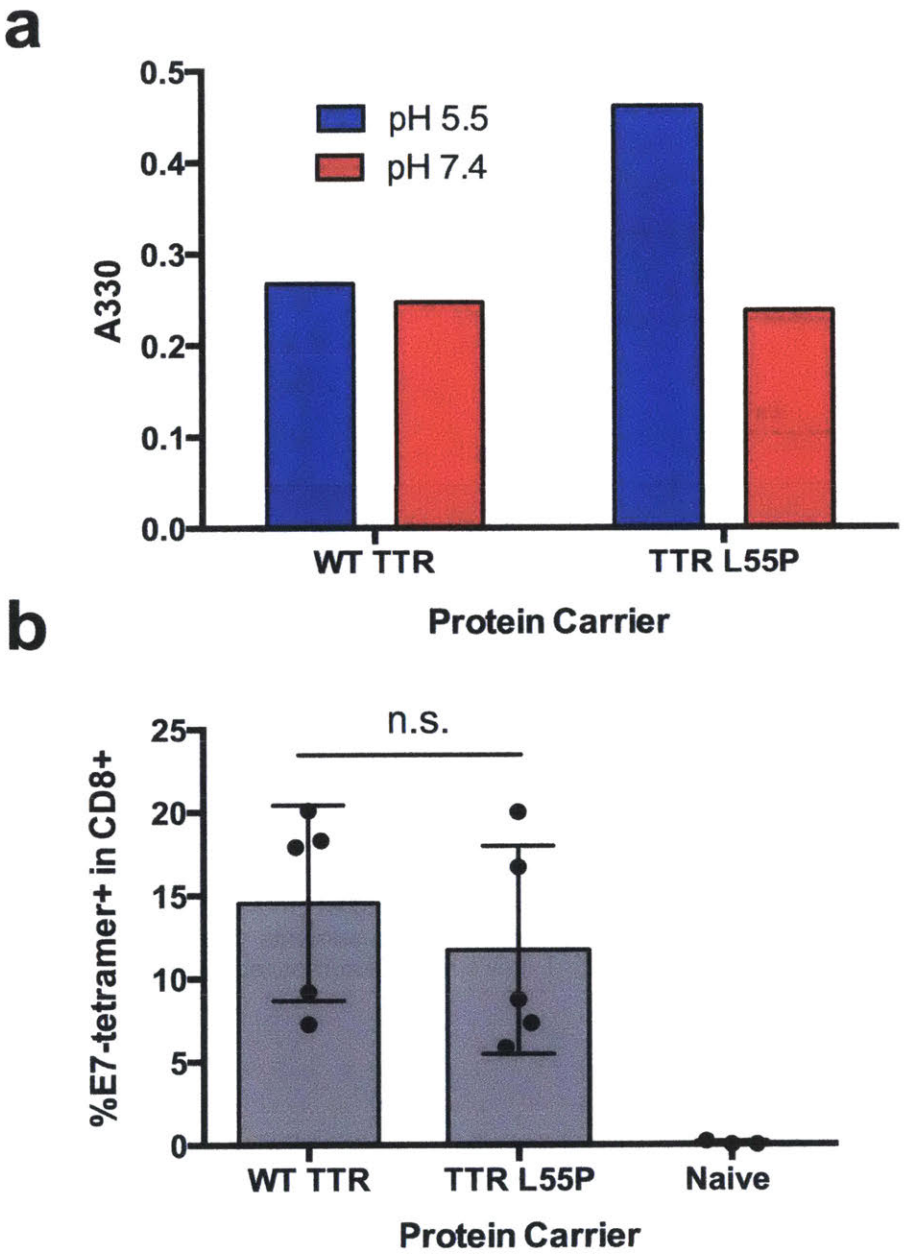

Figure 2.15. TTR-E7$_{38-57}$ is not enhanced by destabilization

(a) WT TTR-E7$_{38-57}$ or TTR-E7$_{38-57}$ L55P was incubated in acetate buffer at the indicated pH at 0.2 mg/ml for 48 hours followed by assessment of light scattering as measured by A330 on a plate reader. **(b)** Mice were vaccinated WT-TTR-E7$_{38-57}$ or TTR-E7$_{38-57}$ L55P and CDN subcutaneously. Shown are tetramer stain data 6 days after boost (n = 5 mice per group). Data are representative of two independent experiments. Statistics in **(b)** calculated via one-way ANOVA with Tukey's multiple comparisons test.

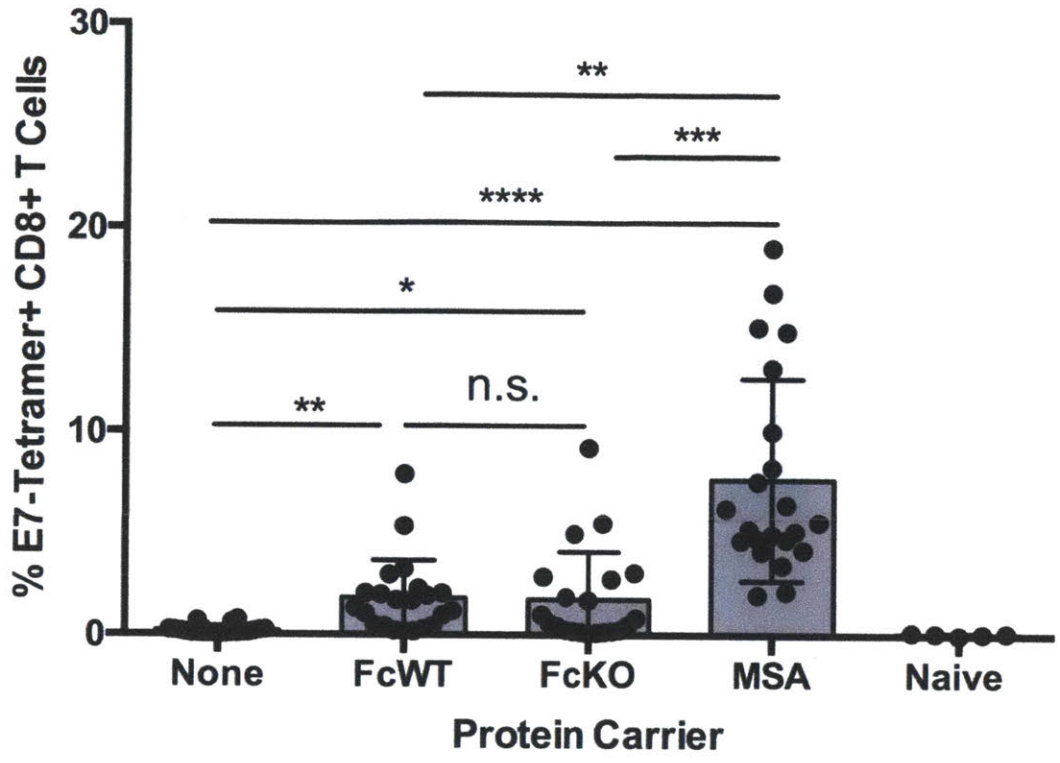

Figure 2.16. Fc-$E7_{38-57}$ efficacy is receptor-independent

Mice were primed and boosted with 3 μg $E7_{38-57}$ or equimolar doses of the indicated protein-$E7_{38-57}$ fusion plus CDN subcutaneously. Shown are tetramer stain data among CD8+ T cells 6 days after boost (n = 5 - 22 mice per group). Data are pooled from four independent experiments. * $P < 0.05$; ** $P < 0.01$; *** $P < 0.001$; **** $P < 0.0001$ by one-way ANOVA with Tukey's multiple comparisons test.

Table 2.1. Summary of measured quantities

	1. Size Exclusion from Systemic Absorption			2. Proteolytic Stability			3. Avoidance of Distal Priming	Immunogenicity
Quantity	*MW (kDa)*	*Radius (nm)*	k_{abs} (hr^{-1})	$log(EC_{50,fresh})$	$log(EC_{50,serum})$	$EC_{50,serum}$ / $EC_{50,fresh}$	k_{clear} (hr^{-1})	*Vaccine Response (% of CD8+ T Cells)*
$E7_{38-57}$ Peptide	2.2	-	1.37 ± 0.40	-8.23 ± 0.95	-6.55 ± 0.13	47.9	0.55 ± 0.11	0.12 ± 0.07
Fc-$E7_{38-57}$	57.8	3.4	0.13 ± 0.02	-6.80 ± 0.18	-6.85 ± 0.31	1.12	0.006 ± 0.002	1.94 ± 0.69
MSA-$E7_{38-57}$	69.4	3.3	0.14 ± 0.03	-6.01± 0.75	-6.05± 0.67	0.91	0.019 ± 0.004	5.94 ± 1.38
TTR-$E7_{38-57}$	68.5	3.5	0.16 ± 0.03	-6.19 ± 0.09	-5.89 ± 0.04	0.5	0.059 ± 0.006	12.45 ± 4.70

TTR as a delivery vehicle in tumor immunotherapy

We next explored the generalizability of TTR delivery in the context of other tumor-associated antigens. As measured by IFNγ^+ $CD8^+$ T cells in peripheral blood, TTR-antigen fusion vaccines outperformed MSA-antigen vaccines by 4-fold for $Trp1_{455-63}$ and 2-fold for $gp100_{20-39}$ APL; while TTR-CEA_{567-84} generated equivalent IFNγ^+ responses as MSA-CEA_{567-84}, polyfunctional IFNγ^+TNFα^+ responses were statistically primed over background only in the TTR-CEA_{567-84} case (**Fig. 2.17a**).

As a tetramer, TTR also provides the opportunity to develop higher valency constructs, which offer manufacturing advantages. For example, TTR fusions carrying 2 copies of the $E7_{38-57}$ epitope per subunit (8 copies per tetramer) could be produced at 4.7-fold more vaccine doses per liter of production cell culture compared to MSA-$E7_{38-57}$ constructs (**Fig. 2.18a**). Immunization with this higher-valency construct elicited T cell responses equivalent to TTR fused with a single copy of $E7_{38-57}$ per subunit when equivalent molar doses of the peptide were adminstered (**Fig. 2.18b**). We reasoned that if fusion of multiple copies of epitopes to TTR preserved immunogenicity, then the protein carrier could be designed to deliver multiple

antigens simultaneously. To this end, we compared TTR-gp100$_{20-39}$ and TTR-Trp1$_{1455-463}$ vaccines administered separately or together, and compared immune responses against TTR fused to gp100$_{20-39}$ and Trp1$_{1455-463}$ simultaneously in either orientation (**Fig. 2.17b**). TTR carriers delivering both antigens together elicited T cell responses that were not statistically different from the individual or mixed antigens, and we observed no dependence on antigen order in the fusion constructs (**Fig. 2.17b**).

To test the therapeutic efficacy of TTR carriers delivering multiple target antigens, we assessed therapeutic responses to Trp1 and gp100 vaccination in the aggressive B16F10 melanoma model. B16F10 subcutaneous tumors were treated with vaccinated with free Trp1 and gp100 peptides or TTR-Trp1-gp100 fusions every six days with or without anti-PD1 combination therapy (**Fig. 2.17c**). Six days after the first boost, ICS confirmed that Trp1 and gp100 responses were only generated above PBS-treated negative control mice in groups vaccinated with TTR-Trp1-gp100: strong mean responses >25% were generated in both groups utilizing TTR to co-deliver Trp1 and gp100 (**Fig. 2.17d**). As a result, TTR-Trp1-gp100-treated mice had significantly slower tumor outgrowth than mice treated with Trp1 and gp100 peptide without delivery vehicle (**Fig. 2.17e**). Anti-PD-1 therapy in this model had no efficacy as monotherapy, but together with the TTR fusion vaccine elicited substantially enhanced anti-tumor efficacy (**Fig. 2.17f**). Statistically significant improvements in overall survival relative to PBS controls was observed only in mice receiving TTR fusion vaccines (**Fig. 2.17g**).

An exciting potential clinical application of protein-epitope fusions is the targeting of shared neoantigens, or epitopes consisting of oncogenic mutations that arise in a relatively large

frequency of the patient population with a particular HLA allele. We chose to target two shared neoantigens: Kras G12D, which is mutated in a number of tumors, most notably pancreatic cancer[104,105], and H3.3 K27M, a common mutation that epigenetically drives transcriptional modifications in pediatric gliomas[106–108]. HLA-A11- and HLA-A2-restricted TCRs and their corresponding epitopes have been identified against Kras G12D and H3.3 K27M mutations, respectively[109,110]. $Kras_{2\text{-}21,G12D}$ and $H3.3_{21\text{-}40,K27M}$ epitopes were fused to TTR and prime/boosted in HLA-A11 and HLA-A2 transgenic mice, followed by an ELISPOT read-out to detect the magnitude of response. In both cases, antigen-specific cellular immunity above background was observed only when epitopes were delivered via TTR (**Fig. 2.17h,i**). Taken together, these data demonstrate the utility of TTR-mediated delivery for viral antigens (E7), tumor-associated antigens (Trp1, gp100), oncofetal antigens (CEA), and shared neoantigens (Kras, H3.3).

The protein-epitope fusions described here avoid a number of manufacturing and scale-up issues commonly associated with nanoparticulate formulations. Mass production of protein biologics is a well-developed art, and recombinant proteins can be manufactured in cGMP processes at scale to high purity. Albumin has a decades-long history of helping solubilize challenging cargo; while TTR is a more novel carrier, it can also be homogeneously produced, and as a tetramer its manufacturing efficiency is improved several-fold.

The protein-epitope fusion approach also has a potential application in nucleic acid vaccination, a cheaper, rapidly deployable modality. Intramuscular transfection with plasmid DNA and/or mRNA are both commonly studied vaccination strategies[111–113]. Encoding protein-epitope fusions in these systems could allow for the expression of antigen payload fused to

protein delivery vehicle to shepherd antigen from the site of secretion to the dLN. Non-encodable, particulate- or conjugate-based delivery systems are not amenable to such an approach.

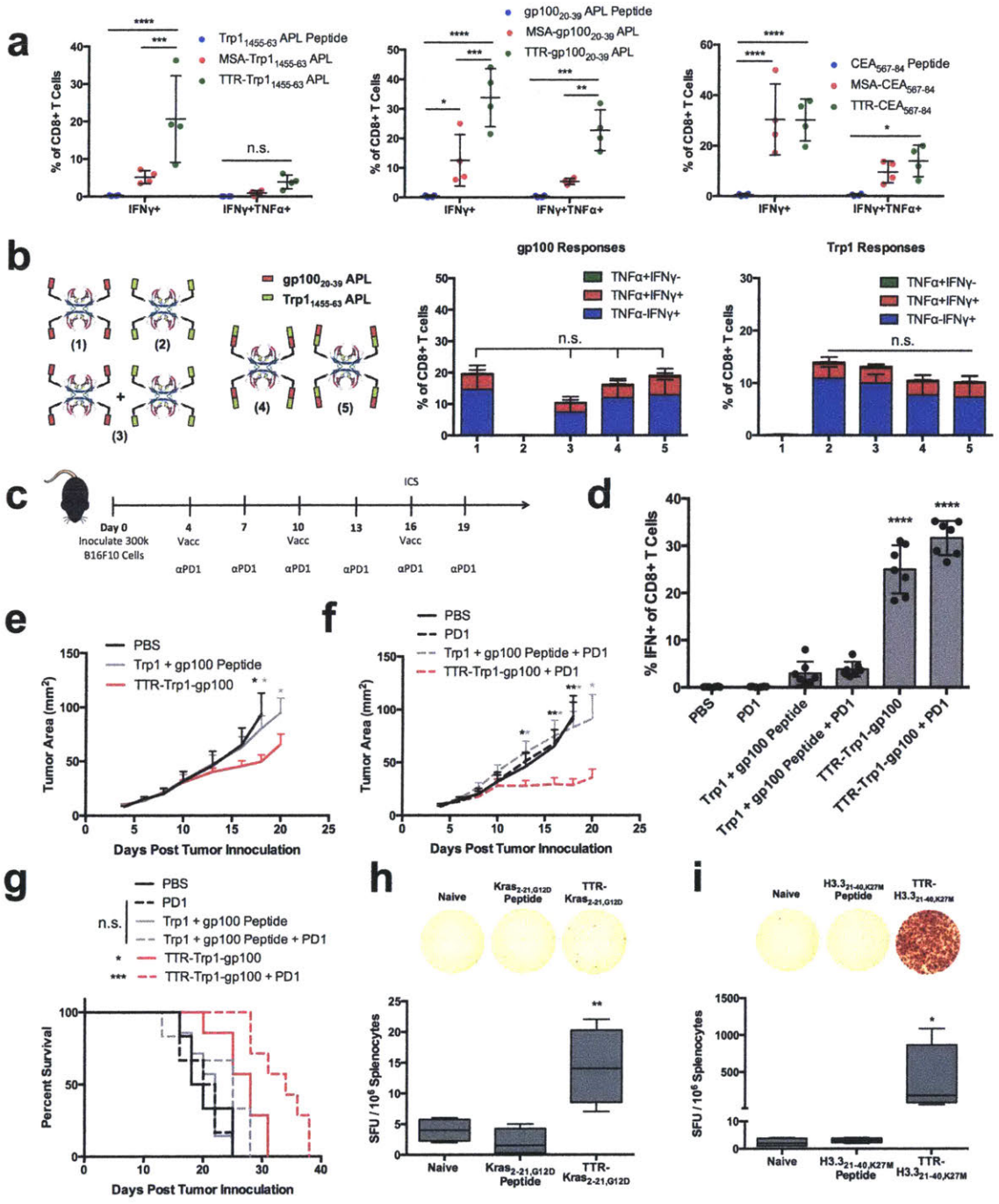

Figure 2.17. TTR-antigen fusions in cancer immunotherapy

(a) Mice were primed and boosted with the indicated antigens in peptide, MSA-fusion, or TTR-fusion form along with CDN subcutaneously, then assed with ICS (n = 4 mice per group) **(b)** Schematic of the TTR constructs used to test Trp1 and gp100 orientation during co-delivery. Mice were vaccinated with constructs along with CDN. Shown are ICS data 6 days after boost (n = 4-5 mice per group). **(c)** Schematic of the anti-B16F10 tumor immunotherapy study timeline used to generate panels **(d-g)** (n = 7 mice per group). **(d)** ICS data collected from PBMCs on day 16 of B16F10 study. Shown are pooled Trp1 and GP100 responses among CD8+ T cells in blood. **(e,f)** Shown are tumor growth curves of the indicated groups (mean + SEM). Curves are plotted until the first mouse is euthanized in each group. **(g)**

Survival curves. **(h,i)** The indicated shared neoantigen-targeting vaccines were administered with prime/boost in HLA-A11 **(h)** and HLA-A2 **(i)** transgenic mice, followed by an ELISPOT read-out with splenocytes stimulated with neoantigen-containing overlapping peptides. Throughout, * $P < 0.05$; ** $P < 0.01$; *** $P < 0.001$; **** $P < 0.0001$; by one-way ANOVA with Tukey's multiple comparisons test **(a,b,d,h,i)**; by one-tailed t-test at each measurement time point comparing samples against TTR-Trp1-gp100 **(e)** or TTR-Trp1-gp100 + PD1 **(f)**; or by log-rank (Mantel-Cox) test versus PBS **(g)**.

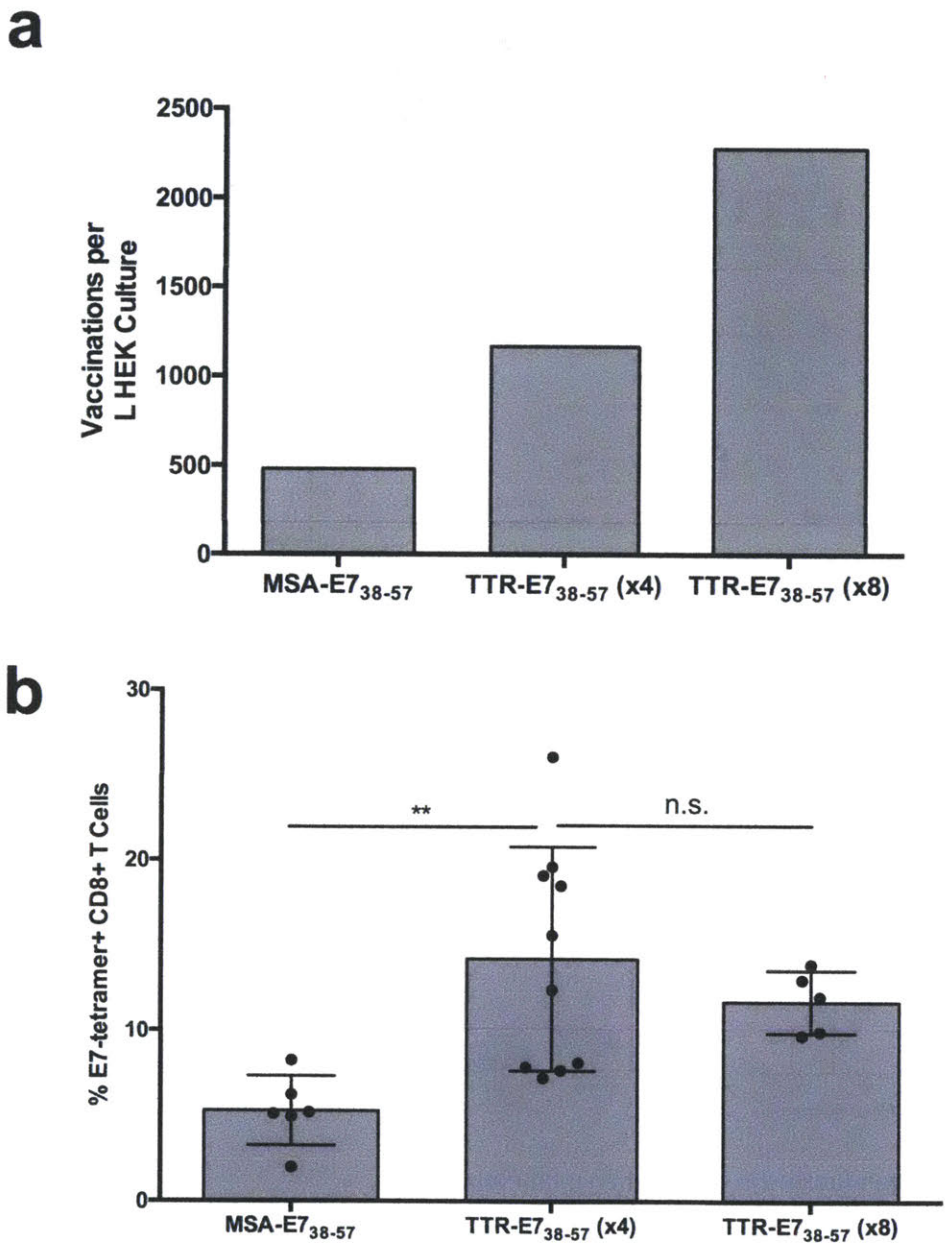

Figure 2.18. TTR-mediated delivery of highly valent antigen.

(a) Yields from the supernatant of HEK cell culture one week after transfection with the indicated constructs, calculated in terms of numbers of typical 3 μg peptide-equivalent doses of vaccine per liter of culture. **(b)** Mice were vaccinated with MSA-E7$_{38-57}$ or TTR-E7$_{38-57}$ with the indicated E7$_{38-57}$ copy number.

Shown are tetramer stain data 6 days after boost (n = 5-10 mice per group). ** P < 0.01 by one-way ANOVA with Tukey's multiple comparisons test **(b)**.

2.3 Materials and Methods

Mice

B6 mice (C57BL/6NTac) and HLA-A11 mice (B6-Tg(HLA-A*1101/H2-Kb)A11.01) were purchased from Taconic. Batf3$^{-/-}$ mice (B6.129S(C)-Batf3^{tm1Kmm}/J), pmel Thy1.1^{+} mice (B6.Cg-Thy1a/Cy Tg(TcraTcrb)8Rest/J), and HLA-A2 mice (C57BL/6-Mcph1Tg(HLA-A2.1)1Enge/J) were purchased from the Jackson Laboratory. OTI mice (C57BL/6-Tg(TcraTcrb)1100Mjb/J) and Thy1.1 mice (B6.PL-Thy1a/CyJ) were purchased from Jackson Laboratory and crossed to generate an OTI Thy1.1^{+} colony. All animal work was conducted under the approval of the Massachusetts Institute of Technology (MIT) Division of Comparative Medicine in accordance with federal, state, and local guidelines.

Cells

HEK cells (FreeStyle 293-F) were purchased from Thermo Fisher Scientific. TC-1 cells were kindly provided by T.C. Wu (Johns Hopkins University). B16F10 cells were purchased from ATCC. HEK cells were cultured in FreeStyle 293 Expression Medium (Thermo Fisher Scientific) and passaged every two days to a density of 300k/ml. TC-1 cells were cultured in RPMI-1640 (GE Healthcare Life Sciences) supplemented with 10% FBS, 100 units/ml penicillin, 100 μg/ml streptomycin, and 4 mM L-alanyl-L-glutamine. B16F10 cells were cultured in DMEM (GE Healthcare Life Sciences) supplemented with 10% FBS, 100 units/ml penicillin, 100 μg/ml

streptomycin, and 4 mM L-alanyl-L-glutamine. Both tumor cells were passaged 1:10 every two days. All cells were cultured at 37°C and 5% CO_2. All cells were tested regularly for mycoplasma contamination and for rodent pathogens, and none used tested positive at any point.

Protein production and characterization

Codon-optimized genes encoding desired proteins were cloned into gWiz expression vectors (Genlantis) using the In-Fusion HD Cloning Kit (Clontech), prepared endotoxin free (Macherey-Nagel) and incubated with Opti-Pro (Thermo Fisher Scientific) and polyethylenimine (PEI) 25K (Polysciences) prior to drop-wise addition to HEK cell culture at 1 million cells/ml. 1 mg of DNA was mixed with 40 ml of Opti-Pro and 2 mg of PEI per 1 L of cell culture. One week after transfection, cell culture was spun down in endotoxin-free centrifuge tubes at 15000xg for 30 min, supernatant filtered, pH neutralized by addition of 10X PBS, and run through TALON metal affinity resin (Clontech) by gravity flow per manufacturer instructions. Fc-$E7_{38-57}$ and variants were prepared as heterodimers with one copy of $E7_{38-57}$ per Fc dimer by co-transfecting gWiz-Fc-His_6-$E7_{38-57}$ and gWiz-Fc-FLAG (0.5 mg of each plasmid per 1 L of cell culture). Purification proceeded as above, but eluate from TALON resin was subsequently run through an anti-DYKDDDDK G1 affinity resin kit (Genscript) per manufacturer instructions to ensure purification of the heterodimer. In addition to wild-type Fc fusions, a pair of mutations (G236R/L328R) were introduced to knock out binding to FcγRs. Following purification, proteins were buffer exchanged into PBS with 30 kDa molecular weight cutoff Amicon Ultra-15 centrifugal filters (Millipore), filtered using Spin-X centrifuge tube filters (Corning) or 0.2 μm

syringe filters (VWR), and flash-frozen in aliquots with liquid nitrogen, then stored at -80°C. After thaw, proteins were used within one month and stored at 4°C in sterile conditions. Protein and dextran hydrodynamic radii were assessed by DLS (DynaPro NanoStar), purity analyzed by SEC (Superdex 200 Increase), and endotoxin levels measured using a chromogenic LAL assay (Lonza). A maximum of 5 EU/kg, or 0.1 EU/mouse was accepted for all injected proteins.

PK studies

5-FAM-E7$_{38-57}$ was purchased from Genscript, and recombinantly expressed proteins (MSA-E7$_{38-57}$, TTR-E7$_{38-57}$, and Fc-E7$_{38-57}$) were labeled with NHS-5/6-FAM (Thermo Fisher Scientific) per manufacturer instructions. Following protein conjugation, the concentration of labeled protein was calculated using A493. Mice were s.c. or i.v. vaccinated with 1 nmol labeled peptide or protein. At the indicated time points, <10 μl of blood was collected from tail snip into heparin-coated microhematocrit capillary tubes (VWR). Capillaries were parafilmed and stored upright in the dark at 4°C overnight to separate serum from cellular components. On a Typhoon Trio variable mode imager, serum in capillaries was measured (526 SP filter, 532 nm laser) against a standard curve of analytes prepared in PBS and added directly into capillaries. FIJI image analysis software was used to calculate serum concentrations of analyte. I.v. curves were fit to $C = C_0e^{-kclear*t}$ and s.c. curves were fit to $C = F*C_0*k_{abs}/(k_{abs}-k_{clear})*(e^{-kclear*t}-e^{-kabs*t})$, where C_0 and k_{clear} were fixed by the i.v. fit. F is systemic absorbance, and k_{clear} and k_{abs} are the clearance and absorbance rates, respectively (hr^{-1}). Curves were fit using nonlinear regression on GraphPad Prism software.

Vaccinations

All activating vaccinations were performed by s.c. prime at the tail base on day 0, boost on day 14, and read-out on day 20, except for the i.v. vaccination in Fig. 2.12a. All studies utilized 25 μg cyclic di-GMP (InvivoGen) as the adjuvant unless otherwise specified: in Fig. 2.7c utilizing alternative adjuvants, 1 nmol ODN1826 (CpG) (InvivoGen), 50 μg poly(I:C) HMW (Invivogen), and 1 nmol lipo-CpG[43] were instead used; in TC-1 tumor bearing animals, 50 μg cyclic di-GMP was used instead; in the amphiphile test, 1 nmol lipo-CpG[43] was used instead; in the B16F10 tumor study, 1 nmol lipo-CpG was used as the adjuvant. Antigen dosing (expressed as peptide equivalence): 3 μg for all $E7_{38-57}$ studies in non-tumor bearing mice; 10 μg $E7_{38-57}$ in TC-1 tumor-bearing mice; in Fig. 2.7e and 2.17a, 2.5 μg $Trp1_{1455-63}$ APL, and 5 μg $gp100_{20-39}$ APL and CEA_{567-84}; 3 μg for $gp100_{20-39}$ APL in pmel adoptive transfer studies; for bivalent forms of TTR-Trp1-gp100, 2.5 nmol in non-tumor bearing mice and 4 nmol in tumor-bearing mice; 10 μg $Kras_{2-21,G12D}$ and $H3.3_{21-40,K27M}$. For tolerizing vaccinations (Fig. 2.12b-c), PBS or 3 μg peptide equivalence $E7_{38-57}$ or MSA-$E7_{38-57}$ with or without adjuvant (25 μg cyclic di-GMP or 1 nmol lipo-CpG) was i.v. administered 14 days before s.c. prime/boost with TTR-$E7_{38-57}$ plus cyclic di-GMP as described above. In all cases, vaccine responses were measured by tetramer stain, ICS (see flow cytometry section), or by mouse IFN-γ ELISPOT (BD Biosciences) per manufacturer instructions, where 1M splenocytes were plated per well and stimulated with overlapping peptides ($Kras_{2-21,G12D}$ or $H3.3_{21-40,K27M}$) for 24 hours.

Flow cytometry

Antibodies against CD16/32 (Fc block, clone 93), CD8α (53-6.7), TNF-α (MP6-XT22), IFN-γ (XMG1.2), CD3 (17a2), B220 (RA3-6B2), CD11b (M1/70), CD11c (N418), F4/80 (BM8), CD69 (H1.2F3), CD86 (GL-1), PD1 (29F.1A12), Lag3 (C9B7W), and Tim3 (RMT3-23) were purchased from BioLegend. Cell viability was assessed with DAPI (Sigma) for tetramer stains and LIVE/DEAD fixable aqua dead cell stain (Thermo Fisher Scientific) for all other studies. *Tetramer staining:* E7 tetramer (iTAg Tetramer/PE - H-2 Db HPV 16 E7) was purchased from MBL; during tetramer staining, PBMCs were Fc blocked and stained with tetramer for 15 minutes prior to addition of anti-CD8α antibody, and cells were incubated with all antibodies for another 30 minutes. All labeling was performed in PBS + 0.1% BSA. *Ex vivo stimulation studies:* Intracellular cytokine staining (ICS) to assess the magnitude of T cell response was performed as previously reported[114]. Briefly, PBMCs were re-stimulated in RPMI-1640 + 10% FBS at 37°C with optimal WT peptide at 10 μg/ml ($Trp1_{455-63}$, $gp100_{25-33}$, $CEA_{572-579}$) for 2 hrs followed by addition of brefeldin A (Thermo Fisher Scientific) for another 4 hrs prior to staining. In the B16F10 study, re-stimulation was performed with 10 μg/ml of both $Trp1_{455-63}$ and $gp100_{25-33}$. When ICS was instead used to assess stability/immunogenicity instead of a vaccine read-out, whole protein or long peptide antigen was used for stimulation (see antigenic stability analysis section), and cells were re-stimulated for 18 hours followed by addition of brefeldin A for another 6 hours prior to staining. In all cases, surface staining was performed first (Fc block, anti-CD8α) in PBS + 0.1% BSA followed by fixation and permeabilization using BD Cytofix/Cytoperm fixation/permeabilization kit per manufacturer instructions and intracellular staining (anti-IFN-γ and/or anti-TNF-α) in perm/wash buffer. To assess the immunogenicity of protein or peptide antigens at stimulating OTI cells, pooled ACK-lysed splenocytes from OTI mice were cultured

in RPMI-1640 + 10% FBS and varying concentrations of SIINFEKL-containing antigen for 24 hours; after culture, cells were surface labeled with anti-CD8α and anti-CD69. *Organ processing:* In studies where T cells from lymph nodes were assessed by flow cytometry (Figs. 2.12d-g, and 2.13e), LNs were excised, mashed through 74 μm Netwell inserts (Corning), and washed into PBS + 0.1% BSA prior to antibody labeling. In studies where dendritic cells and/or other APCs were assessed by flow cytometry (Figs. 2.12d, 2.13c, 2.13e, and Supplementary Fig. 2.11c), LNs were excised, digested in RPMI-1640 + 0.8 mg/ml collagenase/dispase (Sigma) + 0.1 mg/ml DNase I (Sigma), mashed through 74 μm Netwell inserts, and washed into PBS + 0.1% BSA prior to antibody staining. In all cases, spleens were excised and mashed through 70 μm filters (Corning), lysed in ACK buffer, and washed into PBS + 0.1% BSA prior to antibody staining. To assess CD86 expression on DCs post-immunization, mice were s.c. injected with 25 μg cyclic-d-GMP (InvivoGen) and the spleen, inguinal LN, and mesenteric LN excised and processed 1, 4, or 7d later. Cells were analyzed using BD FACSCanto and BD FACS LSR Fortessa, and data were analyzed using FlowJo.

Antigenic stability analysis

Ex vivo stimulation method: 20 days in advance, mice were primed with $E7_{38-57}$ fusion protein mixed with CDNs, boosted 6 days in advance, and strong peripheral antigen-specific CD8+ T cell responses confirmed on day 0. On day of experiment, spleens from vaccinated animals were excised, mashed through 70 μm filters (Corning), lysed in ACK buffer, pooled, and plated in 96 well V-bottom plates (1 spleen per 30 wells). 24 hours before *ex vivo* stimulation, mouse serum from naïve animals was freshly collected in collection tubes with Z-Gel to remove clotting

factors (Sarstedt) and used to prepare RPMI-1640 + 10% mouse serum media. 4 μM antigen solutions were prepared in RPMI-1640 + 10% mouse serum and incubated at 37°C. After a 24 hour incubation, fresh antigen was similarly prepared at 4 μM in RPMI-1640 + 10% mouse serum and both solutions were immediately diluted 1:4 in RPMI-1640 + 10% FBS to make a 1 μM solution. 6-point 2.5-fold serial dilutions of both fresh and serum-treated antigen solutions were prepared and used to re-stimulate the aforementioned splenocytes from vaccinated animals. IFN-γ^+CD8^+ T cell responses were measured with ICS (see flow cytometry section), normalized to the highest response well per analyte, and the EC_{50} calculated using nonlinear regression on GraphPad Prism, fitting to a log(agonist) vs. response (three parameters) model. *ELISA method*: fresh mouse plasma was prepared by bleeding directly into microcentrifuge tubes and spin removal of cellular matter, maintaining functional complement and clotting factor components. 3 μM FLAG-$E7_{38-57}$-His_6 peptide and MSA-FLAG-$E7_{38-57}$-His_6 were incubated in PBS + 20% mouse plasma for 4 hours at 37°C and immediately quenched by addition of 100X EDTA and 100X protease inhibitor cocktail (Thermo Fisher Scientific). ELISA protocol: MaxiSorp plates (Thermo Fisher Scientific) were coated with anti-FLAG M2 antibody (Sigma) at 10 μg/ml overnight, then blocked with PBS + 2% BSA + 5% non-fat milk + .01% Tween-20. Antigen in quenched reaction solution and freshly prepared antigen at equivalent concentration were diluted 200x in blocking buffer + EDTA + protease inhibitor and incubated on coated ELISA plate for 1.5 hours at room temperature. Detection was performed using an HRP-conjugated polyclonal rabbit anti-His_6 antibody (Abcam) diluted 1:1000 in blocking buffer for 1.5 hours at 4°C and developed using TMB (Thermo Fisher Scientific) and sulfuric acid.

Separate standards for peptide and protein analytes were prepared. Wash buffer consisted of PBS + 0.01% Tween-20, and at least 3x washes were performed between each incubation step.

Biodistribution studies

IVIS imaging: 5-FAM-conjugated peptides (GenScript), FITC-conjugated dextrans of various molecular weights (Sigma), or 5/6-FAM-conjugated proteins, in saline or Montanide ISA 51 VG ST formulation (Seppic) were s.c. injected at the tail base of B6 mice; the inguinal LN was excised 8 hours later and imaged on an IVIS Spectrum Imaging System (Caliper Life Sciences), excitation: 500 nm, emission: 540 nm. In our analysis of Montanide formulation trafficking (Fig 2.6), the injection site of the animal was imaged as well. Images were analyzed on Living Image software. Following protein conjugation, the concentration of labeled protein was calculated using A493. Dosing: In Fig. 2.1f, 2.7 nmol of labeled MSA-$E7_{38-57}$ and up to 27 nmol of $E7_{38-57}$; in Fig. 2.13b, 2.5 nmol of MSA-$E7_{38-57}$ and TTR-$E7_{38-57}$; in Fig. 2.6, 1.2 nmol of labeled MSA-$E7_{38-57}$ and up to 6 nmol of $E7_{38-57}$; in Fig. 2.11d, 0.5 nmol of labeled MSA-$E7_{38-57}$ and DEC1-MSA-$E7_{38-57}$. *Cellular biodistribution:* Alexa Fluor 488-NHS Ester (Thermo Fisher Scientific) was conjugated to recombinantly expressed proteins and injected s.c. at the tail base of B6 mice. Following protein conjugation, the concentration of labeled protein was calculated using A495. The inguinal LN was excised 24 hours later and processed for single cell analysis (see flow cytometry section). Dosing: In Fig. 2.13c, 2.5 nmol of MSA-$E7_{38-57}$ and TTR-$E7_{38-57}$; in Fig. 2.11c, 0.5 nmol of labeled MSA-$E7_{38-57}$ and DEC1-MSA-$E7_{38-57}$.

Detection of anti-MSA and anti-TTR antibodies

Titrating serum on an analyte-coated ELISA plate is an ineffective way to detect antibodies against serum proteins because of the potential for competition between serum in solution and the analyte on the coated plate surface. Instead, we first purified IgG from serum using Pierce protein A spin plates (Thermo Fisher Scientific), per manufacturer instructions, prior to detection in ELISA format. 10 μg/ml MSA (Alpha-Diagnostic International) or TTR (Aviva Systems Biology) were coated on MaxiSorp plates (Thermo Fisher Scientific) overnight, then blocked with PBS + 0.1% bovine IgG (Sigma) + 0.1% Tween-20 for anti-MSA antibody detection or PBS + 5% non-fat milk + 0.1% Tween-20 for anti-TTR antibody detection. IgG eluate from the spin plate was diluted 3x in blocking buffer, then added to the plate for a 1.5 hr incubation at room temperature. Goat anti-mouse HRP detection antibody (Bio-Rad) was used at a 1:5000 dilution in blocking buffer and incubated for 1 hr at 4°C. Controls included IgG isolates from Ova-vaccinated animals on 10 μg/ml Ova-coated wells, and MSA/TTR-coated wells assessed with chicken polyclonal anti-MSA/TTR antibodies (Abcam) and with goat anti-chicken HRP (Abcam) detection, followed by TMB and sulfuric acid development. Wash buffer consisted of PBS + 0.01% Tween-20, and at least 3x washes were performed between each incubation step.

Yeast surface display

Engineered sso7d binders have been previously described[93]. Fibronectin domains were engineered to bind the DEC-205 ectodomain as previously described[115]. Briefly, the two outermost extracellular domains of DEC-205 (the N-terminal cysteine-rich and type II fibronectin domains) were produced from HEK cells and used to select for binders from the G4 library. Four rounds of magnetic enrichment were followed by seven rounds of flow cytometry-

based sorting, with additional diversity introduced via error-prone PCR in between sorting rounds. After sorting and sequencing, 4 individual clones were displayed on yeast as sinle controls and binding to soluble DEC-205 was measured with flow cytometry to calculate the K_d. DEC-1 was measured to have a K_d of 0.66 nM.

Adoptive transfer

$CD8^+$ T cells from pmel $Thy1.1^+$ spleens were isolated using the EasySep mouse CD8+ T Cell Isolation Kit (STEMCELL Technologies). To assess the kinetics of TCR engagement, we retro-orbitally i.v. transferred 500k pmel $Thy1.1^+$ cells into animals that had previously been s.c. vaccinated with 3 μg peptide equivalence MSA-$gp100_{20-39}$ APL or TTR-$gp100_{20-39}$ APL mixed with 25 μg cyclic di-GMP (InvivoGen) 1, 4, or 7 days earlier. 24 hours after transfer, the spleen, inguinal LNs, and mesenteric LNs were excised and $Thy1.1^+$ cells assessed for CD69 expression by flow cytometry (see flow cytometry section). Area under the curve calculations were performed using the trapezoidal method. To assess T cell phenotype in response to tolerization, $CD8^+$ T cells from pmel $Thy1.1^+$ mice isolated as above and labeled with carboxyfluorescein succinimidyl ester (CFSE) (Thermo Fisher Scientific) at a cell density of 10M/ml and a CFSE concentration of 5 μM for 20 min at 37°C in PBS + 0.1% BSA and subsequently quenched by addition of FBS. 1M CFSE-labeled pmel $Thy1.1^+$ cells were retro-orbitally transferred into naïve animals in PBS. 24 hrs later, recipient mice were i.v. vaccinated with 3 μg $gp100_{20-39}$ APL peptide, MSA-$gp100_{20-39}$, or PBS control. 72 hrs post-immunization, the spleen, inguinal LNs, and mesenteric LNs were excised and $Thy1.1^+$ cells assessed by flow cytometry (see flow cytometry section). Proliferation index = $\log_2(FI_{nd}/MFI_{all})$ where MFI_{all} = MFI of live $Thy1.1^+$ pmel

T cells and FI_{nd} = peak fluorescence intensity of viable non-divided Thy1.1$^+$ pmel T cells.

Tumor studies

300k TC-1 or B16F10 cells were subcutaneously administered in 50 μl sterile PBS on the right flank of shaved WT B6 mice. Mice bearing TC-1 tumors were treated on days 5, 12, and 19; mice bearing B16F10 tumors were vaccinated on days 4, 10, and 16, and/or treated with 200 μg anti-PD1 antibody (clone 29F.1A12, BioXCell) on days 4, 7, 10, 13, 16, and 19. Mice were randomized into groups prior to treatment initiation. Tumor size was measured by area (longest dimension x perpendicular dimension), and mice were euthanized when tumor area exceeded 100 mm^2. Memory from $E7_{38-57}$ vaccinated animals was assessed by inoculating 300k TC-1 cells in mice 66 days post-boost and assessing survival as above.

TTR amyloidosis

To determine whether TTR variant fusions formed fibrils, protein was diluted to a concentration of 0.2 mg/ml in either pH 5.5 acetic acid buffer or pH 7.4 PBS in 96 well plate format. Protein solution was incubated for 48 hours at 37°C. The emergence of fibrils was assessed via A330 measurements on a Tecan plate reader.

Statistical analysis

All statistical analyses were performed using GraphPad Prism software. The specifics of the statistical test performed, p-values, and number of replicates are stated in the figure legends. For all tests, the threshold for significance was $P < 0.05$.

2.4 Conclusions

A major factor limiting the potency of peptide vaccines is their poor transport to lymph nodes following injection[43]. This transport limitation has spurred the development of a broad set of delivery platforms to improve antigen delivery to lymph nodes; these strategies have mostly entailed nanoparticulate formulation and/or chemical modification of synthetically produced peptide vaccines[43,82,83,116–118] Here, we altered peptide biodistributions by fusing these antigens to protein-based delivery vehicles to develop a fully recombinant protein solution. We show that protein-epitope fusions are strong candidate vehicles for off-the-shelf vaccination against targets like viral antigens, tumor-associated antigens, oncofetal antigens, and shared neoantigens.

Analysis of the biodistribution behavior of several protein carrier-epitope fusion vaccines revealed principles for optimizing vaccine immunogenicity via pharmacokinetic tuning. We found that maximizing bioavailability in the dLN but reducing uptake in distal lymphoid organs ensures that antigen is presented at the right site at the right time. Two rate constants controlling local lymphatic vs. systemic distribution, k_{abs} and k_{clear}, predictably influenced antigen biodistribution, and thus had a dominant effect on vaccine immunogenicity. In particular, appropriately bulky protein carriers reduced k_{abs} sufficiently to reduce systemic absorption following subcutaneous injection, improving lymphatic uptake and subsequent accumulation in the dLN.

While dLN bioavailability is a prerequisite to potent vaccination, increasing k_{clear} can improve immunogenicity even further by limiting antigen accumulation in distal lymphoid organs that have not received adjuvant stimulation. Adjuvants are typically designed to avoid systemic dissemination, preventing unacceptable toxicities[42,43,119], and inflaming only the local draining lymph nodes as observed here with cyclic dinucleotides. Antigens with low k_{clear}, however, will systemically distribute into non-inflamed distal lymphoid organs, leading to dysfunctional priming of T cells at these sites. This principle is supported by the hierarchy of immunogenicity we observed with TTR, MSA, and Fc fusions. Recognition of this phenomenon has practical implications in vaccine engineering. For example, the observation of priming in distal nodes was noted in early antibody-mediated DEC-205 targeted immunization studies, necessitating the co-administration of systemic adjuvant, which would likely be too toxic for clinical translation[84]. Simply matching the pharmacokinetics of antigen and adjuvant such that they similarly distribute *in vivo* may be a facile alternative to manufacturing antigen/adjuvant conjugates or co-encapsulations. The use of appropriately persistent protein-antigen fusions to treat autoimmunity should also be further explored.

2.5 Acknowledgments

Roma V. Pradhan, my UROP, was incredibly helpful at cloning and producing many of the constructs. Kelly D. Moynihan was instrumental in helping me get situated with *in vivo* experiments at the start of this project. Ava P. Soleimany, from Sangeeta N. Bhatia's lab, was heavily involved in the finding that protein carriers with low k_{clear} rates induced tolerance in distal lymphoid organs.

CHAPTER 3. PROTEIN CARRIERS IN GENETICALLY ENCODED VACCINES

Abstract

While patient-specific cancer vaccine strategies have recently become a clinical reality, the processes required from biopsy to vaccine administration remain cumbersome, slow, and expensive. Genetically encoded vaccine modalities, including DNA and RNA vaccines, represent potentially quicker, cheaper, and more reliable alternatives to traditional peptide or protein vaccines. Here, we adapt our protein-fusion strategy as a transgene in either plasmid DNA or self-replicating RNA vaccines. We find that vaccines that encode albumin-epitope fusions outperform vaccines encoding epitopes alone by over 15-fold for both DNA and RNA. We identify antigen expression as a critical process in the vaccine response, and observe that albumin fusion significantly enhances this key early step. Unexpectedly, however, we find that albumin fusion fails to enhance efficacy in the case of multi-antigen vaccination.

3.1 Introduction

While recent efforts to vaccinate against patient-specific neoantigens have yielded promising results[120], there remain a number of challenges to overcome. Of important consideration is manufacturing time and cost of goods. Current approaches to develop personalized peptide vaccines have not only been costly but also quite slow, with a median time of 18 weeks from surgery to vaccine administration. One shortcoming of peptide vaccines is their batch-to-batch variability, leading some promising antigens to drop out of clinical

development because of their inability to be produced and/or purified at scale. If peptide antigens could instead be expressed using nucleic acid vectors, such as plasmid DNA or self-replicating RNA, then the final drug product could have biophysical properties virtually identical from patient to patient, allowing for scalability and a reduction in manufacturing time.

As described here, self-replicating RNA vaccines, or replicons, consist of viral RNA genomes with structural proteins removed replaced with transcripts of interest. The natural self-replicating machinery of the RNA genome allows for intracellular transcriptional amplification, enhancing the vaccine response. RNA replicons are typically packaged in nanoparticles to preserve their stability and promote transfection in vivo[113]. Plasmid DNA, on the other hand, does not require particulate delivery but must be transfected into muscle cells via gene gun or electroporation[121,122]. Local tissue damage in the case of DNA and inherent TLR3 agonism in the case of RNA[123] obviates the need for additional adjuvants.

While vaccinologists have long been interested in DNA and RNA vaccines, mechanistic detail remains relatively sparse. Although both intramuscularly administered plasmid DNA and replicon RNA vaccines robustly transfect myocytes, APCs ultimately prime T cells, suggesting mechanisms of antigen transfer that have thus far been poorly defined[124–126]. Given our finding that subcutaneously administered protein-antigen fusions readily convect into the local lymphatics (see chapter two), we believed that antigens secreted from transfected myocytes would similarly access the draining lymph nodes and potentiate vaccine responses given the appropriate protein carrier. Unlike other particulate- or conjugate-based delivery strategies, the protein-fusion approach is amenable to DNA and RNA applications due to its

genetically-encodable nature. Most clinically and preclinically promising DNA vaccines to date have primarily expressed whole protein antigens, rather than expressing the peptide epitopes most relevant to immuno-oncology[127,128]. We hypothesized that the use of encoded inert protein carriers would allow us to coopt the advantages of whole protein transgenes to instead direct immunity against defined epitopes.

In this study, we fuse peptide antigens onto the C-terminal end of mouse serum albumin (MSA), and express the whole construct with either plasmid DNA or RNA replicons. In both cases, intramuscular transfection of constructs encoding MSA-epitope fusions, but not constructs encoding epitope alone, led to robust antigen-specific CD8+ T cell responses. We find that antigen expression is significantly enhanced when MSA is used as a protein carrier, and that secretion of antigen is critical to the immune response, supporting our hypothesis that secretion and subsequent drainage may be an effective means of antigen handoff from myocytes to APCs. Additionally, because the same MSA-antigen fusion strategy is amenable to DNA, replicon, and protein vaccines, we explore the use of heterologous prime/boost strategies and find DNA vaccine prime followed by protein vaccine boost to be most efficacious. Overall, we have identified the MSA-fusion strategy as an enabling technology that allows for the expansion of vaccination modalities available for cancer immunotherapy.

3.2 Results and Discussion

Plasmid vaccines encoding albumin-antigen fusions prime functional therapeutic CD8+ T cell responses

As described in Chapter 2, we found that recombinant albumin-antigen fusions could potentiate the immunogenicity of the antigenic payload via protection from proteolytic degradation and by enhancement of lymphatic uptake. Here, we demonstrate the versatility of this approach by introducing nucleic acid vaccines that encode for the recombinant protein vaccine, enabling the simultaneous production of carrier (albumin) and payload (antigen) *in situ*, a strategy that is not possible with particulate/conjugate delivery strategies.

We first developed plasmid DNA vaccines that encoded for human papillomavirus (HPV) $E7_{38-57}$ as a model antigen. $E7_{38-57}$ contains the H-$2D^b$-restricted CD8+ T cell epitope[87] $E7_{49-57}$ that can be detected by commercially available H-$2D^b$/$E7_{49-57}$ tetramers. To assess the role of albumin as a fusion partner, a second plasmid was prepared that encoded for mouse serum albumin (MSA) fused to $E7_{38-57}$ via a GGGS linker. For both plasmids, mouse codon-optimized genetic sequences encoding for the desired transgene were cloned downstream of an IgE leader peptide to promote secretion, under control of a CMV promoter and Kozak sequence to enhance expression.

To test the immunogenicity of pVax1 MSA-$E7_{38-57}$ relative to pVax1 $E7_{38-57}$, mice were primed and boosted with 25 μg pVax1 $E7_{38-57}$ or equimolar doses of pVax1 MSA-$E7_{38-57}$ by

intramuscular (IM) injection followed by electroporation. Post-boost, inclusion of MSA fusion enhanced $E7_{49-57}$-specific responses 17-fold relative to the $E7_{38-57}$-only transgene as measured by tetramer stain (**Fig. 3.1a,b**). We next assessed whether the enhanced immunogenicity of pVax1 MSA-$E7_{38-57}$ vaccines similarly demonstrated enhanced efficacy in the treatment of established tumors. Mice bearing TC-1 tumors, which are E7+, were treated weekly with equimolar doses of pVax1 $E7_{38-57}$ or pVax1 MSA-$E7_{38-57}$. Mice treated with pVax1 MSA-$E7_{38-57}$ delayed tumor outgrowth, while mice treated with pVax1 $E7_{38-57}$ experienced no significant delay. (**Fig. 3.1c,d**).

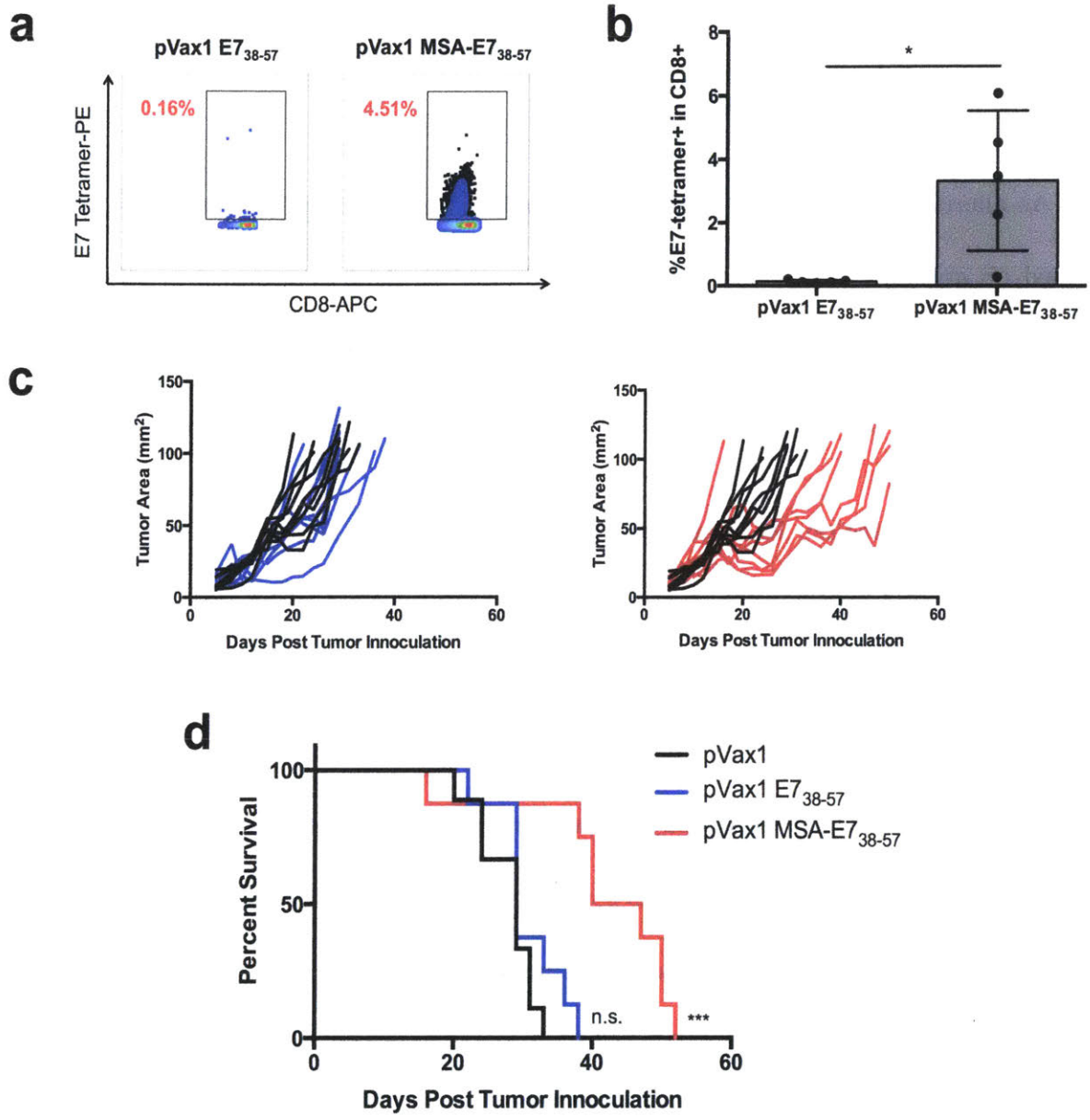

Figure 3.1. Plasmid DNA vaccines encoding MSA-E7$_{38-57}$

(**a-b**) Mice were primed and boosted with intramuscular transfection of 25 μg pVax1 E7$_{38-57}$ or 40 μg pVax1 MSA-E7$_{38-57}$. Following boost, the frequency of E7-specific CD8+ T cells in the blood were measured via tetramer stain (**a**) and quantification (**b**) (n = 4, and data are representative of three independent experiments). (**c-d**) Mice were inoculated with 300k TC-1 tumor cells; on day 6, mice were vaccinated weekly for three doses with the indicated plasmid vaccines. Shown are tumor growth curves (**c**) and survival curves (**d**). * $P < 0.05$; *** $P < 0.001$ by two-tailed t test (**b**) or by log-rank (Mantel-Cox) test versus pVax1 (**c**).

Self-replicating RNA vaccines encoding albumin-antigen fusions prime functional therapeutic CD8+ T cell responses

An alternative nucleic acid vaccine platform is self-replicating RNA, or "replicons" that are based on an alphaviral genome that are made non-virulent by removal of all structural proteins and with insertion of the desired vaccine cargo. Plasmids encoding the replicon structure with $E7_{38-57}$ or MSA-$E7_{38-57}$ were cloned, and RNA produced by in vitro transcription.

In a similar fashion, RNA replicon transcripts encoding MSA-$E7_{38-57}$ and $E7_{38-57}$ were developed, packaged into liposomal nanoparticles (LNPs), and injected IM into mice. After prime alone, inclusion of MSA fusion enhanced $E7_{49-57}$-specific responses 31-fold relative to the $E7_{38-57}$ only replicon (**Fig. 3.2a,b**). Similar to the DNA vaccine setting, replicon-encoded MSA-$E7_{38-57}$ vaccinations allowed mice to delay the outgrowth of established TC-1 tumors, but did not lead to any cures; replicons encoding $E7_{38-57}$, however, did not induce any delay in tumor growth (**Fig. 3.2c,d**). Thus, we conclude that albumin-fusion is an enabling platform that can improve cellular responses for both DNA and RNA-based vaccines.

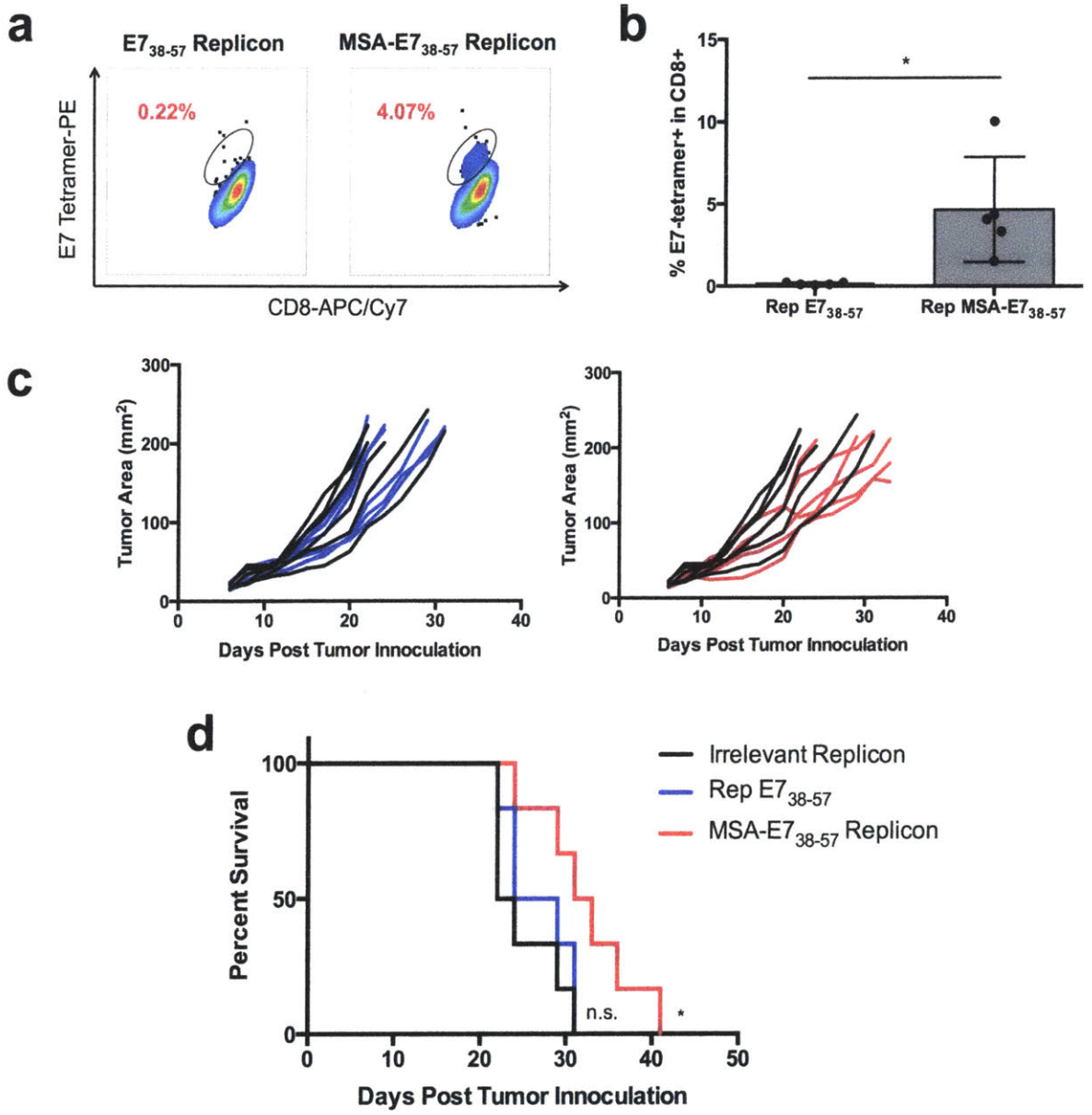

Figure 3.2. Replicon RNA vaccines encoding MSA-E7$_{38-57}$

(**a-b**) Mice were primed with intramuscular transfection of 1 µg replicons encoding E7$_{38-57}$ and MSA-E7$_{38-57}$. Two weeks following vaccination, the frequency of E7-specific CD8+ T cells in the blood were measured via tetramer stain (**a**) and quantification (**b**) (n = 5). (**c-d**) Mice were inoculated with 300k TC-1 tumor cells; on day 6, mice were vaccinated weekly for three doses with the indicated plasmid vaccines. Shown are tumor growth curves (**c**) and survival curves (**d**). * $P < 0.05$ by two-tailed t test (**b**) or by log-rank (Mantel-Cox) test versus irrelevant replicon (**c**).

Albumin fusion enhances antigen expression

We next sought to explore the mechanisms by which MSA fusion potentiates the immunogenicity of DNA and RNA vaccines. Our previous work with MSA-antigen fusion proteins injected subcutaneously demonstrated that MSA-antigen fusions are better protected from proteolytic degradation and better access the lymphatics relative to naked peptide antigens. We reasoned that some of the same mechanisms are likely at play for nucleic acid vaccines following secretion from myocytes into the interstitium, improving bioavailability in local lymph nodes where immune responses are orchestrated.

A pre-requisite for lymphatic uptake, however, is antigen expression, a process that we also find to be boosted by MSA-fusion. As measured by secretion of antigen into the supernatant following *in vitro* transfection, MSA-fusion enhanced expression of both plasmid DNA (**Fig. 3.3a**) and replicon RNA (**Fig. 3.3b**) by 300-fold and 65-fold, respectively. To confirm the importance of antigen secretion, we removed the leader sequence of pVax1 MSA-E7$_{38-57}$ and found that vaccine responses were reduced by 75% (**Fig. 3.3c**).

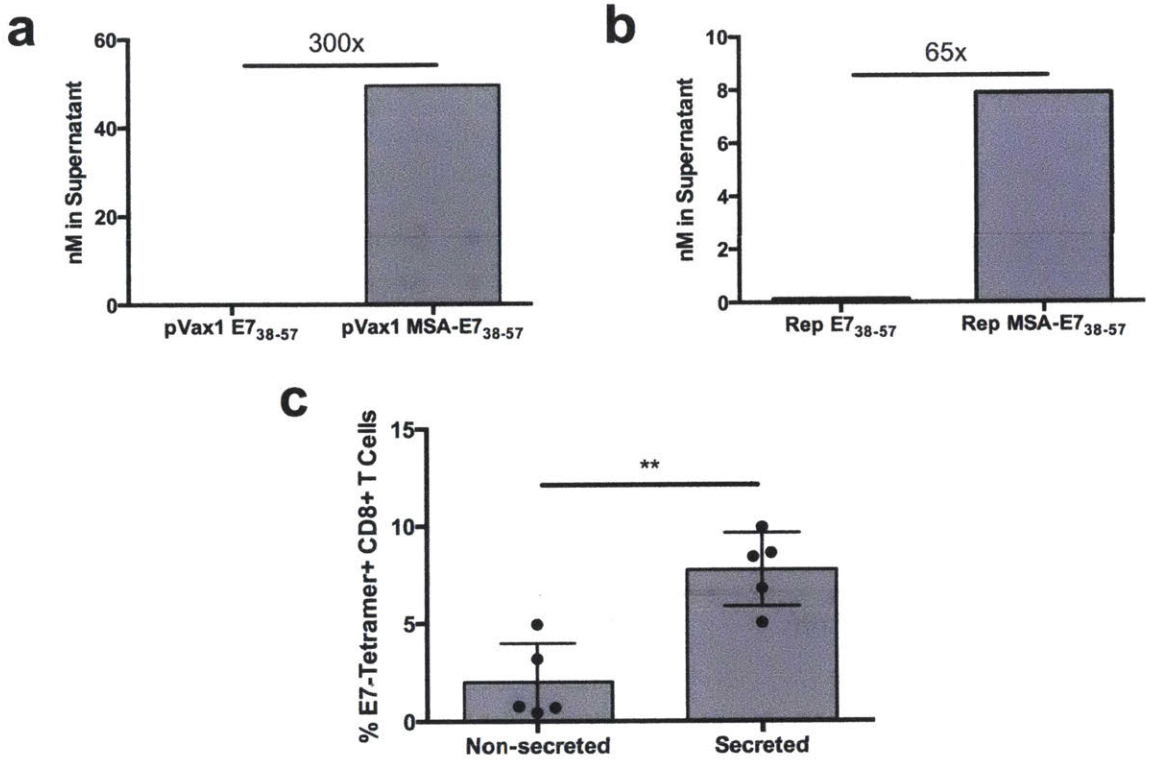

Figure 3.3. MSA fusions have enhanced immunogenicity in part due to improved expression

(**a**) Six days following transfection of HEK cells with the indicated plasmid, supernatant was harvested and assessed for expression by His_6 competition ELISA. (**b**) One day following transfection of BHK-21 cells with the indicated replicon, supernatant was harvested and assessed for expression by His_6 competition ELISA. (**c**) Mice were intramuscular primed and boosted as earlier with pVax1 MSA-E7$_{38-57}$ including leader sequence (secreted) or without (non-secreted). ** $P < 0.01$ by two-tailed t test (**c**).

In a clinical setting, however, vaccines are typically designed to target multiple antigens simultaneously, not just single copies of single antigens, as is the case with pVax1 MSA-E7$_{38-57}$. To assess whether MSA fusions could also enhance the immunogenicity of constructs that encode several antigens, we cloned strings of epitopes (Trp1-gp100-Mut25-Mut30-CEA) with or without a leader sequence to enable secretion, and with or without MSA fusion in the transgene. Unexpectedly, we found that the consistently best performing strategy after prime and boost was without MSA and without secretion, suggesting that different design criteria apply when strings of epitopes are expressed (**Fig. 3.4**). We conclude that the use of albumin-

fusions to enhance the potency of nucleic acid vaccines may only be applicable in a narrow set of circumstances, such as single antigen vaccines.

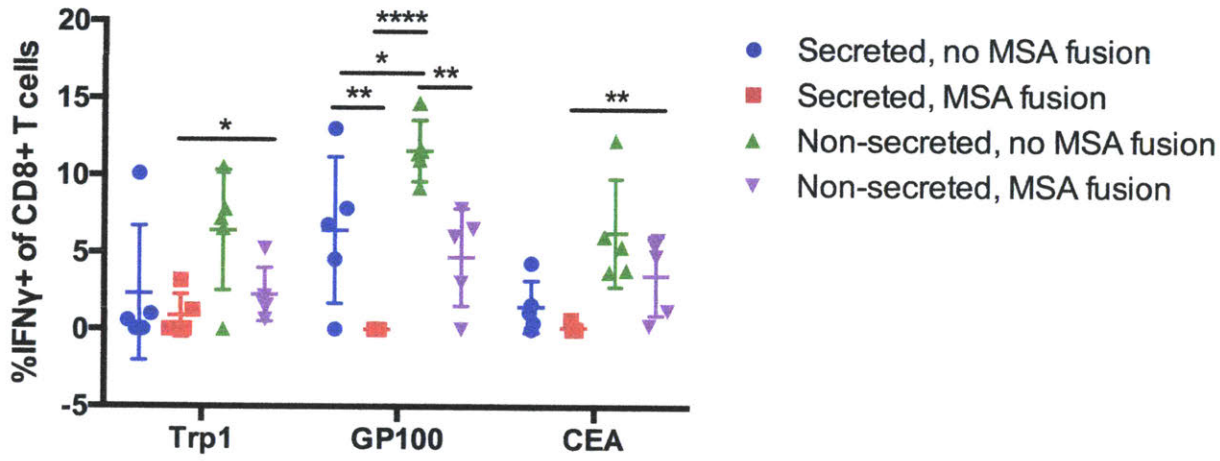

Figure 3.4. MSA fusion fails to enhance immunogenicity of strings of epitopes

Mice were primed and boosted with intramuscular transfection of 1 μg replicons encoding Trp1-gp100-Mut25-Mut30-CEA with or without the indicated elements (leader sequence to induce secretion or MSA fusion). Following boost, ICS was performed against all relevant antigens to assess magnitude of response. * $P < 0.05$; ** $P < 0.01$; ** $P < 0.0001$ by two-way ANOVA and Tukey's multiple comparisons test.

Albumin fusion enables heterologous prime-boost approaches

The versatility of MSA-fusion with regard to modality led us to assess heterologous prime/boost strategies via exploration of all nine combinations of DNA/RNA/protein MSA-fusion prime and boost schedules (**Fig. 3.5**). Post-prime, we observed a rank order of DNA > RNA > protein in terms of magnitude of $E7_{49-57}$-specific CD8+ T cell responses (8.3%, 2.3%, and 0.7%, respectively). However, despite being the least immunogenic modality post-prime, protein vaccination was the most potent post-boost. Therefore, nucleic acid-based MSA-fusions appear most optimally suited for prime, while protein-based MSA-fusions may be ideal boosting agents.

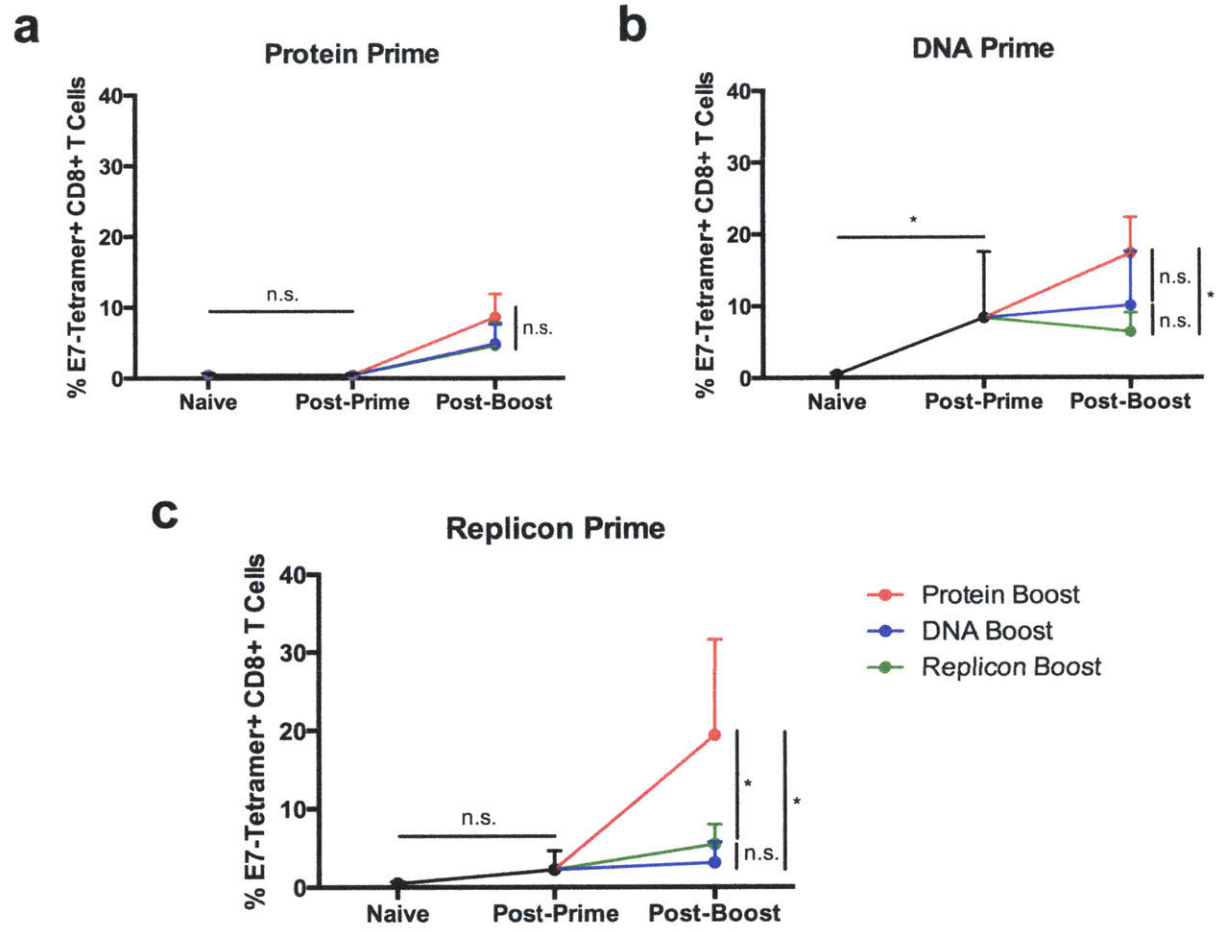

Figure 3.5. Heterologous prime/boost vaccination

(**a-c**) Mice were primed on day 0 and boosted on day 28 with the indicated form of MSA-E7$_{38-57}$. Six days following prime or boost, the frequency of E7-specific CD8+ T cells were assessed by tetramer stain. Shown are representative response trajectories under different heterologous and homologous prime/boost strategies. * $P < 0.05$ by one-way ANOVA with Tukey's multiple comparisons test.

3.3 Materials and Methods

Mice

B6 mice (C57BL/6NTac) were purchased from Taconic. All animal work was conducted under the approval of the Massachusetts Institute of Technology (MIT) Division of Comparative Medicine in accordance with federal, state, and local guidelines.

Cells

TC-1 cells were kindly provided by T.C. Wu (Johns Hopkins University). HEK cells (FreeStyle 293-F) were purchased from Thermo Fisher Scientific. BHK-21 cells were kindly provided by Ron Weiss. HEK cells were cultured in FreeStyle 293 Expression Medium (Thermo Fisher Scientific) and passaged every two days to a density of 300k/ml. TC-1 cells were cultured in RPMI-1640 (GE Healthcare Life Sciences) supplemented with 10% FBS, 100 units/ml penicillin, 100 μg/ml streptomycin, and 4 mM L-alanyl-L-glutamine. BHK-21 cells were cultured in EMEM (ATCC) supplemented with 10% Tetracycline Screened HyClone FBS (GE Healthcare Life Sciences). All cells were cultured at 37°C and 5% CO_2. TC-1s were tested regularly for mycoplasma contamination and for rodent pathogens, and none used tested positive at any point.

Transfections

HEK cell transfection: Endotoxin-free plasmid was incubated with Opti-Pro (Thermo Fisher Scientific) and polyethylenimine (PEI) 25K (Polysciences) prior to drop-wise addition to HEK cell culture at 1 million cells/ml. 1 mg of DNA was mixed with 40 ml of Opti-Pro and 2 mg of PEI per 1 L of cell culture. One week after transfection, cell culture was spun down, and supernatant filtered and flash frozen. *BHK-21 cell transfection:* Cells at approximately 70%

confluence were electroporated using the Neon Transfection System (Life Technologies), according to manufacturer's instructions. 1 μg of RNA was transfected per 100,000 BHK-21 cells. Electroporation conditions: 1,100 mV, 40 ms, 1 pulse. 24h after transfection, media was filtered and flash frozen. Following both transfection protocols, antigen expression was determined using a His tag ELISA detection kit (Genscript). *Protein purification*: Codon-optimized genes encoding desired proteins were cloned into gWiz expression vectors (Genlantis) using the In-Fusion HD Cloning Kit (Clontech), prepared endotoxin free (Macherey-Nagel) and incubated with Opti-Pro (Thermo Fisher Scientific) and polyethylenimine (PEI) 25K (Polysciences) prior to drop-wise addition to HEK cell culture at 1 million cells/ml. 1 mg of DNA was mixed with 40 ml of Opti-Pro and 2 mg of PEI per 1 L of cell culture. One week after transfection, cell culture was spun down in endotoxin-free centrifuge tubes at 15000xg for 30 min, supernatant filtered, pH neutralized by addition of 10X PBS, and run through TALON metal affinity resin (Clontech) by gravity flow per manufacturer instructions.

Flow cytometry

Antibodies against CD16/32 (Fc block, clone 93), CD8α (53-6.7), and IFN-γ (XMG1.2) were purchased from BioLegend. Cell viability was assessed with DAPI (Sigma) for tetramer stains and LIVE/DEAD fixable aqua dead cell stain (Thermo Fisher Scientific) for all other studies. *Tetramer staining:* E7 tetramer (iTAg Tetramer/PE - H-2 Db HPV 16 E7) was purchased from MBL; during tetramer staining, PBMCs were Fc blocked and stained with tetramer for 15 minutes prior to addition of anti-CD8α antibody, and cells were incubated with all antibodies for another 30 minutes. All labeling was performed in PBS + 0.1% BSA. *Intracellular cytokine*

staining (ICS): Performed as previously reported[114]. Briefly, PBMCs were re-stimulated in RPMI-1640 + 10% FBS at 37°C with optimal WT peptides mixed at 10 μg/ml each (Trp1, gp100, CEA, Mut25, Mut30) for 2 hrs followed by addition of brefeldin A (Thermo Fisher Scientific) for another 4 hrs prior to staining. In all cases, surface staining was performed first (Fc block, anti-CD8α) in PBS + 0.1% BSA followed by fixation and permeabilization using BD Cytofix/Cytoperm fixation/permeabilization kit per manufacturer instructions and intracellular staining (anti-IFN-γ and/or anti-TNF-α) in perm/wash buffer. Cells were analyzed using BD FACSCanto and BD FACS LSR Fortessa, and data were analyzed using FlowJo.

Vaccinations

Plasmid DNA: Each vaccine was prepared with 100 μl volume: 50 μl was IM injected in both the right and left hind quadriceps. Immediately after each injection, a 5 mm 2-needle array electrode (BTX) connected to an ECM 830 Square Wave Electroporation System (BTX) was inserted flanking the injection site. A connected footswitch (BTX) was used to initiate electroporation; following resolution, the electrode leads were switched and pulsing was resumed for another cycle at reverse polarity, for a total of four cycles per animal. Electroporation protocol: 50 ms pulse, 200 ms gap, 3x100V. Dosing: 40 μg pVax1 encoding MSA fusion and 25 μg pVax1 encoding peptide only to deliver equimolar dosing.

Replicon RNA:

Preparing template DNA[129]: The gene of interest was PCR amplified to include SapI sites; next, a Modular Cloning (MoClo) reaction was initiated that contained 100 ng pTW072M (containing

non-structural proteins), 25 ng pTW614 (containing the wild-type 26S subgenomic promoter), 25 ng pEP433 (containing the 3′ untranslated region), 50 ng PCR product, along with T4 DNA ligase, ligase buffer, and SapI. Reaction was incubated for 37°C for 1 hr, 50°C for 5 min, and 80°C for 5 min prior to transformation and plating on ampicillin plates. DNA was prepared from expanded single colonies.

Preparing RNA[129]: Replicon plasmids constructed using the MoClo assembly strategy were linearized using I-SceI (NEB) and PCR purified (Macherey-Nagel) before in vitro transcription (IVT). IVTs were performed using either the mMESSAGE mMachine T7 Kit (Life Technologies) or the MEGAscript T7 Transcription Kit (Life Technologies) at 37 °C for 4 h. The resulting RNA was DNase treated and purified using either the RNeasy Mini Kit (Qiagen) or lithium chloride precipitation. For lithium chloride precipitation, ½ volume of ice-cold LiCl solution (7.5 M LiCl, 50 mM EDTA) was added to the IVT RNA and incubated at −20°C for 30 min. After incubation, the mixture was centrifuged at max speed (~18,000 *g*) for 20 min at 4°C. The supernatant was discarded and the resulting pellet was washed with 10× volume of ice-cold 70% EtOH and centrifuged for 1–3 min at max speed. This step was repeated two more times. After the final wash, the supernatant was discarded and the pellet was air dried for approximately 5 min before it was resuspended in water. When the MEGAscript T7 Transcription Kit was used for IVT, purification was followed by denaturation of the RNA at 65 °C and enzymatic (Cap1) capping of the RNA using the ScriptCap 2′-*O*-methyltransferase Kit (Cellscript) and ScriptCap m7G Capping System (Cellscript) for 30–60 min at 37 °C. A second purification using either the RNeasy Mini Kit (Qiagen) or lithium chloride precipitation was then performed.

Packaging RNA: Replicon RNA was packaged into LNPs of the following composition: 40% DOTAP : 10% DSPC : 48% Cholesterol : 2% DSPE-PEG with a DOTAP:RNA ratio of 8. Briefly, lipid content dissolved in ethanol was mixed in one tube; RNA was diluted into citrate buffer of equal volume in a second tube; RNA solution was added to lipid solution, and rapid mixing induced the formation of encapsulated liposomes. Following encapsulation, particles were buffer exchanged into PBS using Slide-A-Lyzer MINI Dialysis Device, 20K MWCO (Thermo Fisher Scientific) for 1 hour. An aliquot was lysed with 0.5% Triton-X, and RNA content measured using Quant-iT RiboGreen RNA Assay Kit (Thermo Fisher Scientific) to determine dosing.

Vaccination: 1 μg of encapsulated RNA was IM injected per mouse, split between each hind gastrocnemius muscle. Tetramer stain performed two weeks after vaccination.

Note: Neither DNA nor replicon RNA were filter sterilized, but were instead presumed to be sterile following ethanol precipitation.

Protein: 100 μg MSA-$E7_{38-57}$ was mixed with 25 μg cyclic di-GMP (InvivoGen) and injected subcutaneously in 100 μl at the tail base, 50 μl on each side.

Heterologous prime/boost: Dosing and methodology performed as above. Mice were primed on day 0, post-prime T cell responses read out on day 6 via tetramer stain, boosted on day 28, and post-boost T cell responses read out again on day 34.

Tumor Studies

300k TC-1 or B16F10 cells were subcutaneously administered in 50 μl sterile PBS on the right flank of shaved WT B6 mice. Mice bearing TC-1 tumors were treated on days 5, 12, and 19. Mice were randomized into groups prior to treatment initiation. Tumor size was measured by area (longest dimension x perpendicular dimension), and mice were euthanized when tumor area exceeded 100 mm^2 (plasmid DNA study) or 200 mm^2 (replicon RNA study).

Statistical analysis

All statistical analyses were performed using GraphPad Prism software. The specifics of the statistical test performed, p-values, and number of replicates are stated in the figure legends. For all tests, the threshold for significance was $P < 0.05$.

3.4 Conclusions

A potentially exciting way to administer vaccines to patients in a cheap, fast, and scalable manner is by the delivery of nucleic acid vaccines. While these vaccines have shown promise in eliciting humoral immunity against infectious disease, their ability to induce T cell responses against specific epitopes has not been optimized. Here, we utilize our albumin-epitope fusion approach from Chapter 2, but instead of injecting the protein product as a subunit vaccine, we encode the construct in plasmid DNA or replicon RNA and vaccinate via *in vivo* transfection. We find that encoding albumin-antigen fusions in either plasmid DNA or replicon RNA vaccine systems is a viable strategy to improve T cell responses in the case of single epitope, but not multi-epitope, vaccination. The reason why albumin fusions fail to enhance multi-epitope vaccines remains unclear. In the single-epitope context, however, we

find that albumin fusion imparts its potency benefit due to the significant enhancement of antigen expression, as measured *in vitro*. Although albumin-fused transgenes in DNA and RNA vaccines can generate T cell responses after a single vaccination, they are poor boosting agents. Protein vaccines co-administered with adjuvant can more appropriately boost responses following prime, suggesting that a heterologous scheduling strategy with DNA prime and protein boost is optimal.

3.5 Acknowledgements

Roma V. Pradhan, my UROP, was incredibly helpful at cloning and producing many of the constructs, particularly with regard to plasmid DNA vaccines, and conducted the plasmid DNA associated tumor study. Wuhbet Abraham, Kelly D. Moynihan, Adrienne M. Rothschilds, and Noor Momin were all helpful at helping me optimize the *in vivo* electroporation protocol necessary to obtain satisfactory DNA vaccine responses. Brian Dobosh, Jacob R. Becraft, and Bremy Alburquerque from Ron Weiss' lab, were all very generous with their time in making replicons for me as needed. Mariane B. Melo, Na Li, and Yuan Zhang were all instrumental in helping me learn how to package replicon RNA in liposomal nanoparticles.

CHAPTER 4. ALBUMIN-ANTIGEN FUSIONS AS TOLERIZING VACCINES

Abstract

Persistent antigen presentation in the absence of co-stimulation can induce tolerization, characterized by exhaustion, anergy, and apoptosis of antigen-specific T cells. In this work, we fused peptide antigens to serum albumin to prolong circulatory half-life and impart tolerization against subsequent antigenic challenge. We find that responses to vaccination can be decreased over 20-fold if mice are first administered albumin-fused tolerizing vaccines. Additionally, we used the albumin-fusion vaccine system as a tool to explore the mechanism of action of tolerizing vaccines. We describe the dominant role played by peripheral lymph nodes, despite intravenous vaccine administration; we observe more persistent antigen presentation and the induction of Foxp3 in the nodes relative to the spleen. Additionally, by comparing albumin-fusion tolerizing vaccines against alternative carrier proteins with distinct half-lives, we identify a threshold persistence requirement, whereby vaccines must have a half life >24h to induce maximal tolerization. Finally, we show that prophylactic administration of albumin fused to myelin oligodendrocyte glycoprotein peptide can prevent the induction of experimental autoimmune encephalomyelitis.

4.1 Introduction

Autoimmune disorders occur when a patient's immune system recognizes a self-antigen as foreign, thereby initiating a toxic response against healthy tissue. Because these diseases are

chronic in nature, they have a staggering cost on the healthcare system. It is estimated that 50 million Americans suffer from autoimmune related diseases, leading to annual costs of $100 billion annually[50]. Some of the most common autoimmune disorders include rheumatoid arthritis (RA), characterized by the inflammatory degradation of cartilage, which has 1.3 million patients; multiple sclerosis (MS), in which the immune system attacks the myelin sheath, which has 400 thousand patients; and type 1 diabetes, whose disease etiology consists of autoimmune destruction of pancreatic beta cells, and which has 1.25 million patients.

While vaccines have traditionally been designed to activate immune responses against pathogens or cancer, there is an emerging field of tolerizing vaccine engineering to address autoimmune disorders in an antigen-specific manner. Tolerizing vaccines take advantage of the observation that antigen persistence in the absence of inflammatory cues can lead to exhaustion, dysfunction, anergy, and apoptosis among T cells in a variety of settings including chronic inflammation[130], adoptive transfer studies[97,98], and long-lived vaccination[88,96]. Current approaches to engineer tolerizing vaccines in preclinical development include particulate delivery of antigen[69], red blood cell associated antigen infusion[66–68], and the use of pMHC-conjugated particles to trigger T cell receptor priming in the absence of co-stimulation[71,131].

This work builds upon the conclusions of chapter two, where we found that persistent and systemic albumin-antigen fusions detracted from overall immune responses due to apparent access to poorly inflamed distal lymph nodes following subcutaneous injection. Here, we transform this observation into an advantage in the engineering of tolerizing vaccines: we purposefully introduce albumin-antigen fusions intravenously in the absence of adjuvant to

promote tolerization. We find that in spite of intravenous administration, the peripheral lymph nodes play a major role in antigen presentation and the induction of tolerance, and we use various protein carriers with defined pharmacokinetic properties to identify a 24 hour systemic half-life threshold beyond which the efficacy of tolerization is maximized. Finally, we apply the albumin-antigen fusion approach to a murine model of experimental autoimmune encephalomyelitis.

4.2 Results and Discussion

Intravenous administration of albumin-antigen fusions tolerizes against subsequent challenge

When co-administered with adjuvant subcutaneously (s.c.), albumin-antigen fusions prime high magnitude and functional T-cell responses. However, albumin's long half-life, and the known understanding that persistent antigen can induce tolerance[88,98], led us to suspect that if appropriately delivered in the absence of inflammatory cues albumin-antigen fusions could instead be tolerizing instead of activating for a potential application in the treatment of T-cell mediated autoimmune disorders.

As a preliminary read-out for tolerization, we first asked whether an initial tolerizing vaccine could reduce the magnitude of a subsequent challenge vaccination against the same antigen. To maximally deliver albumin-antigen fusions to secondary lymphoid organs in the absence of inflammation, we administered the vaccine intravenously (i.v.) without adjuvant.

Two weeks later, mice were primed and boosted subcutaneously against the same antigen. In an effort to keep the tolerizing vaccine and activating vaccine as orthogonal as possible, different protein carriers were used for tolerization and activation. CD8+ T cells in peripheral blood were analyzed six days after boost by either pMHC tetramer or intracellular cytokine staining following *ex vivo* antigen restimulation to assess the frequency of antigen-specific cells (**Fig. 4.1a**).

MSA-antigen fusions were compared against direct i.v. administration of unformulated peptide, the current gold standard in tolerizing vaccines. We tested three different antigens: HPV-associated $E7_{38-57}$, vitiligo-associated $gp100_{20-39}$, and a long peptide form of OTI derived from Ova protein as a model antigen. In all three cases, MSA-antigen fusions were able to induce tolerance relative to control mice that only received i.v. PBS (**Fig. 4.1b-d**). The frequency of antigen-specific CD8+ T cells was reduced by 97% for $E7_{38-57}$ (**Fig. 4.1b**), 86% for $gp100_{20-39}$ (**Fig. 4.1c**), and 75% for OTI (**Fig. 4.1d**). Unexpectedly, there was notable variability in the efficacy of peptide tolerizing vaccine from antigen to antigen; while no peptide tolerization regimen induced statistically significant reduction in T cell response relative to PBS control, $E7_{38-57}$ and $gp100_{20-39}$ did appear to induce some degree of tolerance (albeit to a lesser extent than their MSA-fusion counterparts) (**Fig. 4.1b-c**), while OTI peptide was less effective (**Fig. 4.1d**).

An ideal tolerizing vaccine would not be chronically administered, but would instead impart long-term tolerance, obviating the need for high frequency dosing. To test whether MSA-$E7_{38-57}$ could impart tolerance beyond the two weeks assessed above, we waited up to over 200 days after administration of tolerizing vaccine before beginning challenge, and found that

the frequency of E7-specific CD8+ T cells was similarly reduced at all time points (by >80%) (**Fig. 4.1e**). These data suggest that there is an induced "memory" of tolerance that is sustained long after the initial tolerizing vaccine has cleared.

To ensure that tolerance was induced not just in terms of frequency of CD8+ T cells but also in terms of functionality, we next asked whether tolerizing against E7 would quicken the growth rate of TC-1 tumor cells, which are E7+. Indeed, we found that i.v. administration of MSA-$E7_{38-57}$ in the absence of adjuvant two weeks prior to TC-1 tumor inoculation resulted in mice with larger tumors relative to PBS- or E7 peptide-treated animals starting on day 16 post tumor inoculation (**Fig. 4.1f**). Consistent with the presumed mechanism of action, the initial tumor growth phase from days 0-13 were unaffected, as these are time points that are expected to be prior to the induction of an adaptive immune response.

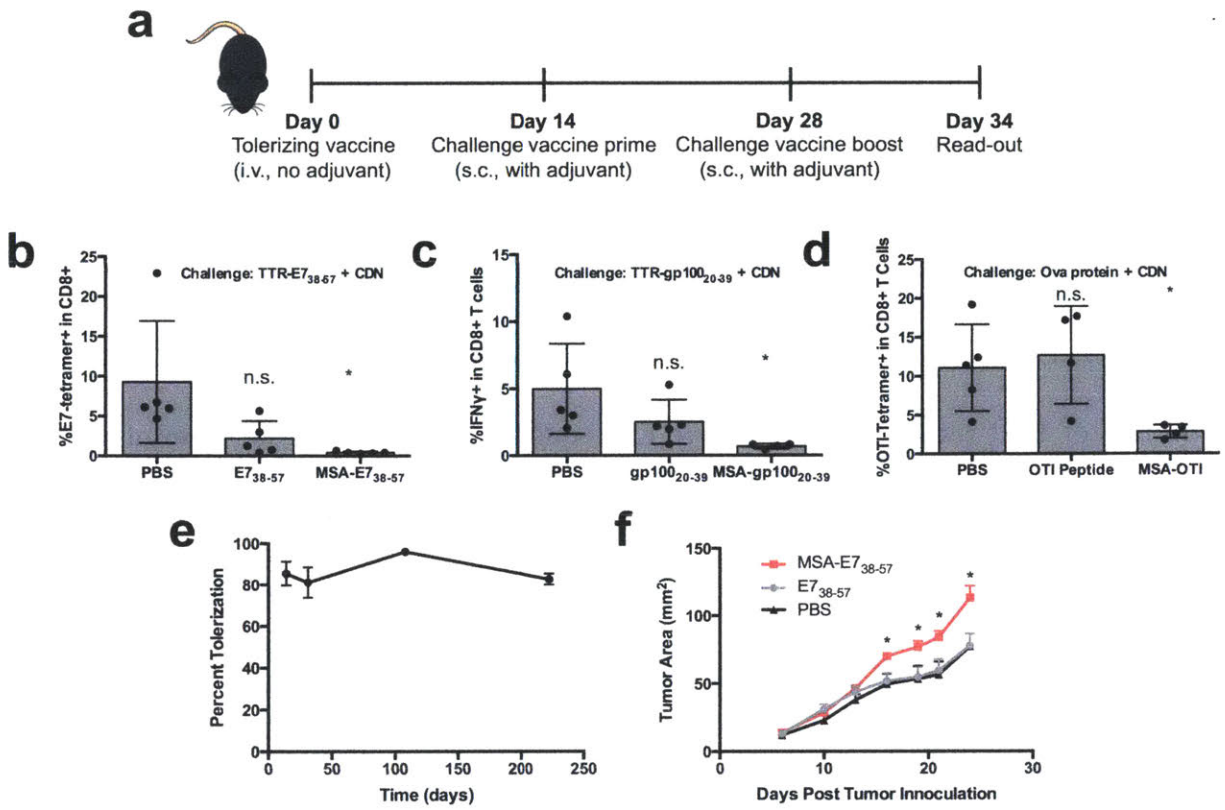

Figure 4.1. Intravenous administration of albumin-antigen fusions tolerizes against subsequent challenge

(**a**) Schematic of typical experiment used to measure tolerance against subsequent challenge. 3 μg peptide equivalence tolerizing vaccine was administered intravenously; two weeks later, mice were primed and boosted with the indicated subcutaneous vaccine, and the magnitude of the CD8+ T cell response was assessed by tetramer staining or intracellular cytokine staining. (**b-d**) Tolerization studies with three different antigens: $E7_{38-57}$ (**b**), $gp100_{20-39}$ (**c**), and OTI peptide (**d**) (n = 5 mice/group in all cases). The specific challenge regimen is indicated. Data are representative of at least two independent studies. (**e**) Mice were tolerized with MSA-$E7_{38-57}$ i.v. and prime/boost challenged s.c. with TTR-$E7_{38-57}$ and CDN the indicated number of days later. Percent tolerization was calculated as the percent reduction in tetramer+ frequency relative to PBS control. (**f**) Mice were tolerized with MSA-$E7_{38-57}$ and two weeks later inoculated with TC-1 tumors. Throughout, * $P < 0.05$ by one-way ANOVA with Dunnett's multiple comparisons test against PBS (**b-d**) or one-tailed t tests at each indicated time point against PBS (**f**).

T cells are tolerized in the spleen and lymph nodes

Having confirmed that MSA-antigen fusions effectively induced tolerance against subsequent challenge, we next explored their mechanism of action. We first sought to understand in which organs antigen-specific CD8+ T cells were being primed. A first pass

approach to answering this question is to elucidate the biodistribution of MSA-antigen fusions to generate a shortlist of possible sites of T cell priming. When injected i.v., we found that Alexa Fluor 647 labeled MSA-gp100$_{20-39}$ did distribute to canonical lymphoid organs like the inguinal lymph node (LN) and the spleen, but that very bright signal was detectable in both the liver and the lungs (**Fig. 4.2a**).

The efficient biodistribution of MSA-gp100$_{20-39}$ to the liver was particularly exciting because of a robust literature describing the liver as a tolerizing organ[132,133] that serves to prevent the generation of unregulated immune responses against food antigens, for example. However, the liver does not have the same anatomical architecture of spleens and LNs, which bring antigen presenting cells (APCs) and circulating T cells in sufficiently close compartments to maximize the probability of T cells contacting their cognate pMHC[56,134,135]. Thus, we were skeptical that the initial priming event could truly happen in the liver. To investigate where T cells are initially primed, we transferred 500k Thy1.1+ pmel T cells (which are specific for gp100$_{20-39}$) into recipient mice, then administered either PBS or MSA-gp100$_{20-39}$ i.v. 24 hours later. 24 hours after vaccination, the same organs analyzed for gross biodistribution (inguinal LN, kidney, spleen, liver, and lungs), were processed into single cell suspensions, and Thy1.1+ cells analyzed for CD69 expression, as a marker of TCR triggering. Within the first 24 hours of activation, CD69 prevents T cell egression from lymphoid organs, so we can be reasonably confident that at this time point CD69+ T cells were primed at the organ of recovery[136,137]. Activated Thy1.1+ pmels were only recovered in the canonical secondary lymphoid organs

(inguinal LN and spleen) (**Fig. 4.2b-c**), making it unlikely that the liver is the site of initial priming, despite significant organ uptake at the gross level (**Fig. 4.2a**).

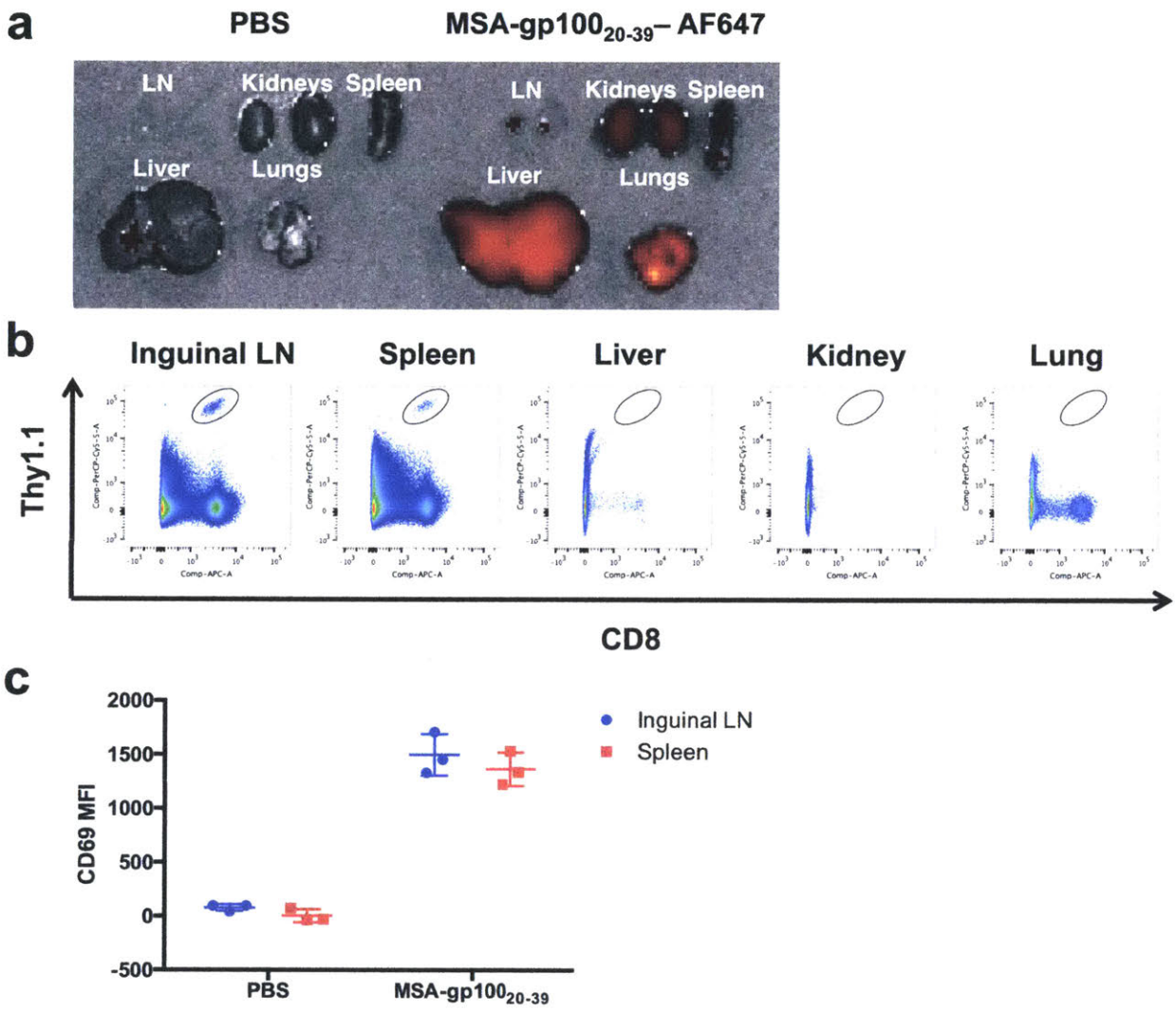

Figure 4.2. Tolerizing vaccines prime CD8+ T cells in secondary lymphoid organs despite their distribution to the liver and lungs

(**a**) AF647-labeled MSA was administered i.v. and the indicated organs excised and imaged 24 hours later (where LN represents the inguinal LNs). (**b-c**) 500k Thy1.1+ pmel T cells were transferred into recipient mice, which were subsequently administered MSA-gp100$_{20-39}$ i.v. (**b**) The indicated organs were excised and Thy1.1+ cells assessed by flow cytometry. Shown are representative Thy1.1+ identification plots, demonstrating in which organs Thy1.1+ cells were recovered. (**c**) CD69 expression measurements from Thy1.1+ cells recovered from the inguinal LN and the spleen.

We next assessed the phenotype of T cells as they respond to tolerizing vaccination within secondary lymphoid organs. In addition to the peripheral inguinal LN, we added the intestine-draining mesenteric LNs to our analysis to try and observe behavior in the presumably tolerizing gut environment. To examine mechanisms of T cell tolerization, we transferred 1M CFSE-labeled CD45.2+ OTI T cells into recipient CD45.1+ mice; 24 hours later we administered PBS, $gp100_{20-39}$ peptide, or MSA-$gp100_{20-39}$ intravenously. Three days after vaccination, the spleen, inguinal LN, and mesenteric LN were excised and CD45.2+ cells were analyzed for proliferation as measured by CFSE dilution, markers to assess exhaustion (PD1, Tim3, Lag3) and the induction of regulatory cells (Foxp3).

CD45.2+ cells from mice that received the MSA-OTI vaccine had proliferated significantly more than CD45.2+ cells from mice that received PBS or OTI peptide in all lymphoid organs assessed, with nearly 100% of CD45.2+ cells divided in the MSA-OTI (**Fig. 4.3a-b**). Additionally, CD45.2+ T cells from MSA-OTI-vaccinated animals showed markers consistent with an exhaustive phenotype. While OTI peptide and MSA-OTI vaccination induced PD1 expression in the spleen, only MSA-OTI triggered PD1 expression in the inguinal LN and mesenteric LN (**Fig. 4.3c**). To differentiate between activated T cells and exhausted cells, we also stained for Tim3 and Lag3, where double positive cells can more confidently be described as exhausted[130]. By this measurement, only MSA-OTI induced an exhaustive phenotype (**Fig. 4.3d-e**). Finally, we assessed the regulatory phenotype of CD45.2+ cells with Foxp3 staining, and intriguingly found Foxp3 expression only in the LNs of mice that had been vaccinated with MSA-OTI (**Fig. 4.3f**). Collectively, we conclude that upon i.v. administration of MSA-antigen

tolerizing vaccine, antigen-specific T cells in the spleen and lymph nodes proliferate but become rapidly exhausted, preventing response to future challenge, and antigen-specific T cells in the lymph nodes adopt a regulatory phenotype, actively dampening subsequent antigen-specific immune responses.

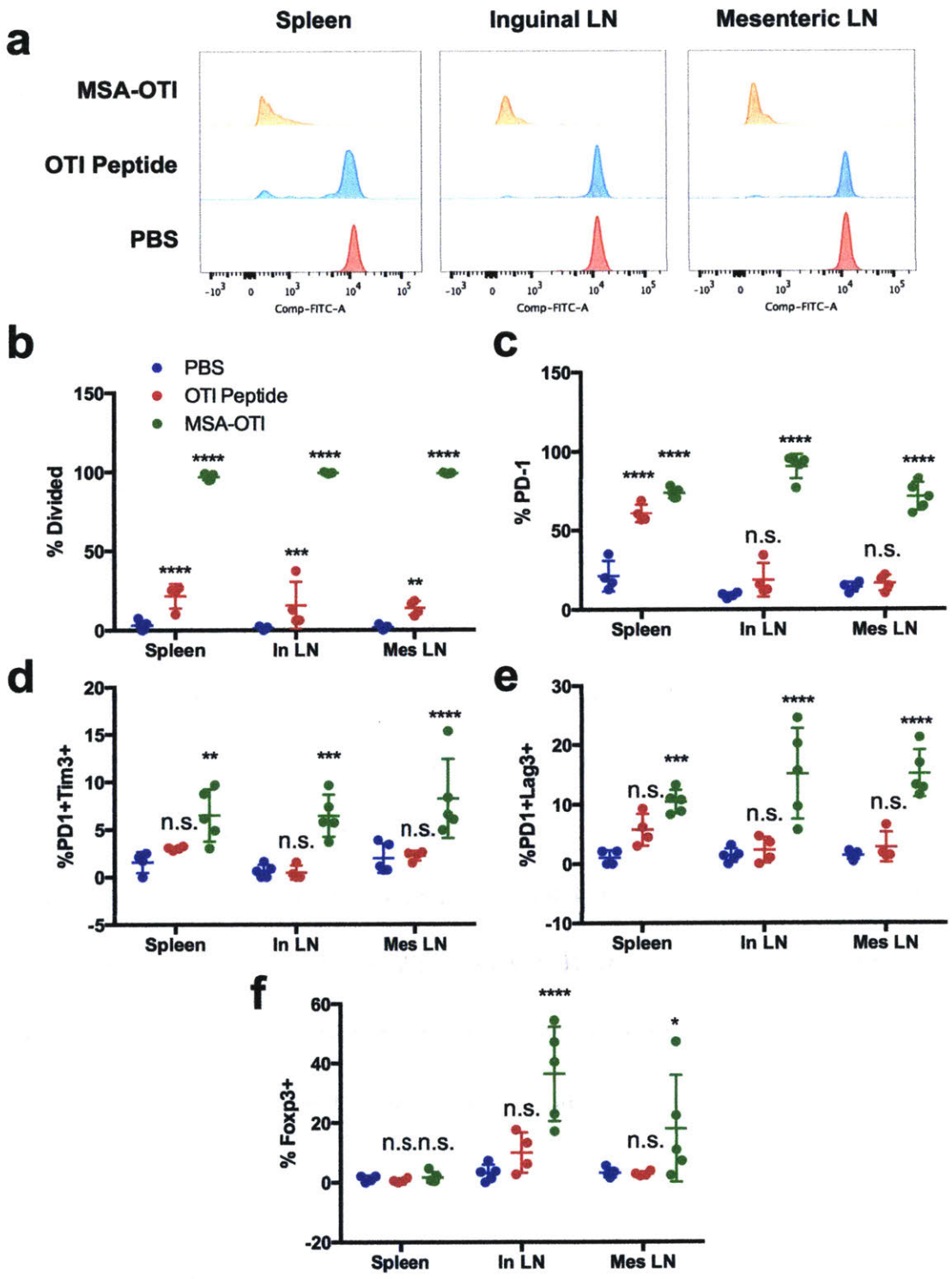

Figure 4.3. Phenotype of CD8+ T cells in response to tolerization

Throughout, 1M CFSE-labeled CD45.2+ OTI cells were transferred into CD45.1+ recipient mice. 24h later, mice were treated with indicated tolerizing vaccine. 72h later, the indicated organs were excised, and recovered CD45.2+ OTI cells were assessed for the indicated phenotypes (n = 5 mice/group). (**a**) Shown are representative CFSE dilution histograms, quantified in (**b**). (**c-f**) Shown are quantifications of the percent of CD45.2+ OTI cells with the indicated phenotypes. Throughout, * P < 0.05; ** P < 0.01; *** P

< 0.001; **** P < 0.0001 by two-way ANOVA with Dunnett's multiple comparisons test against PBS within each indicated organ (**b-f**).

The degree of tolerization is dependent on antigen persistence and the pharmacokinetics of the protein carrier

We conjectured that a major reason why MSA-antigen fusions are so efficient tolerizing agents is their extended pharmacokinetics, which may lead to persistent T cell priming. To directly assess the kinetics of antigen presentation, we i.v. vaccinated mice with OTI peptide or MSA-OTI. After 1, 3, or 7, or 14 days, 500k OTI Thy1.1+ cells were adoptively transferred into vaccinated animals to serve as reporters of antigen presentation. Twenty-four hours later, inguinal LN, mesenteric LN, and spleen were excised and resident Thy1.1+ cells were assessed for CD69 expression. Antigen presentation was prolonged in mice vaccinated with MSA-OTI: CD69 was still upregulated on OTI T cells in the spleen (**Fig. 4.4a**) and mesenteric LNs (**Fig. 4.4b**) when transferred 7 days after immunization and in the inguinal LN when transferred even 14 days after immunization (**Fig. 4.4c**). OTI peptide administration did not induce CD69 expression at any measured time points (**Fig. 4.4a-c**). We note that the apparent inactivity of the OTI peptide is likely not representative of other peptide antigens, as other peptides administered i.v. tend to perform better than OTI at inducing tolerance (**Fig. 4.1b-d**)

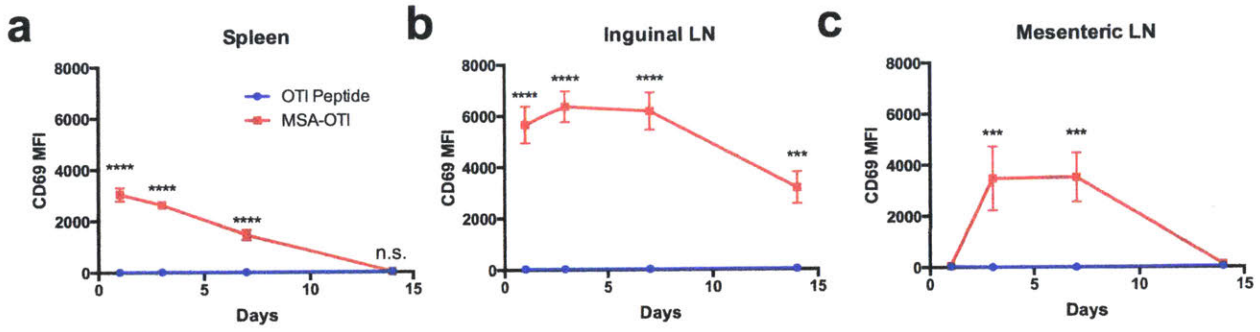

Figure 4.4. Persistence of antigen presentation in secondary lymphoid organs

Throughout, mice were i.v. administered the indicated tolerizing vaccine, then received 500k Thy1.1+ OTI cells after the indicated number of days. 24h after transfer, the indicated organs were excised, and recovered Thy1.1+ OTI cells assessed for CD69 expression by flow cytometry (n = 3 mice/group). *** $P < 0.001$; **** $P < 0.0001$ by two-tailed t tests at each time point with Holm-Sidak multiple comparisons test.

If the persistence of antigen presentation has a dominating impact on tolerization, then choosing carrier proteins with different pharmacokinetic charaacteristics should modulate efficacy in a tolerization model. In addition to MSA-E7$_{38-57}$, we produced E7$_{38-57}$ fused to alternative proteins, including MSA H464Q, a form that fails to interact with the neonatal Fc receptor (FcRn) to shorten the circulating half life, and Fc and transthyretin (TTR), two endogenous serum proteins with notably different half lives. These antigen delivery strategies could be rank ordered: Fc-E7$_{38-57}$ > MSA-E7$_{38-57}$ > MSA-E7$_{38-57}$ H464Q > TTR-E7$_{38-57}$ > E7$_{38-57}$ peptide (**Fig 4.5a**). When compared head-to-head in a tolerizing vaccine study (**Fig. 4.1a**), the fusions with half-lives over 24 hours (Fc-E7$_{38-5}$, MSA-E7$_{38-57}$, and MSA-E7$_{38-57}$ H464Q) all generated mean tolerization >80%, while more rapidly cleared E7$_{38-57}$ peptide (half life of 0.6 hours) and TTR-E7$_{38-57}$ (half life of 11.9 hours) only tolerized 57% and 50%, respectively (**Fig. 4.5b**). Thus, there appears to be a pharmacokinetic threshold requirement to maximize the induction of tolerance.

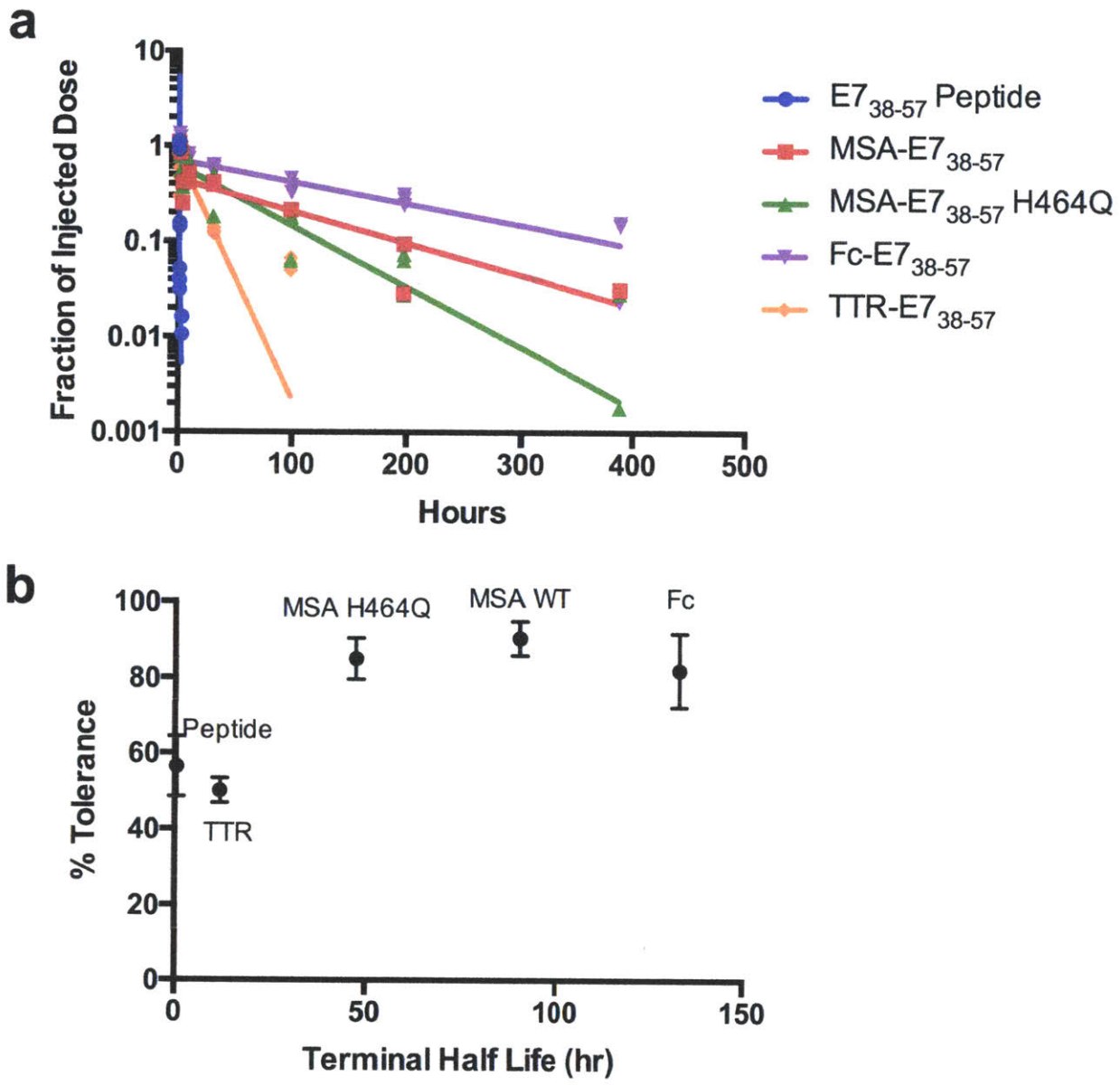

Figure 4.5. Relationship between pharmacokinetics and tolerization

(**a**) The indicated antigens were FITC labeled, injected i.v. and concentrations in blood calculated at the indicated time points (n = 3 mice/group). (**b**) Each antigen was tested for tolerization against subsequent prime/boost s.c. challenge with TTR-$E7_{38-57}$ with CDN (n = 5 mice/group), and percent tolerance calculated as the percent reduction in tetramer+ frequency relative to PBS control. Shown is an overlay of terminal half life calculated from (**a**) and percent tolerance.

Targeting periphal LNs more effectively induces tolerance

A number of the studies described thus far suggested that antigen presentation in the peripheral inguinal LN may have a dominant effect in the induction of tolerance. Lymph nodes, as opposed to the spleen, are prominently involved in the induction of Foxp3+ CD8+ cells (**Fig. 4.3f**), and antigen presentation is robust and significantly more persistent in the inguinal LN than in the mesenteric LN or the spleen (**Fig. 4.4a-c**). We believe this might be a unique feature of a relatively small, antigen carrier like a protein that exchanges between serum and tissue regularly, as opposed to cellular or microparticle delivery strategies that would be excluded from tissues and their draining LNs. However, we were also interested in addressing whether intentionally targeting peripheral LNs could more potently induce tolerance than broad i.v. biodistribution. To target MSA-E7$_{38-57}$ to the inguinal LN for the purposes of tolerization, MSA-E7$_{38-57}$ was administered s.c. rather than i.v. in the absence of adjuvant, then challenged two weeks later as previously described. Indeed, s.c. administered MSA-E7$_{38-57}$ was able to impart tolerance at lower doses than was i.v. administered MSA-E7$_{38-57}$ (**Fig. 4.6**).

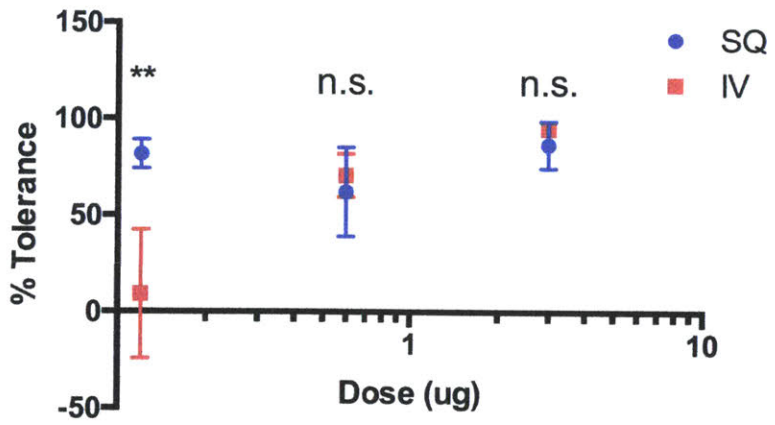

Figure 4.6. Comparison of intravenous versus subcutaneous administration of tolerization vaccines

Mice were tolerized with MSA-E7$_{38-57}$ at the indicated equivalent peptide dose, followed by prime/boost challenge with TTR-E7$_{38-57}$ (n = 5 mice/group). Percent tolerance was calculated as the percent reduction in tetramer+ frequency relative to PBS control. ** $P < 0.01$ by two-tailed t tests at each dose followed by Holm-Sidak multiple comparisons test.

Albumin-antigen fusions in a preclinical model of multiple sclerosis

A commonly utilized preclinical model in autoimmunity is the experimental autoimmune encephalomyelitis (EAE) model of multiple sclerosis. In this model, mice are immunized against MOG$_{35-55}$ along with Pertussis toxin to induce an anti-myelin response, leading to debiliting muscular destruction and the onset of paralysis which can be measured by clinical score. We prophylactically administered MOG$_{35-55}$ or MSA-MOG$_{35-55}$ i.v. in mice 7 days prior to induction of disease, then tracked disease score starting on day 10 after disease induction. Starting on day 17 and onwards, mice that had received MSA-MOG$_{35-55}$ had significantly lower disease score than either the no treatment control or MOG$_{35-55}$ peptide controls, and 90% of MSA-MOG$_{35-55}$-treated mice exhibited no disease score at all (**Fig. 4.7**). While more preclinical work is needed to thoroughly characterize the mechanism of action here, the early data are promising.

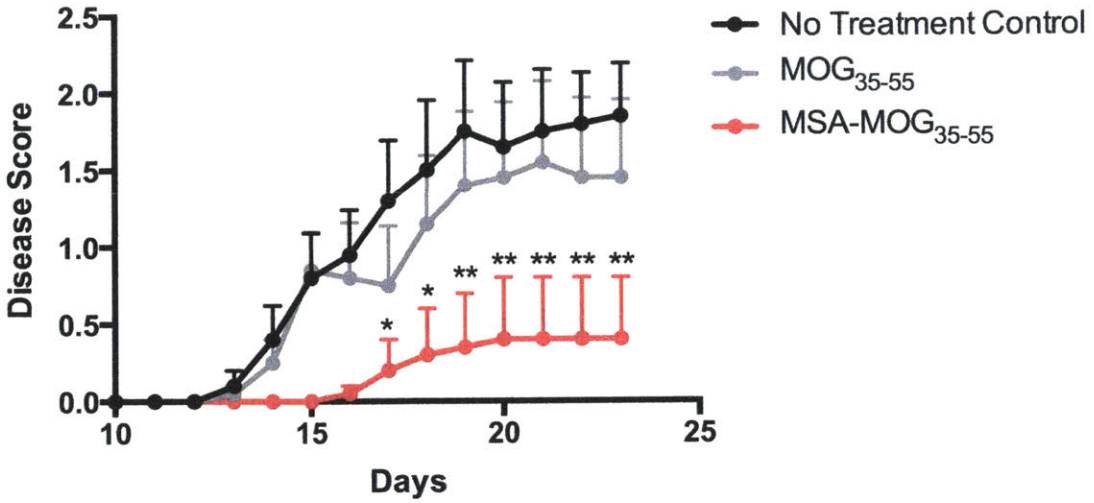

Figure 4.7. MSA-MOG_{35-55} tolerizing vaccine effectively prevents induction of EAE

Mice were i.v. administered the indicated tolerizing vaccine on day -7, followed by induction of EAE on day 0, and disease score was assessed daily from days 10-23 (n = 10 mice/group). * $P < 0.05$ and ** $P < 0.01$ by two-way ANOVA with Dunnett's multiple comparisons test at each time point against no treatment control.

4.3 Materials and Methods

Mice

B6 mice were purchased from Taconic. OTI mice (C57BL/6-Tg(TcraTcrb)1100Mjb/J) and Thy1.1 mice (B6.PL-Thy1a/CyJ) were purchased from Jackson Laboratory and crossed to generate an OTI Thy1.1$^+$ colony. Pmel Thy1.1$^+$ mice (B6.Cg-Thy1a/Cy Tg(TcraTcrb)8Rest/J) were purchased from Jackson Laboratory. All animal work was conducted under the approval of the Massachusetts Institute of Technology (MIT) Division of Comparative Medicine in accordance with federal, state, and local guidelines.

Cells

HEK cells (FreeStyle 293-F) were purchased from Thermo Fisher Scientific. TC-1 cells were kindly provided by T.C. Wu (Johns Hopkins University). HEK cells were cultured in FreeStyle 293 Expression Medium (Thermo Fisher Scientific) and passaged every two days to a density of 300k/ml. TC-1 cells were cultured in RPMI-1640 (GE Healthcare Life Sciences) supplemented with 10% FBS, 100 units/ml penicillin, 100 μg/ml streptomycin, and 4 mM L-alanyl-L-glutamine. TC-1 cells were passaged 1:10 every two days. All cells were cultured at 37°C and 5% CO_2. All cells were tested regularly for mycoplasma contamination and for rodent pathogens, and none used tested positive at any point.

Protein production and characterization

Codon-optimized genes encoding desired proteins were cloned into gWiz expression vectors (Genlantis) using the In-Fusion HD Cloning Kit (Clontech), prepared endotoxin free (Macherey-Nagel) and incubated with Opti-Pro (Thermo Fisher Scientific) and polyethylenimine (PEI) 25K (Polysciences) prior to drop-wise addition to HEK cell culture at 1 million cells/ml. 1 mg of DNA was mixed with 40 ml of Opti-Pro and 2 mg of PEI per 1 L of cell culture. One week after transfection, cell culture was spun down in endotoxin-free centrifuge tubes at 15000xg for 30 min, supernatant filtered, pH neutralized by addition of 10X PBS, and run through TALON metal affinity resin (Clontech) by gravity flow per manufacturer instructions. Following purification, proteins were buffer exchanged into PBS with 30 kDa molecular weight cutoff Amicon Ultra-15 centrifugal filters (Millipore), filtered using Spin-X centrifuge tube filters (Corning) or 0.2 μm syringe filters (VWR), and flash-frozen in aliquots with liquid nitrogen, then stored at -80°C. After thaw, proteins were used within one month and stored at 4°C in

sterile conditions. Endotoxin levels measured using a chromogenic LAL assay (Lonza). A maximum of 5 EU/kg, or 0.1 EU/mouse was accepted for all injected proteins.

PK studies

5-FAM-E7$_{38-57}$ was purchased from Genscript, and recombinantly expressed proteins (MSA-E7$_{38-57}$, TTR-E7$_{38-57}$, and Fc-E7$_{38-57}$) were labeled with NHS-5/6-FAM (Thermo Fisher Scientific) per manufacturer instructions. Following protein conjugation, the concentration of labeled protein was calculated using A493. Mice were i.v. injected with 5 nmol labeled peptide or protein. At the indicated time points, <10 μl of blood was collected from tail snip into heparin-coated microhematocrit capillary tubes (VWR). Capillaries were parafilmed and stored upright in the dark at 4°C overnight to separate serum from cellular components. On a Typhoon Trio variable mode imager, serum in capillaries was measured (526 SP filter, 532 nm laser) against a standard curve of analytes prepared in PBS and added directly into capillaries. FIJI image analysis software was used to calculate serum concentrations of analyte. I.v. curves were fit to biphasic decay kinetics and the terminal half-life calculated. Curves were fit using nonlinear regression on GraphPad Prism software.

Vaccinations

To test tolerizing vaccinations, epitope-containing peptide or protein-epitope fusions were i.v. administered retro-orbitally 14 days before s.c. prime with adjuvanted challenge vaccine, and boost 14 days after prime; the magnitude of the T cell response was read-out 6 days after boost with either tetramer staining or intracellular cytokine staining (Fig. 4.1a). Dosing and details of

challenge: In Fig. 4.1, 3 μg equivalent of indicated peptide tolerization and challenge with 3 μg peptide equivalent TTR-E7$_{38-57}$ (Fig. 4.1b), 3 μg peptide equivalent TTR-gp100$_{20-39}$ (Fig. 4.1c), or 5 μg ovalbumin (Fig. 4.1d), mixed with 25 μg cyclic di-GMP (CDN) in all cases in Fig. 4.1. Fig. 4.1d was performed like Fig. 4.1b but the indicated time period elapsed before initiation of prime/boost challenge. Fig. 4.5b was performed like Fig. 4.1b but the tolerizing vaccine dose was reduced from 3 μg peptide equivalent to 0.6 μg; challenge dose remained the same. Fig. 4.6 was performed like Fig. 41b but the tolerizing vaccine dose was titrated as indicated, and administered either i.v. or s.c. as indicated.; challenge dose and route of administration remained the same.

Flow cytometry

Antibodies against CD16/32 (Fc block, clone 93), CD8α (53-6.7), TNF-α (MP6-XT22), IFN-γ (XMG1.2), CD45.2 (104), Thy1.1 (OX-7), CD69 (H1.2F3), PD1 (29F.1A12), Lag3 (C9B7W), Tim3 (RMT3-23), and Foxp3 (MF-14) were purchased from BioLegend. Cell viability was assessed with DAPI (Sigma) for tetramer stains and LIVE/DEAD fixable aqua dead cell stain (Thermo Fisher Scientific) for all other studies. *Tetramer staining:* E7 tetramer (iTAg Tetramer/PE - H-2 Db HPV 16 E7) and OTI tetramer (iTAg Tetramer/PE - H-2 Kb OVA) were both purchased from MBL; during tetramer staining, PBMCs were Fc blocked and stained with tetramer for 15 minutes prior to addition of anti-CD8α antibody, and cells were incubated with all antibodies for another 30 minutes. All labeling was performed in PBS + 0.1% BSA. *Ex vivo stimulation studies:* Intracellular cytokine staining (ICS) to assess the magnitude of T cell response was performed as previously reported[114]. Briefly, PBMCs were re-stimulated in RPMI-1640 + 10%

FBS at 37°C with optimal WT peptide at 10 μg/ml ($gp100_{25-33}$) for 2 hrs followed by addition of brefeldin A (Thermo Fisher Scientific) for another 4 hrs prior to staining. In all cases, surface staining was performed first (Fc block, anti-CD8α) in PBS + 0.1% BSA followed by fixation and permeabilization using BD Cytofix/Cytoperm fixation/permeabilization kit per manufacturer instructions and intracellular staining (anti-IFN-γ and/or anti-TNF-α) in perm/wash buffer. *Organ processing:* LNs were excised, mashed through 74 μm Netwell inserts (Corning), and washed into PBS + 0.1% BSA prior to antibody labeling. Other organs were excised and mashed through 70 μm filters (Corning) and washed into PBS + 0.1% BSA prior to antibody staining. Spleens were also treated with ACK lysis to remove red blood cells. Cells were analyzed using BD FACSCanto and BD FACS LSR Fortessa, and data were analyzed using FlowJo.

Tumor studies

Two weeks after the administration of 3 μg $E7_{38-57}$ or equimolar doses of MSA-$E7_{38-57}$ (or PBS control), 300k TC-1 cells were subcutaneously administered in 50 μl sterile PBS on the right flank of shaved WT B6 mice. Tumor size was measured by area (longest dimension x perpendicular dimension), and mice were euthanized when tumor area exceeded 100 mm^2.

Biodistribution

IVIS imaging: 2 nmol AF647-conjugated MSA-$gp100_{20-39}$ or PBS control was i.v. administered retro-orbitally; the indicated organs were excised 24 hours after injection and imaged on an IVIS Spectrum Imaging System (Caliper Life Sciences), excitation: 640 nm, emission: 700 nm.

Adoptive transfer

$CD8^+$ T cells from pmel $Thy1.1^+$, OTI $Thy1.1^+$, or OTI mouse spleens were isolated using the EasySep mouse CD8+ T Cell Isolation Kit (STEMCELL Technologies). To determine in which organs antigen is presented, $CD8^+$ T cells from pmel $Thy1.1^+$ mice were isolated as above and retro-orbitally transferred into naïve mice in PBS. 24 hrs later, recipient mice were i.v. immunized with 3 μg peptide equivalence MSA-$gp100_{20\text{-}39}$; 24 hrs after injection, the indicated organs were probed for $Thy1.1^+$ cells, and if sufficient $Thy1.1^+$ cells were recovered, then CD69 expression was measured by flow cytometry (see flow cytometry section). To assess T cell phenotype in response to tolerization, $CD8^+$ T cells from OTI mice were isolated as above and labeled with carboxyfluorescein succinimidyl ester (CFSE) (Thermo Fisher Scientific) at a cell density of 10M/ml and a CFSE concentration of 5 μM for 20 min at 37°C in PBS + 0.1% BSA and subsequently quenched by addition of FBS. 1M CFSE-labeled OTI cells were retro-orbitally transferred into naïve $CD45.1^+$ animals in PBS. 24 hrs later, recipient mice were i.v. vaccinated with 3 μg OTI peptide, MSA-OTI, or PBS control. 72 hrs post-immunization, the spleen, inguinal LNs, and mesenteric LNs were excised and $Thy1.1^+$ cells assessed by flow cytometry (see flow cytometry section). Proliferation index = $\log_2(FI_{nd}/MFI_{all})$ where MFI_{all} = MFI of live $Thy1.1^+$ pmel T cells and FI_{nd} = peak fluorescence intensity of viable non-divided $Thy1.1^+$ pmel T cells. To assess the kinetics of TCR engagement (Fig. 4.4), we retro-orbitally i.v. transferred 500k OTI $Thy1.1^+$ cells into animals that had previously been i.v. vaccinated with 3 μg peptide equivalence MSA-OTI at the indicated time points. 24 hours after transfer, the spleen, inguinal LNs, and mesenteric LNs were excised and $Thy1.1^+$ cells assessed for CD69 expression by flow

cytometry (see flow cytometry section).

EAE studies

EAE was induced as previously reported[138]. Mice were administered 3 μg MOG_{35-55} or equimolar dose of MSA-MOG_{35-55} i.v. 7 days prior to initiation of EAE. EAE was induced via MOG_{35-55} vaccination and injection of Pertussis toxin. 2 days later, Pertussis toxin was re-injected. Starting on day 8 after EAE initiation, mice were scored daily until day 22.

Statistical analysis

All statistical analyses were performed using GraphPad Prism software. The specifics of the statistical test performed, p-values, and number of replicates are stated in the figure legends. For all tests, the threshold for significance was $P < 0.05$.

4.4 Conclusions

Given our conclusion from chapter 2 that albumin-antigen fusion proteins are bioactive and immunogenic, and because of albumin's known ability to extend circulating half-life, we hypothesized that albumin-antigen fusions would be effective at inducing tolerization if administered in the absence of adjuvant. Surprisingly, we found that intravenously administered albumin fusions were effective at preventing responses to subsequent antigenic challenge both with and without co-administration of adjuvant. The reason why the approach is agnostic to adjuvant has not been fully elucidated, but is likely due to different pharmacokinetic

clearance rates between antigen and adjuvant, or their partitioning into distinct anatomic or cellular compartments.

To understand how albumin-epitope fusions function, we analyzed 1) the pharmacokinetics of fusion protein clearance; 2) the pharmacodynamics of antigen presentation; and 3) the phenotype of T cells as they respond to tolerizing vaccine. We report a threshold half-life requirement of approximately 24h, beyond which tolerizing vaccines achieve maximal efficacy. Surprisingly, we find that peripheral lymph nodes play a dominant role in the induction of tolerance, even following intravenous administration of tolerizing vaccine: antigen presentation is more persistent in the inguinal node than in the spleen, and Foxp3 expression is induced exclusively in T cells of the lymph nodes three days after injection of antigen. As a result, subcutaneous administration of tolerizing vaccines, such that the draining inguinal lymph node is more specifically targeted, is effective at lower doses relative to intravenous administration. Finally, we report that mouse serum albumin fused to MOG_{35-55} peptide effectively prevents the induction of EAE, although the fusion approach is ineffective in a therapeutic context after EAE has already been induced (data not shown).

4.5 Acknowledgements

This work is the product of a fruitful collaboration between our labs and a dedicated team at Pfizer, including Aaron Winkler, Michael Look, Kellie Kravarik, Andre M. Mueller, and Xiao Chen. Roma V. Pradhan, my UROP, helped clone and produce many of the protein products in this study, and helped out with several tetramer stains. Ava P. Soleimany, a graduate student

from Sangeeta N. Bhatia's lab, was also a major help in the flow cytometry-based phenotyping studies.

CHAPTER 5. ELUCIDATING THE MECHANISM OF ACTION OF LIPO-CPG

Abstract

In the development of therapeutic subunit vaccines, we must pay careful consideration to our choice of adjuvant, which triggers the appropriate inflammatory environment needed to sustain a productive T cell response. Previously, we conjugated CpG, a TLR agonist, to a diacyl lipid tail (lipo-CpG), to develop a moiety that bound serum albumin *in situ* upon subcutaneous injection, improving lymph node targeting and enhancing T cell responses over vaccines with unformulated CpG by over 10-fold. Here, we explore lipo-CpG's mechanism of action in more depth and find that its advantage over CpG goes beyond improved lymph node accumulation to include enhanced monocyte uptake. We uncover a cascade of cellular events and soluble signals triggered by monocyte activation following immunization with lipo-CpG, including monocyte-produced IL-12, NK cell-secreted IFNγ, and a number of chemokines that aid in antigen-presenting cell recruitment. Collectively, we conclude that the key advantage of lipo-CpG over CpG is its ability to enhance the cytokine milieu in the lymph node during early events in T cell priming to generate a more productive response.

5.1 Introduction

We previously published on the use of 1,2-Distearoyl-sn-glycero-3-phosphoethanolamine (DSPE) conjugates to improve responses to molecular vaccines[43]. In this work, DSPE-peptide and –CpG conjugates were amphiphiles with a hydrophilic head and a

hydrophobic tail. These amphiphilic vaccine components were named amph-peptide and lipo-CpG. In solution, both amph-peptide and lipo-CpG formed micelles that could be disrupted by the presence of serum albumin due to the several lipid-binding pockets present in the globular protein[45,46]. Lipid-mediated albumin binding was found to have a direct correlation with lymph node (LN) uptake upon subcutaneous injection, as measured by whole organ *in vivo* imaging systems (IVIS). Lipo-CpG adjuvanted OVA vaccination resulted in tremendous increases in potency of protein antigens, generating 32-fold higher numbers of OVA-specific CD8+ T cells in the blood compared to CpG. Over 30% of the CD8+ T cells in the blood were OVA-specific, a high frequency rivaling that seen during natural infection[48]. Similarly potent responses were seen when lipo-CpG and amph-peptide were co-injected in vaccination.

Intriguingly, however, neither *in vitro* nor *in vivo* studies on dendritic cells (DCs) revealed any significant differences in potency between CpG and lipo-CpG[43]. In addition to presenting antigen (signal one) and danger-signal associated co-receptors (signal two), APCs also provide a third signal via the secretion of soluble inflammatory cytokines[139]. We began to suspect that it is along this axis that lipo-CpG may gain its marginal efficacy over CpG. With CpG in particular, TLR9 expression has been found to be inessential on both the DC presenting antigen and on the T cell responding to antigen, instead implicating other immune cells in the lymph node[140]. CpG has also been shown to induce high levels of IL-12 secretion, a cytokine that can shape the quality and phenotype of T cell responses[141]. Monocytes and macrophages, despite being sub-optimal antigen-presenting cells relative to DCs, have been shown to be responsible for directing the cytokine milieu in response to CpG, secreting both IL-12 and

chemokines to further recruit APCs[142,143]. The role of CpG in shaping the immune response is complex, however, as high doses can ultimately be immunosuppressive rather than stimulatory[144,145].

Here, we modulate the dosing of CpG relative to lipo-CpG such that both accumulate in the draining LN equivalently, and we find that lipo-CpG remains a superior adjuvant. We show that lipo-CpG is preferentially taken up by monocytes, expanding their numbers and triggering high degrees of IL-12 production, directing an inflammatory cascade that recruits additional monocytes via chemokines and induces a highly proliferative CD8+ T cell response modulated by the transcription factor T-bet. We conclude that lipo-CpG outperforms CpG not solely due to better lymph node accumulation nor due to enhanced maturation of cells directly presenting antigen, but rather due to superior uptake by monocytes and the production of the most appropriate signals to direct the immune response in trans.

5.2 Results and Discussion

High dose CpG fails to replicate lipo-CpG efficacy despite enhanced lymphatic retention

Previously, the Irvine lab had systematically explored various formulation strategies to improve the bioavailability of CpG in the draining lymphatics, and found a tight correlation between lymphatic retention and vaccine responses when combined with ovalbumin[43,44]. This work suggested that, in a generalizable matter, strategies that enhance the lymphatic uptake of

CpG should also improve its potency, and that the primary bottleneck in CpG efficacy is its mass transport to the lymph node, where the immune response is orchestrated. The conclusion drawn from this work is that lipo-CpG gained efficacy over CpG because of its propensity to form complexes with serum albumin, which helped solve the delivery problem associated with naked CpG.

To directly test the role of lymphatic bioavailability on CpG potency, we sought to dose through the mass transport deficiencies of CpG to identify a dosing regimen that matched the dLN retention characteristics of lipo-CpG. 1 nmol of TAMRA-labeled CpG only weakly accumulated in the draining inguinal lymph node (dLN) while 1 nmol of labeled lipo-CpG demonstrated potent dLN uptake as measured by IVIS, consistent with previous findings; however, simply administering a five-fold higher dose of labeled CpG (5 nmol) also led to robust accumulation (**Fig. 5.1a,b**). In addition to early mass uptake, lipo-CpG is notable for its persistence in the dLN, a feature that was also replicated by high dose CpG, where strong TAMRA signal was detected even 7 days after administration of labeled CpG (**Fig. 5.1a,b**). Thus, 5-fold higher dosing of CpG seemed to appropriately replicate the dLN accumulative characteristics of lipo-CpG.

We next assessed whether improved dLN uptake by high dose CpG led to matched potency compared to lipo-CpG in a vaccination model. CpG or lipo-CpG, at 1 nmol or 5 nmol as indicated, were mixed with 5 μg ovalbumin as a model antigen, and administered using a prime/boost vaccination schedule (prime on day 0, boost on day 14, read-out with tetramer staining on day 20). Surprisingly, 5 nmol CpG failed to improve upon 1 nmol CpG at triggering

high-frequency anti-OVA CD8+ T cell responses responses, and continued to underperform relative to lipo-CpG by 8.4-fold (**Fig. 5.1c**). This result decoupled dLN bioavailability from potency and suggested that there may be some underlying biological mechanism of action that differs between CpG and lipo-CpG.

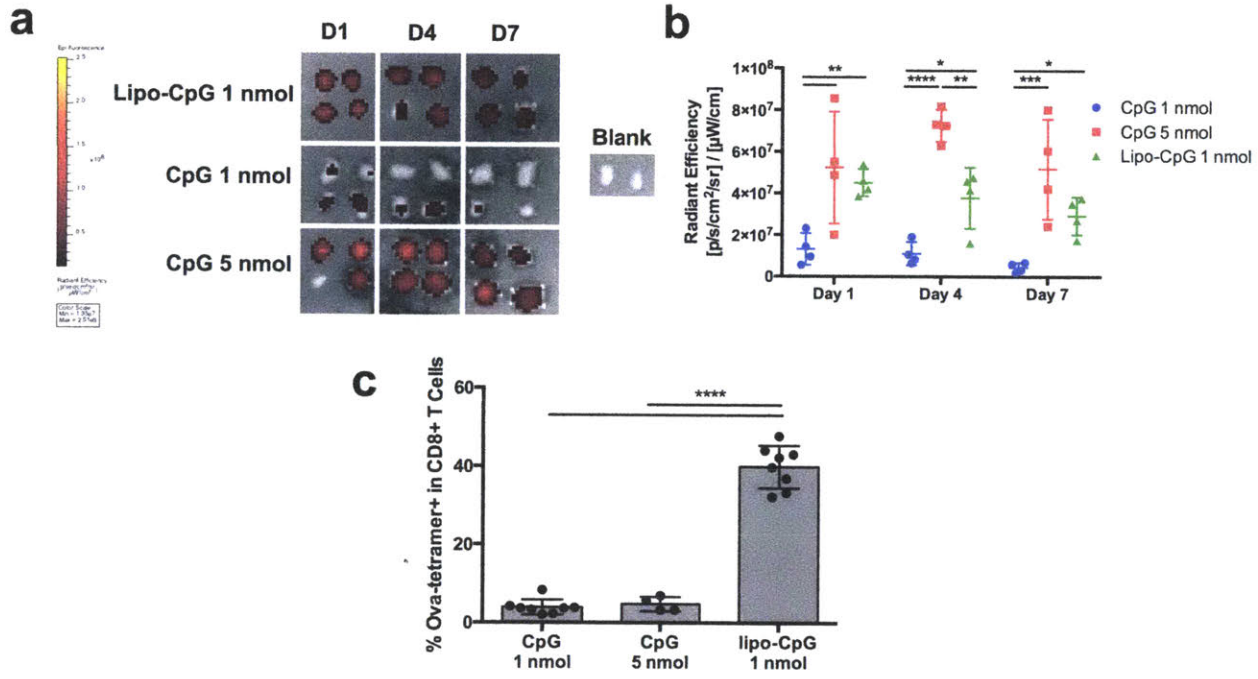

Figure 5.1. High dose CpG fails to replicate lipo-CpG efficacy

(**a**) TAMRA-conjugated CpG variants at the reported dose were subcutaneously administered, and the draining inguinal LNs were excised and imaged on IVIS at the indicated time points (n = 4 lymph nodes/group). (**b**) Quantification of IVIS signals from (**a**). (**c**) Mice were prime/boost vaccinated with the indicated CpG variants mixed with ovalbumin. Six days after boost, the frequency of Ova-specific CD8+ T cells was assessed via tetramer stain (n = 4-8 mice/group). * $P < 0.05$; ** $P < 0.01$; *** $P < 0.001$; **** $P < 0.0001$ by two-way ANOVA with Tukey's multiple comparisons test within each time point (**b**) or one-way ANOVA with Tukey's multiple comparisons test (**a**).

Lipo-CpG potently activates and expands monocyte populations

To understand the biological differences between low dose CpG, high dose CpG, and lipo-CpG, we performed single cell RNA-seq (scRNA-seq) on cells isolated from the dLN 24

hours after administration of CpG mixed with ovalbumin, compared against PBS control. Several immune cells were successfully isolated and reliably clustered (**Fig. 5.2a**), allowing for the assessment of differences between groups on a cell-by-cell level in terms of both gene expression and numerical expansion.

We observed notable differences between the groups in the monocyte population, both in terms of numbers and activation. During sample preparation, equivalent numbers of cells were run in each group, so total absolute numbers of cells are not available for this dataset; however, it was apparent that both high dose CpG and lipo-CpG expand the frequency of monocytes relative to PBS control (**Fig. 5.2b**). Due to the greater number of total cells recovered from lipo-CpG immunized animals, this suggests that lipo-CpG should significantly outperform CpG in terms of the absolute number of monocytes per dLN following immunization. This finding is consistent with previous reports that show dramatic monocyte expansion in the nodes in response to CpG immunization, and suggested that it is on this mechanistic axis that lipo-CpG may outperform CpG. The apparent reduced expansion of monocytes by high dose CpG intriguingly suggested that an auto-regulatory feedback might be triggered at higher doses of CpG[144,145], reducing its propensity to expand monocytes. Importantly, gene set enrichment analysis within the identified monocyte populations demonstrated signatures of activation, including apparent responses to IFNγ, NFκB, and JAK/Stat3 (**Fig. 5.2c).**

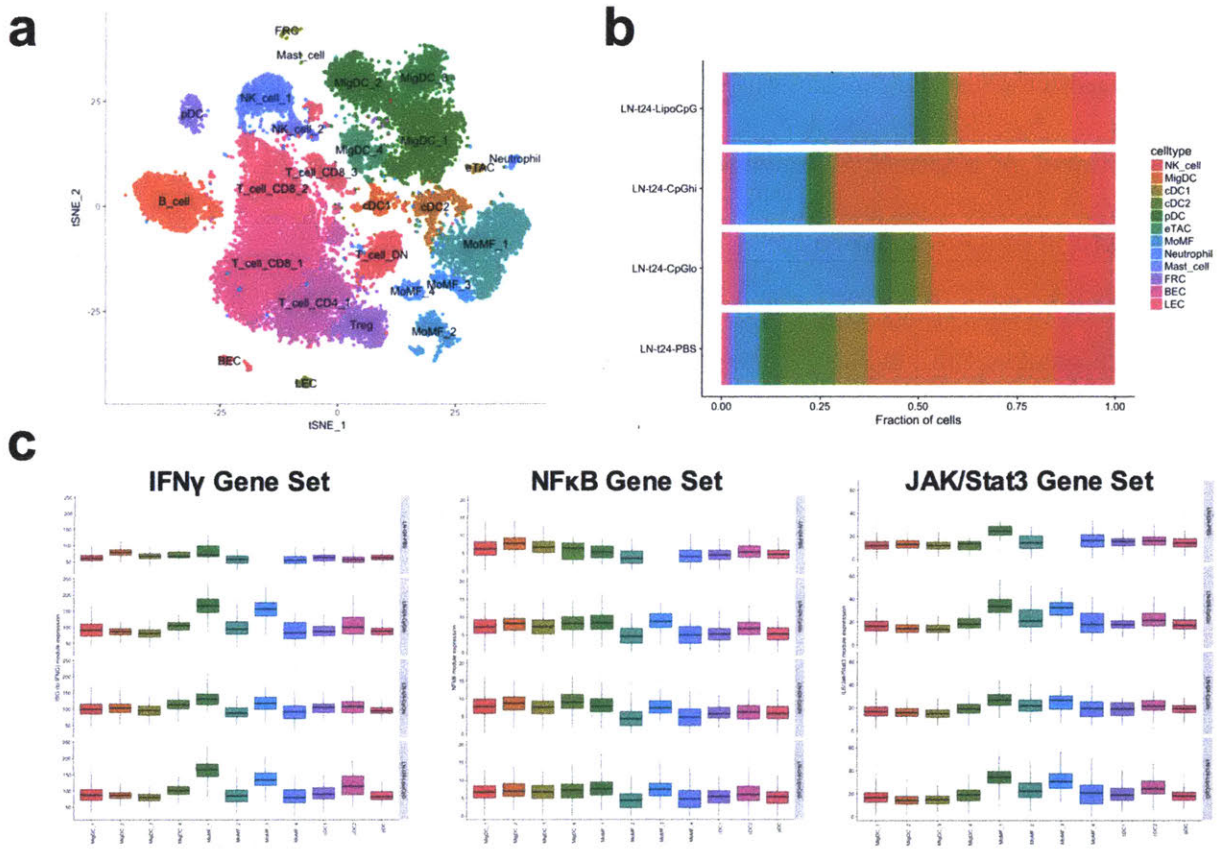

Figure 5.2. Single-cell RNA-seq analysis of CpG-treated lymph nodes

(**a-c**) Mice were s.c. immunized with PBS, 1 nmol CpG, 5 nmol CpG, or 1 nmol lipo-CpG mixed with ovalbumin. The draining inguinal LNs were excised 24h later and assessed by scRNA-seq (n = 1 mouse/group). (**a**) Shown is a tSNE plot of identified cell types. (**b**) Distribution of all identified cells per sample. (**c**) Gene set analysis of the indicated signaling pathways, where each row represents a different sample, and each column represents a distinct cell type.

The scRNA-seq data begged the question whether monocytes are drivers of immune activation or instead downstream responders to a distinct initiation event. To address this question, we utilized flow cytometry to understand the cellular biodistribution of CpG relative to lipo-CpG in the dLN, with the hypothesis that cell types that took up adjuvant were the likely initiators of the response. Consistent with the notion that monocytes are likely drivers, we found TAMRA-labeled lipo-CpG to preferentially accumulate in activated (Ly6C+) monocytes and macrophages, in addition to all other CD11b+ myeloid cells analyzed (neutrophils, and

CD11b+ cDC2s) (**Fig 5.3a**). Conversely, and unexpectedly, high dose TAMRA-CpG tended to segment into NK1.1+ cells, including NK cells and NKT cells (**Fig. 5.3a**). Thus, although high dose CpG equivalently drained into the dLN as measured by IVIS (**Fig. 5.1a,b**), cellular uptake was strikingly different between CpG and lipo-CpG.

We found that lipo-CpG not only segmented into monocytes/macrophages, but also expanded their numbers, validating the similar observation made with scRNA-seq (**Fig. 5.2b**), while high dose CpG instead only expanded NKT cells over PBS control (**Fig. 5.3b**). To understand the mechanism for monocyte expansion in the case of lipo-CpG immunization, but not high dose CpG immunization, we returned to the scRNA-seq dataset to analyze gene expression differences in monocytes between the two conditions. Among a cluster of genes upregulated in lipo-CpG treated monocytes were chemokines including CXCL10 and CCL2 that induce monocyte recruitment (**Fig. 5.3c**). Collectively, these data suggest that lipo-CpG distributes in a biased fashion to monocyte cell populations and facilitates a positive feedback loop, whereby activated monocytes trigger the chemoattraction of additional monocytes, inducing significant increases in numbers of activated monocytes in the dLN.

Previous studies have shown that CpG can stimulate IL-12 production by monocytes, leading us to hypothesize that lipo-CpG may further potentiate this effect. To assess this, we immunized mice with CpG or lipo-CpG, excised lymph nodes 24 hours later, and isolated monocytes using negative magnetic bead selection. After culturing primary monocytes for 48 hours without any additional treatment, we measured IL-12p70 production in culture media via ELISA; we observed 9.3-fold higher concentrations of IL-12p70 in the conditioned media of lipo-

CpG-immunized monocytes than of CpG-immunized monocytes (**Fig. 5.3d**). To confirm the functional significance of IL-12 in vaccination, we administered an anti-IL-12p40 depleting monoclonal antibody throughout the 20-day prime/boost vaccination timecourse, and found that IL-12 depletion eliminated the advantage of lipo-CpG over CpG as an adjuvant in stimulating potent anti-Ova CD8+ T cell responses (**Fig. 5.3e**). We conclude that the potentiating effect of lipo-CpG is dependent on IL-12, and that monocytes are an important contributor of IL-12 to the cytokine milieu in the dLN.

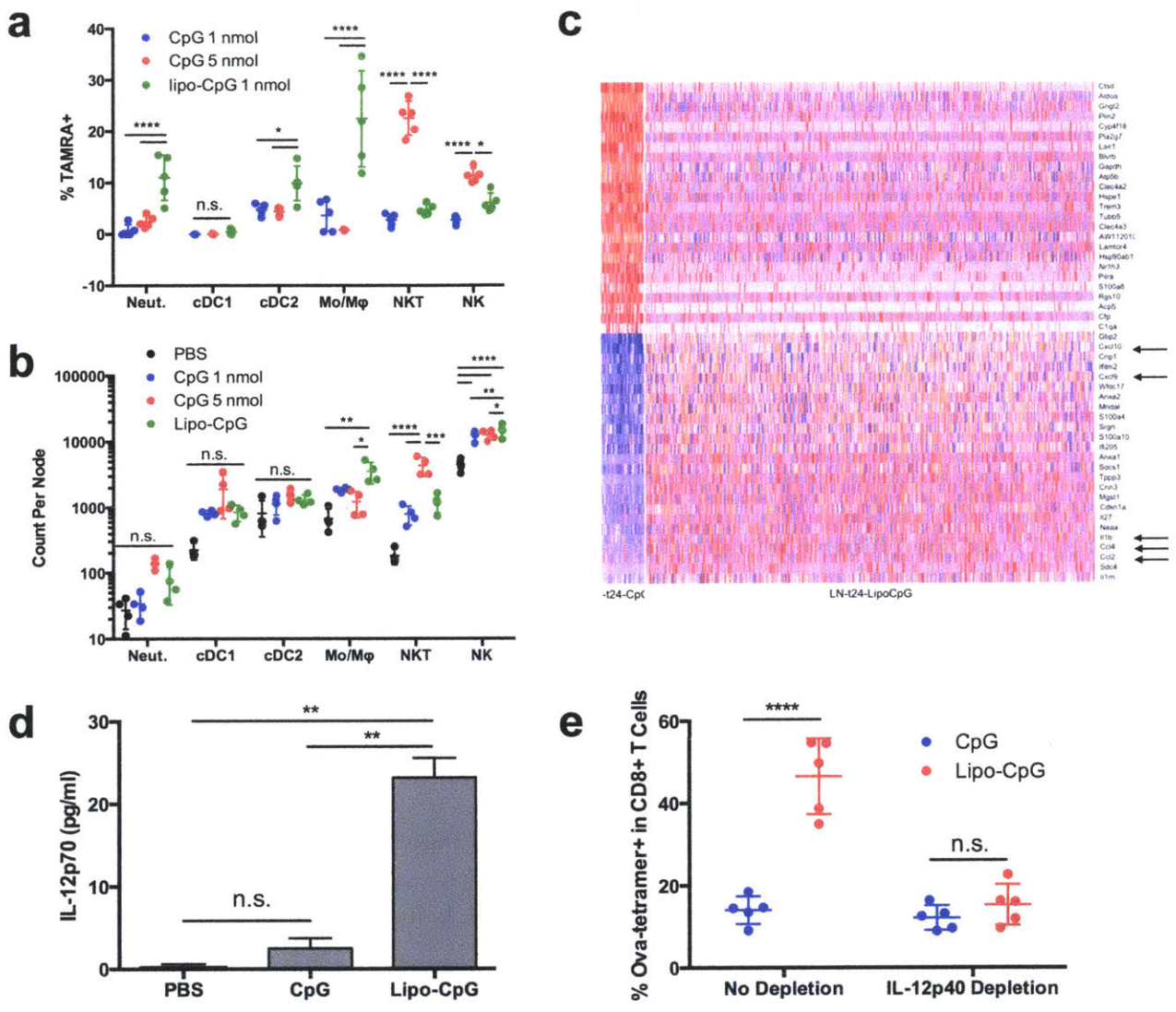

Figure 5.3. Lipo-CpG is uptaken by monocytes and induces proliferation and IL-12 secretion

(**a**) Mice were s.c. immunized with TAMRA-labeled 1 nmol CpG, 5 nmol CpG, or 1 nmol lipo-CpG and ovalbumin. 24h later, the draining inguinal LNs were excised, digested into single cell suspensions, and analyzed by flow cytometry. Shown here are the percent TAMRA+ cells within each identified cell type (*n* = 5 mice/group). (**b**) As in (**a**), mice were s.c.immunized with indicated CpG variant mixed with ovalbumin, and dLNs were digested and analyzed by flow cytometry to assess cell number (n = 4 mice/group). (**c**) Clustered gene expression differences from scRNA-seq within monocytes from high dose CpG and lipo-CpG treated mice (n = 1 mouse/group). (**d**) 15 mice were s.c. treated with either PBS, CpG, or lipo-CpG mixed with ovalbumin. After 24h, the dLNs were isolated, pooled, and isolated monocytes cultured for 48h. IL-12p70 concentrations in media were assessed by ELISA (samples run in duplicate). (**e**) Over the time-course of a prime/boost vaccination with either CpG or lipo-CpG and ovalbumin, mice were either not treated with depleting antibody, or treated with IL-12p40 depletion antibody. Six days after boost, Ova-specific CD8+ T cell response magnitude was assessed by tetramer stain (n = 5 mice/group). * $P < 0.05$; ** $P < 0.01$; *** $P < 0.001$; **** $P < 0.0001$ by two-way ANOVA with Tukey's multiple comparisons test within each cell type (**a-b**), one-way ANOVA with Tukey's multiple comparisons test (**d**), or two-tailed t tests at each condition with Holm-Sidak multiple comparisons test (**e**).

The role of dendritic cells in the lipo-CpG response

Although we observed insignificant accumulation of lipo-CpG in cDC1s (**Fig. 5.3a**) and no difference in expansion of cDC1s between lipo-CpG and CpG (**Fig. 5.3b**), we reasoned that it nonetheless possible that cDC1s played a part in the lipo-CpG response, given their important role as professional antigen presenting cells. We first assessed the activation status of cDC1s: while there was a trend to higher activation among cDC1s, as measured by CD86 staining, results were not statistically significant and unlikely to explain the dramatic differences we observed in vaccine efficacy between CpG and lipo-CpG (**Fig. 5.4a**). However, when Batf3$^{-/-}$ mice that lack cDC1s were vaccinated with optimal E7 peptide and lipo-CpG, the immune response was significantly blunted relative to wild-type animals (**Fig. 5.4b**). Note that the typical cross-presentation role of cDC1s was not involved in this study, because the optimal E7 peptide does not require uptake and processing to load onto MHC. Collectively, we conclude that although lipo-CpG does not preferentially act on cDC1s in terms of activation or expansion, vaccines that utilize lipo-CpG as an adjuvant are nonetheless dependent on cDC1s, likely for direct T cell priming.

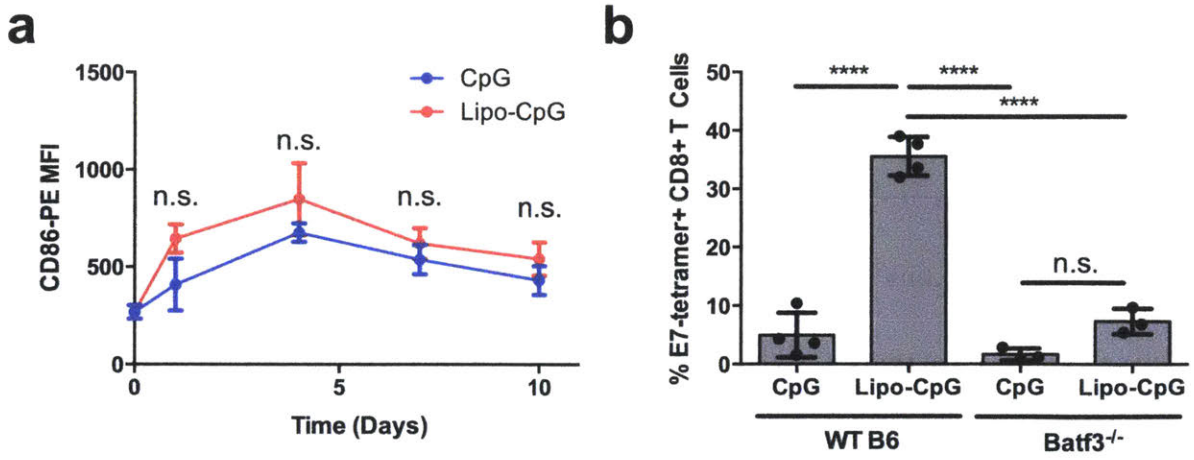

Figure 5.4. Cross-presenting dendritic cells are indispensible to lipo-CpG adjuvanted vaccine responses

(**a**) Mice were s.c. immunized with CpG or lipo-CpG, and the inguinal LNs excised at the indicated time points. Following digestion, CD8+ DCs were assessed for CD86 expression by flow cytometry (n = 3 mice/group). (**b**) Wild-type C57BL/6J or Batf3$^{-/-}$ mice were prime/boost vaccinated with E7 peptide adjuvanted either with CpG or lipo-CpG. Six days after boost, CD8+ T cells in peripheral blood were assessed for E7-specificity via tetramer stain. **** $P < 0.0001$ by two-tailed t tests with Holm-Sidak multiple comparisons test at each time point (**a**) or two-way ANOVA with Tukey's multiple comparisons test (**b**).

IL-12 triggers an IFNγ-directed cytokine milieu in the dLN

The ability of IL-12 to trigger robust IFNγ production by NK cells is well characterized[146,147]. Indeed, as expected, IFNγ was among the genes upregulated in NK cells from scRNA-seq of mice immunized with lipo-CpG compared to mice immunized with high dose CpG (**Fig. 5.5a**). To better characterize the cytokine milieu generated by lipo-CpG compared to CpG, we homogenized the dLN 24 hours after immunization and analyzed cytokine and chemokine concentrations with luminex. When analyte concentrations from lipo-CpG immunized nodes were normalized by concentrations from CpG immunized nodes, we found that several top upregulated cytokines and chemokines could be traced back to an IFNγ-driven network (**Fig. 5.5b**). IFNγ stimulates IL-6 development, which triggers production of

CXCL10 and LIF[148-150]. We were surprised to not find evidence of IL-12 production, but believe that IL-12 may be consumed too rapidly to be appropriately detected.

Although T cells are potent producers of IFNγ in addition to NK cells, at the 24 time point, innate immune cells should dominate the response, so we focused on assessing the propensity of NK cells to produce IFNγ in response to lipo-CpG vaccination. To directly assess whether lipo-CpG immunization *in vivo* leads NK cells to produce more IFNγ than CpG immunization, we excised the dLN from mice that received PBS, 1 nmol CpG, 5 nmol CpG, or 1 nmol lipo-CpG and performed intracellular cytokine staining (ICS) on recovered NK cells to stain for IFNγ. We found that a greater frequency of NK cells from lipo-CpG vaccinated mice produced IFNγ than from CpG vaccinated mice (**Fig. 5.5c**), and that cell-by-cell NK cells from lipo-CpG vaccinated mice produced more IFNγ as well, as measured by MFI (**Fig. 5.5d**).

To understand whether IL-12 is an upstream activator of IFNγ production, we performed a similar ICS study on NK cells from mice vaccinated with CpG or lipo-CpG, with or without IL-12 depletion. Whether mice were immunized with CpG- or lipo-CpG-containing vaccines, IL-12 depletion inhibited IFNγ production, demonstrating that IL-12 triggers an IFNγ response in NK cells in both cases (**Fig. 5.5e**). We conclude that IL-12 from monocytes initiates an IFNγ response that directs the generation of an inflammatory cytokine milieu in the dLN following lipo-CpG vaccination.

The importance of NK cells and their IFNγ product was assessed by administation of depleting antibodies against NK1.1 or IFNγ throughout the timecourse of a prime/boost

immunization schedule with CpG or lipo-CpG mixed with ovalbumin, and found that both depletions reduced the CD8+ T cell responses to ovalbumin; IFNγ depletion erased any advantage lipo-CpG had over CpG, while NK cell depletion still allowed lipo-CpG to generate an anti-ova response with twice the magnitude of the CpG-mediated response (**Fig. 5.5f**). This suggests that perhaps over the entire course of an immune response, IFNγ from alternative sources, like activated T cells, can partially compensate for the lack of NK cells.

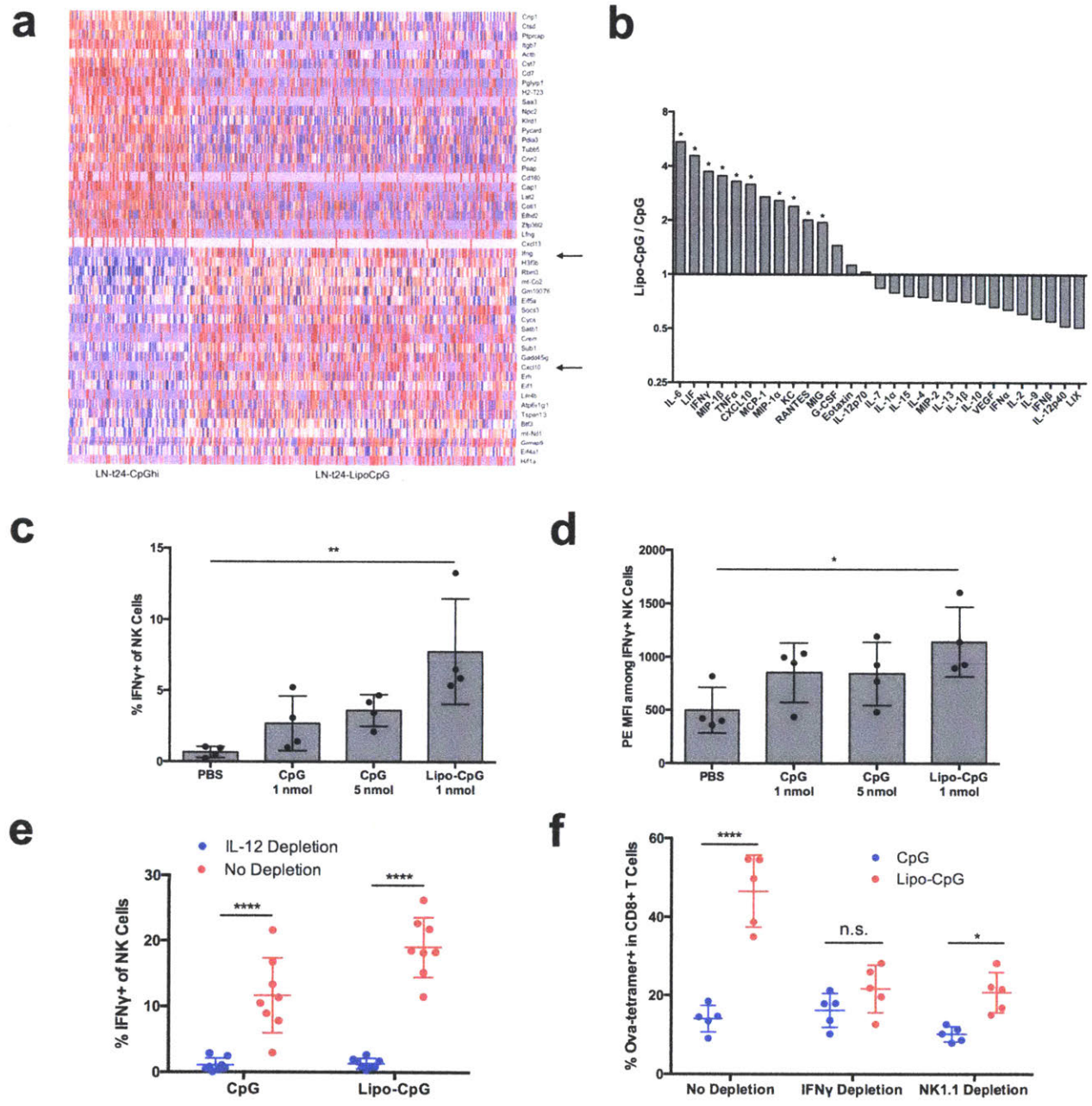

Figure 5.5. Lipo-CpG induces an NK-cell mediated IFNγ-driven cytokine/chemokine milieu

(**a**) Clustered gene expression differences from scRNA-seq within NK cells from high dose CpG and lipo-CpG treated mice (n = 1 mouse/group). (**b**) 24h after s.c. immunization with CpG or lipo-CpG and ovalbumin, dLNs were excised, homogenized, and supernatant analyzed for cytokine/chemokine concentration by luminex analysis. Shown are concentrations from lipo-CpG immunized mice divided by concentrations from CpG immunized mice with analytes ranked accordingly (n = 5 mice/group). (**c-d**) Mice were immunized with the indicated CpG variant and ovalbumin; 24h later, NK cells in the dLN were assessed for IFNγ production by intracellular cytokine staining (n = 4 mice/group). Shown are the frequency of IFNγ+ NK cells in each group (**c**) and the degree of IFNγ production by MFI (**d**). (**e**) Mice were immunized with CpG or lipo-CpG and ovalbumin, and IFNγ production assessed by NK cells as in

(**c-d**) but with or without IL-12 depletion (n = 8 mice/group). (**f**) Over the time-course of a prime/boost vaccination with either CpG or lipo-CpG and ovalbumin, mice were either not treated with depleting antibody, or treated with IL-12p40 or NK1.1 depletion antibody. Six days after boost, Ova-specific CD8+ T cell response magnitude was assessed by tetramer stain (n = 5 mice/group). * $P < 0.05$; ** $P < 0.01$; **** $P < 0.0001$ by two-tailed t test with Holm-Sidak multiple comparisons test between CpG and lipo-CpG for each analyte (**b**) or at each condition on the x-axis (**e-f**), or by one-way ANOVA with Dunnett's multiple comparisons test against PBS (**c-d**).

The cytokine milieu generated by lipo-CpG shapes the phenotype of the T cell response

While we have already demonstrated that IFNγ and IL-12 can collectively produce a positive feedback loop to recruit and activate monocytes and APCs, we also hypothesized that they may directly contribute to the T cell response, and may explain why lipo-CpG is able to generate responses of such high magnitude. High levels of IL-12 and IFNγ can trigger the expression of the transcription factor T-bet and induce a short-lived effector cell (SLEC) phenotype as opposed to a memory precursor effector cell (MPEC) phenotype[151]. During highly inflammatory immune responses in secondary lymphoid organs, where IL-12 and IFNγ are produced to high concentrations, the immune responses tends to favor the generation of SLECs to protect against potentially lethal infections, triggering higher magnitude responses that may suffer from poor memory formation. SLECs and MPECs can be catagorized by the expression of KLRG-1 and CD127 staining (**Fig. 5.6a**).

Following prime/boost vaccination with CpG or lipo-CpG, antigen-specific T cells were assessed for T-bet expression and SLEC/MPEC phenotype. We found that the frequency of T-bet+ CD8+ T cells was increased in animals administered lipo-CpG relative to CpG (**Fig. 5.6b**).

Consistent with an increase in T-bet expression, lipo-CpG generated both a higher frequency of SLECs than CpG (**Fig. 5.6c**), and also a greater total number of antigen-specific SLECs in circulation (**Fig. 5.6d**). Converseley, CpG promoted a higher frequency of MPECs than lipo-CpG (**Fig. 5.6e**); however, the overall much larger number of antigen-specific T cells following lipo-CpG immunization ensured that the total number of MPECs in circulation remained greater from lipo-CpG vaccination than from CpG vaccination in spite of the bias towards SLEC differentiation (**Fig. 5.6f**). This raises the exciting possibility that lipo-CpG may be able to simultaneously trigger a high magnitude response without sacrificing a long-term memory response.

To confirm that these phenotypic differences were dependent on the cytokine milieu, we measured KLRG1 and CD127 expression on antigen-specific T cells from mice that had been depleted of NK cells, IL-12p40, and IFNγ. Note that we have already shown that all three depletions decrease the magnitude of the antigen-specific T cell response among lipo-CpG vaccinated mice, but here we assessed the phenotype of antigen-specific cells. We found that IL-12p40 depletion resulted in the loss of any statistical difference in SLEC frequency between CpG and lipo-CpG, that IFNγ depletion decreases the SLEC phenotype among lipo-CpG vaccinated animals, and that NK cell depletion allows the SLEC phenotypic differences between CpG and lipo-CpG to persist (**Fig. 5.6g**). Collectively, these data are consistent with the literature, which suggests that IL-12 is the primary driver of T-bet expression but that IFNγ can potentiate its effects, and that, as we saw earlier, other cells may be able to compensate for NK cells in the production of cytokines.

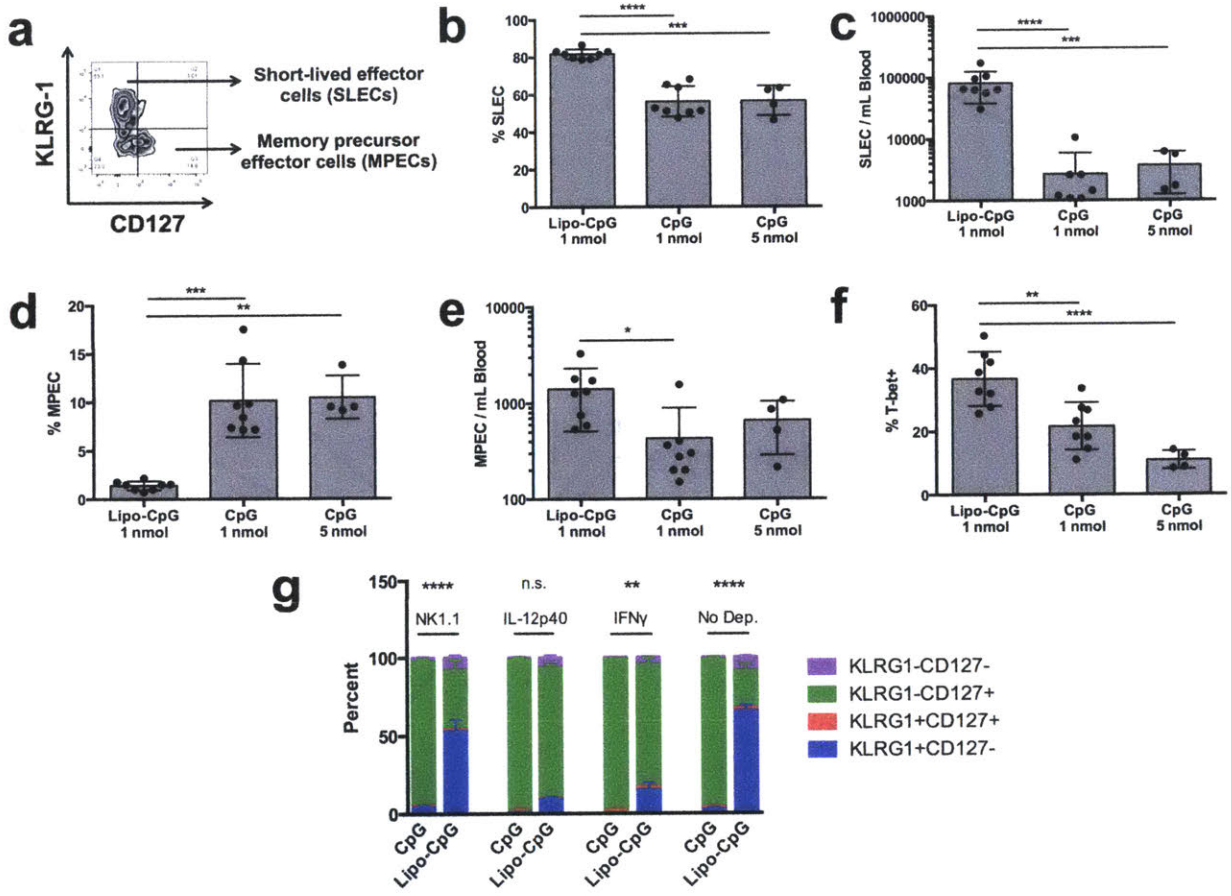

Figure 5.6. The lipo-CpG driven cytokine milieu generates large numbers of short-lived effector T cells

(**a**) Representative gating scheme within antigen-specific T cells to identify short-lived effector cells and memory precursor effector cells. (**b-e**) Following prime/boost vaccination with 1 nmol lipo-CpG, 1 nmol CpG, or 5 nmol CpG combined with ovalbumin, tetramer+ CD8+ T cells were assessed for SLEC and MPEC phenotyping (n = 4-8 mice/group). Shown are relative frequencies (**b, d**) and absolute numbers in blood (**c, e**). (**f**) Following prime/boost vaccination with indicated adjuvant and ovalbumin, tetramer+ CD8+ T cells were assessed for T-bet expression (n = 4-8 mice/group). (**g**) KLRG1 and CD127 expression was analyzed among ovalbumin-specific CD8+ T cells after CpG or lipo-CpG adjuvanted prime/boost ovalbumin vaccination with or without the indicated depletion treatments. * $P < 0.05$; ** $P < 0.01$; *** $P < 0.001$; **** $P < 0.0001$ by one-way ANOVA with Tukey's multiple comparisons test (**b-f**) or two-tailed t tests within each depletion condition with Holm-Sidak multiple comparisons test, comparing the KLRG1+CD127- SLEC population frequencies (**g**).

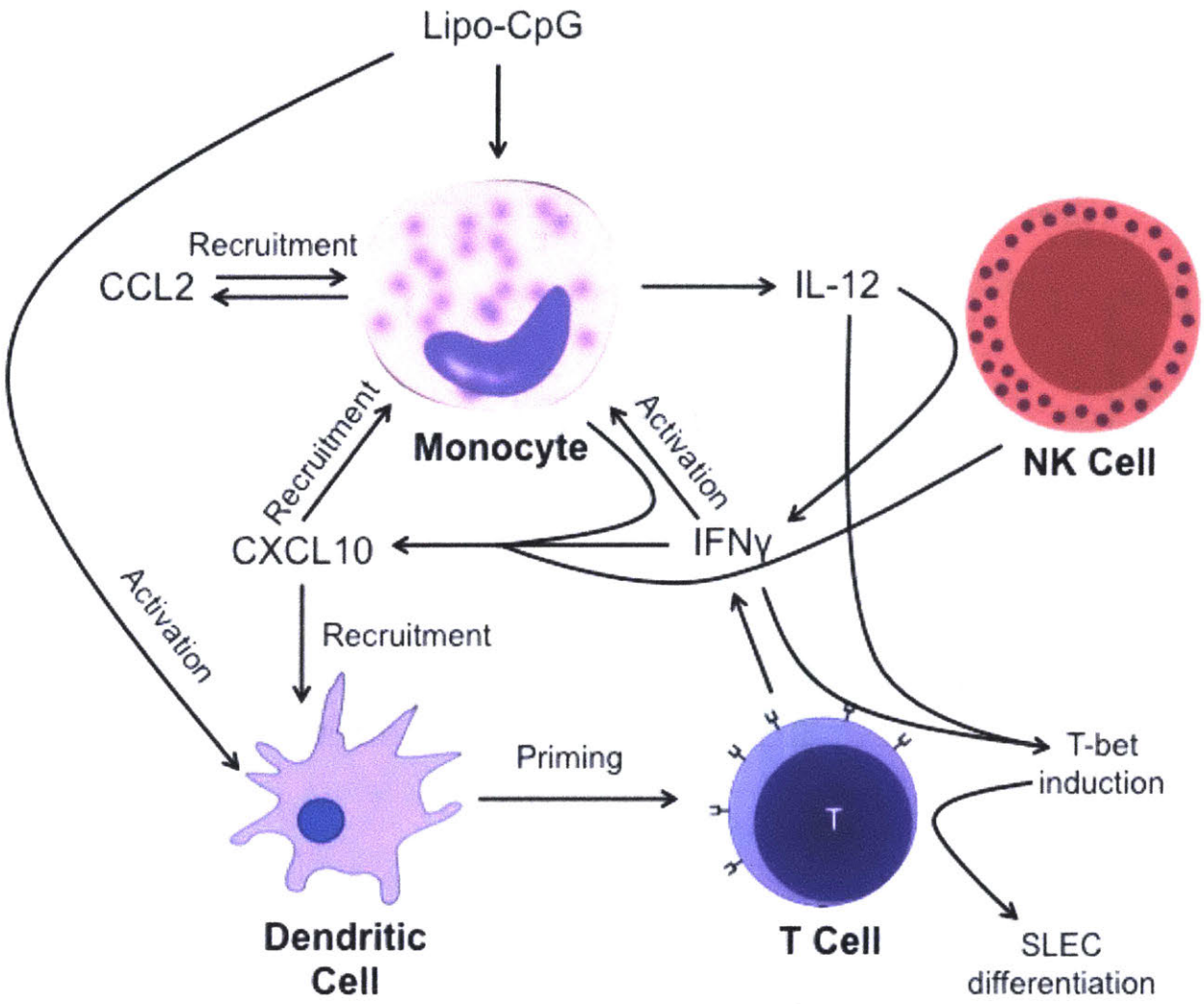

Figure 5.7. Model of lipo-CpG efficacy

Schematic representing the proposed mechanism of action of lipo-CpG. Initial uptake by monocytes triggers an IL-12 driven signaling cascade that modulates the cytokine/chemokine milieu to further recruit antigen-presenting cells and trigger appropriate T cell differentiation.

5.3 Materials and Methods

Mice

B6 mice (C57BL/6NTac) were purchased from Taconic. Batf3$^{-/-}$ mice (B6.129S(C)-Batf3^{tm1Kmm}/J) were purchased from the Jackson Laboratory. All animal work was conducted

under the approval of the Massachusetts Institute of Technology (MIT) Division of Comparative Medicine in accordance with federal, state, and local guidelines.

Vaccinations

All vaccinations were comprised of 10 μg ovalbumin and 1 nmol or 5 nmol of ODN1826 (CpG) (InvivoGen), with or without DSPE-PEG conjugation. DSPE-PEG conjugated ODN1826, or lipo-CpG, was prepared as previously reported[43]. All vaccines were administered s.c. at the tail base. To measure T cell responses, mice were primed on day 0, boosted on day 14, and read-out on day 20. All mechanistic studies (including scRNA-seq, Luminex, biodistribution, monocyte isolation, and IFNγ detection from NK cells) were performed 24 hrs after a single vaccination.

Flow cytometry

Antibodies against CD16/32 (Fc block, clone 93), CD8α (53-6.7), KLRG1 (2F1), CD127 (A7R34), T-bet (4B10), IFN-γ (XMG1.2), CD3 (17a2), B220 (RA3-6B2), NK1.1 (PK136), CD11b (M1/70), CD11c (N418), Ly6C (HK1.4), Ly6G (1A8), and CD86 (GL-1) were purchased from BioLegend. Cell viability was assessed with DAPI (Sigma) for tetramer stains and LIVE/DEAD fixable aqua dead cell stain (Thermo Fisher Scientific) for all other studies. *Tetramer staining:* Ova tetramer (iTAg Tetramer/PE - H-2 Kb OVA) was purchased from MBL; during tetramer staining, PBMCs were Fc blocked and stained with tetramer for 15 minutes prior to addition of anti-CD8α antibody, and cells were incubated with all antibodies for another 30 minutes. All labeling was performed in PBS + 0.1% BSA. *Intracellular staining:* Following surface labeling, cells were fixed and permeabilized using BD Cytofix/Cytperm fixation/permeabilization kit per manufacturer

instructions for IFNγ detection in NK cells, or using BioLegend True-Nuclear Transcription Factor Buffer Set per manufacturer instructions for T-bet detection in T cells. *Organ processing:* In studies where dendritic cells and/or other APCs were assessed by flow cytometry, LNs were excised, digested in RPMI-1640 + 0.8 mg/ml collagenase/dispase (Sigma) + 0.1 mg/ml DNase I (Sigma), mashed through 74 μm Netwell inserts, and washed into PBS + 0.1% BSA prior to antibody staining. Cells were analyzed using BD FACSCanto and BD FACS LSR Fortessa, and data were analyzed using FlowJo.

Biodistribution studies

IVIS imaging: 1 nmol or 5 nmol TAMRA-labeled CpG or lipo-CpG was injected s.c. at the tail base; the inguinal LN was excised 24 hours later and imaged on an IVIS Spectrum Imaging System (Caliper Life Sciences), excitation: 535 nm, emission: 580 nm. *Cellular biodistribution: :* 1 nmol or 5 nmol TAMRA-labeled CpG or lipo-CpG was injected s.c. at the tail base; the inguinal LN was excised 24 hours later and processed for single cell analysis (see flow cytometry section).

Cytokine/chemokine analysis

IL-12p70 production from monocytes: 1 nmol or 5 nmol CpG or lipo-CpG and 10 μg ovalbumin was injected s.c. at the tail base (n = 15 mice per group). 24 hours later, LNs were excised and mashed through 74 μm Netwell inserts to prepare single cell suspensions, and all cells from nodes from a given group pooled. Monocytes were enriched using EasySep Mouse Monocyte Isolation Kit (EasySep). A total of 100-200k monocytes were isolated for each group and plated

in single wells of a 96 well plate in RPMI-1640 + 10% FBS for 48 hours at 37°C and 5% CO_2. Following incubation, cells were spun down, and supernatant assessed for IL-12p70 content with Mouse IL-12p70 Uncoated ELISA Kit (Thermo Fisher Scientific) per manufacturer instructions. *Luminex analysis*: 24 hours after immunization, draining inguinal LNs were excised and kept in 250 µl PBS and protease inhibitors (Protease Inhibitor Tablets from Roche) prior to homogenization. LNs were homogenized using a Mini-Beadbeater. Debris was spun away at max speed, and 200 µl of supernatant collected. Protein concentration was estimated using the Warburg-Christian approximation (protein concentration in mg/ml = 1.55*A280 – 0.76*A260) and samples were diluted in PBS and protease inhibitors to a concentration of 0.4 mg/ml. Samples were submitted to Eve Technologies for analysis with Mouse Cytokine Array / Chemokine Array 31-Plex. During analysis, original concentrations were calculated based on dilution factor.

Depletion studies

Antibodies against IL-12p40 (C17.8), IFNγ (XMG1.2), and NK1.1 (PK136) were purchased from BioXCell. For mechanistic studies measured 24 hrs after immunization, mice were administered depletion antibodies once 24 hrs before vaccination. For full prime/boost vaccination studies, mice were administered depletion antibodies throughout the time-course of the study, starting 24 hrs before prime. Dosing and frequency of depletion: 400 µg of anti-IL-12p40 and anti-NK1.1 administered every 4 days; 600 µg of anti-IFNγ administered every 2 days.

Statistical analysis

All statistical analyses were performed using GraphPad Prism software. The specifics of the statistical test performed, p-values, and number of replicates are stated in the figure legends. For all tests, the threshold for significance was $P < 0.05$.

5.4 Conclusions

In this study, we elucidated a mechanistic explanation for how lipo-CpG functions in relation to CpG. In contrast to previous work suggesting that lipo-CpG gains efficacy over CpG due to improved lymph node uptake and retention, here we show that even if CpG is dosed such that it is equivalently uptaken relative to lipo-CpG, it fails to replicate the efficacy of lipo-CpG in a vaccination study. The primary reason for this is that lipo-CpG preferentially segments into activated monocytes following immunization, whereas CpG is distributed into NK cell populations.

Because of its propensity to be uptaken by monocytes, lipo-CpG triggers a cascade of soluble factors that recruit and activate a wide host of antigen presenting cells while simultaneously inducing the massive proliferation of newly primed T cells (**Fig. 5.7**). Briefly, lipo-CpG induces the secretion of IL-12 from monocytes, triggering the production of IFNγ by NK cells, and both cytokines collectively induce the expression of T-bet in antigen-specific T cells. High T-bet expression leads to rapid T cell responses characterized by the induction of KLRG1+CD127- short-lived effector cells but not at the expense of memory progenitors. Additionally, positive feedback loops are initiated, whereby monocytes are continuously

activated by IFNγ and recruit additional monocytes by the production of chemokines including CXCL10 and CCL2. In summary, rather than directly acting on the dendritic cells that actively present antigen, lipo-CpG is highly effective at triggering a series of signals in trans to enhance the immune response.

5.5 Acknowledgements

Major thanks to Kelly D. Moynihan, Chensu Wang, and Kavya Rakhra for providing the lipo-CpG used in these studies. Additionally, all single-cell RNA-seq studies and data analysis were performed by Ang Cui from Nir Hacohen's lab; these results proved to be essential in honing in on monocytes as the upstream initiator of the inflammatory cascade outlined here.

CHAPTER 6. TOWARD THE DEVELOPMENT OF NOVEL PROTEIN-BASED TLR3 AGONISTS

Abstract

In subunit vaccination, adjuvants are required to provide the appropriate co-stimulation to facilitate productive T cell priming. One of the most common and well-studied classes of adjuvants is the Toll-like receptor (TLR) agonist. Upon engagement with their ligands, TLRs dimerize to trigger an inflammatory cascade that supports the immune response. While TLRs and their natural ligands are well characterized, there is a notable lack of protein-based TLR agonists. Here, we use yeast display to engineer the sso7d protein scaffold into binders of TLR3 in an attempt to make novel multimerized TLR3 agonists. Ultimately, we engineered high affinity binders to soluble TLR3 that nonetheless failed to bind cell surface-bound TLR3, and thus our goal of developing novel TLR3 agonists was unsuccessful. Along the way, however, we learned valuable lessons in sso7d engineering, most importantly the value of performing sorts in the presence of nucleases to prevent either sso7d or TLR3 from binding nucleic acids and skewing selection pressure.

6.1 Introduction

Despite the lofty claim by some that we are living in a golden age of adjuvant design and discovery[152], there remain many potential areas for improvement. If lymph node targeting is indeed important, we are for now limited to lipo-CpG[43]. However, a major limitation of the translational potential of lipo-CpG is that TLR9 is expressed on DCs in mice but only in B cells

and pDCs in humans[153]. Furthermore, there is a striking lack of protein adjuvants available for immunological research, limited to flagellin, a TLR5 agonist, which has been shown to be a weak inducer of cross presentation[154]. There are many benefits to using protein therapeutics as compared to small molecule adjuvants: proteins often have longer *in vivo* half-lives than small molecules; they can be engineered for improved specific to limit off-target effects; and finally, given directed evolution technology, their properties can be finely tuned.

In this work, we sought to engineer a novel protein-based TLR3 agonist for a number of reasons. First, studies have been conducted in both small animals and non-human primates to investigate which TLR is best suited to promote cross presentation. While work in small animals identifies TLR3 and TLR9 agonists as optimal adjuvants for T cell vaccines, work in rhesus macaques recommends the use of TLR3 and TLR7/8 targeting adjuvants[154,155]. The overlap of TLR3 makes future agonists more potentially translatable. Second, TLR3 is a well-understood receptor that benefits from a plethora of structural studies, including a solved crystal structure of its extracellular domain[156]. Third, crystal structures suggest that when TLR3 binds its natural ligand, double-stranded RNA, downstream activity is initiated by TLR3 homodimerization without conformational change[157]. This potential for success is enhanced by evidence that polyclonal anti-TLR3 antibodies can serve as weak activators[158]. Presumably, therefore, multimerized TLR3 binders may serve as effective agonists.

Here, we employed yeast surface display[159] to engineer the sso7d scaffold as a TLR3 binder[93]. Sso7d is a hyperthermophilic small (7 kDa) scaffold with a β sheet consisting of a flat DNA-binding surface with residues that can be randomized without introducing architectural

damage to the rest of the protein[92]. Because sso7d is a DNA binding protein, and TLR3 is an RNA binding protein, we found that selection buffers that include nucleases are necessary to select for true TLR3 binders. After the exploration of three different clones that bound soluble TLR3, however, we were unable to isolate a clone that bound surface displayed TLR3. As a result, multimerization of these binders failed to agonize TLR3 and serve as a novel adjuvant.

6.2 Results and Discussion

Optimizing the selection strategy

To select binders against TLR3, we first expressed TLR3 recombinantly: both the mouse and human TLR3 ectodomain were cloned and expressed in HEK cells. The protein product was biotinylated and a mass increase confirmed with MALD-TOF. We then iterated through a number of different selection strategies to optimize the generation of high affinity binders. In all selection strategies, initial bead sorts were performed with rcSso7d-11 and rcSso7d-18 libraries independently, then enriched libraries were pooled for subsequent bead sorts and flow sorts. Selections were performed at pH 5.5 to mimic the slightly acidic conditions of endosome, where TLR3 is expressed.

In the first selection strategy, yeast were enriched for mouse TLR3 (mTLR3) binding in PBS + 0.1% BSA pH 5.5. After two rounds of bead enrichment and three rounds of flow sorting, however, we sequences 84 clones and found enriched dominant sequences in the variable region: FNYHATWFI (T3.1, 10/84), HWRKRLKWR (6/84), YKHHHHWHI (T3.3, 7/84), and YHKKRWHWR (7/84). Notably, three of these sequences contain a high frequency of basic

residues that would result in highly positive charge at pH 5.5. We hypothesized that mTLR3 may be contaminated with nucleic acid, allowing us to select for highly positively charged binders to nucleic acids. Because sso7d is originally a nucleic acid binder, it may be geometrically optimized for nucleic acid binding, allowing for faster enrichment of DNA/RNA binders than TLR3 binders. Confirming this hypothesis, we found that measuring binding in buffer that included 20 μg/ml RNase A and 4 units/ml DNase I (at 1/500 dilutions from stock concentrations) could decrease binding of mTLR3 to T3.3, but not to T3.1 (**Fig. 6.1**), suggesting that selections in nuclease-containing buffer may be a viable way to avoid nucleic acid binders.

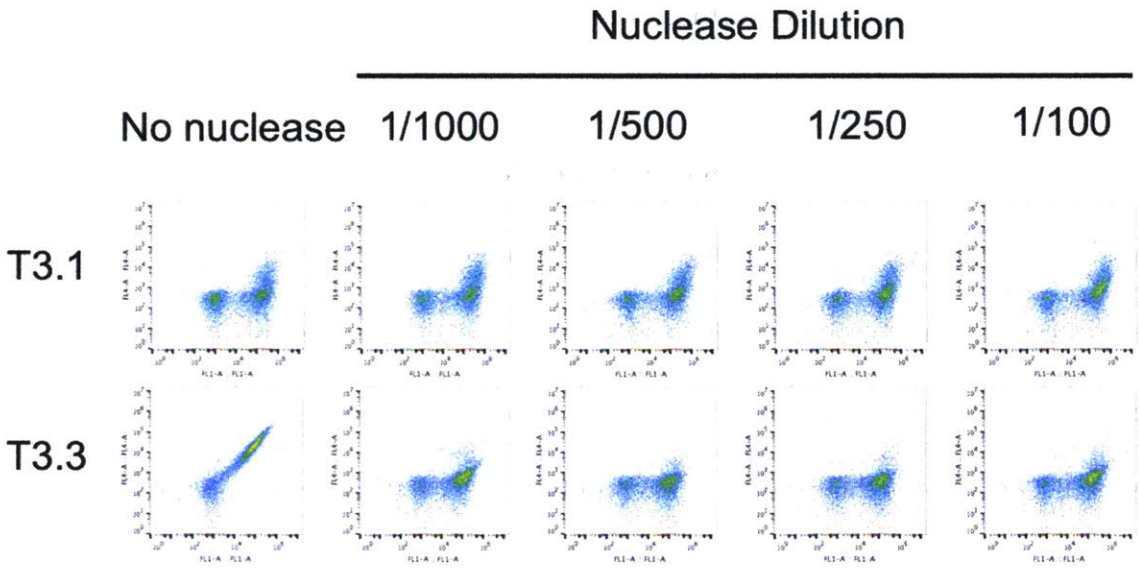

Figure 6.1. The inclusion of DNase I and RNase A in staining buffer can reduce binding to TLR3 via nucleic acids.

Shown are representative flow plots, with cmyc display on the x-axis and biotinylated TLR3 binding on the y-xaxis. T3.3 is a highly cationic binder whose binding is reduced by the inclusion of nucleases at the indicated dilutions, while the binding of T3.1 is unaffected.

Restarting with the naïve libraries, we again performed two bead enrichment rounds, followed by two flow cytometry sorts, this time with pH 5.5 buffer that included RNase A and

DNase I. However, upon sequencing the resulting library, we found no enriched clones. We conjectured that a more stringent selection strategy would be a more effective way to select promising binders, and so we initiated a third selection strategy that added two changes: 1) we measured display using HA detection rather that cmyc detection, because of other work in the lab suggesting that anti-cmyc antibodies may sterically hinder sso7d binding to antigen, and 2) we alternatively selected for binding against biotinylated mTLR3 and human TLR3 (hTLR3) to add selection pressure.

After two bead sorts and four flow sorts, we sequenced the library, chose six clones for further analysis, and chose to further pursue three: T3N.1 (LFVHYAVEL), T3N.3 (GHDWYWAIS), and T3N.4 (YDDYEMVFW). T3N.4 was a particularly interesting clone for its basic nature, whose anionic properties may mimic nucleic acids and thus facilitate productive binding and crosslinking of TLR3. Following subsequent rounds of error-prone PCR and affinity maturation, all three clones had Kd values of at least double-digit nM affinity (**Fig. 6.2**). All clones demonstrated stronger binding to hTLR3 than to mTLR3. Clones are annotated as T3N.x.y, where x represents the original clone number (1, 3, or 4) and y represents the number of affinity maturation rounds.

	Kd Measurements	
T3N.1 affinity maturation	mTLR3	hTLR3
T3N.1: ATVKFTYQGEEKQVDISKIKLVFRVGQHIYFAYDEGGGAVGEGLVSEKDAPKELLQMLEKQ	>10 μM	>10 μM
T3N.1.1: ATVKFTYQGEEKQVDISKIKLVFRVGQHIYVAYDEGGGAVGEGLVSKKDAPEELLQMLEKQ	570 nM	35 nM
T3N.1.2: ATVKFTYQGEEKQVDVSTIKLVFRVGQHIYIAYDEGGGAVGEGLVSKKDAPEELLQMLEEQ	92 nM	25 nM
T3N.1.3: ATVKFTYQGEEKRVDVSTIKLVFRVGQHIYIAYDEGGGAVGEGLVSKKDAPEELLQMLEEQ	29 nM	7.8 nM
T3N.3 affinity maturation		
T3N.3: ATVKFTYQGEEKQVDISKIKGVHRDGQWIYFWYDEGGGAAGIGSVSEKDAPKELLQMLEKQ	>10 μM	>10 μM
T3N.3.1: ATVKFTYYGEEKQVDVSKIKGVHRDGQWIYFWYDEGGGAAGIGSVSEKDAPKELLQMLEEQ	>10 μM	200 nM
T3N.3.2: ATVKFTYYGEEKQVAVSKIKGVHRDGQWIYFWYDEGGGAAGIGSVSEKDAPKELLQMLEEQ	230 nM	51 nM
T3N.3.3: AAVEFTYYGEEKQVAVSKIKGVHRDGQWIYFWYDEGGGAAGIGSVSEKDAPKELLQMLEEQ	95 nM	20 nM
T3N.4 affinity maturation		
T3N.4: ATVKFTYQGEEKQVDISKIKYVDRDGQYIEFMYDEGGGAVGFGWVSEKDAPKELLQMLEKQ	>10 μM	>10 μM
T3N.4.1: ATVKFAYQGGEKQVDISKIKYVDRDGQYIEFMYDEGGGAVGFGWVSEKDAPKELLQMLEEQ	>10 μM	30 nM
T3N.4.2: ATVKFAYQGGEKQVDISKIMYVDRDGQYIEFMYDEGGSAVGFGWVSEKDAPKELLQMLEEQ	>10 μM	13 nM
T3N.4.3: ATVKFAYQGGEKQVDISRIMYVDRDGQYIEFMYDEGGSTVGFGWVSEKDAPKELLQMLEEQ	160 nM	31 nM
T3N.4.4: ATVKFAYQGGEKQMDISRIMYVDRDGQYIEFMYDEGGSTVGFGWVSEKDAPKELLQMLEEQ	46 nM	6.0 nM

Figure 6.2. Summary of affinity maturation

Documentation of accumulated mutations and resulting affinity improvements during affinity maturation of original clones T3N.1, T3N.3, and T3N.4. The nine residues in red in the first row identify the original 9-residue rcSso7d paratope, while red residues in subsequent rows indicated accumulated mutations from error-prone PCR. Affinities were measured on the surface of yeast using flow cytometry at steady state conditions. mTLR3 is mouse TLR3 and hTLR3 is human TLR3.

Expression and characterization of binders

Monomeric T3N binders were expressed either as SUMO-fusions from *E. coli* or as transthyretin (TTR) fusions via HEK cells and assessed for maintained binding. We first confirmed that our selected proteins could bind recombinant TLR3: biotinylated T3N1.2, T3N3.2, and T3N4.3 were all capable of binding immobilized hTLR3 in ELISA format (**Fig. 6.3a**). We kindly received three reporter cell lines from Joshua Leonard's lab to help us assess binding to cell-expressed hTLR3: 1) control HEK that contains a GFP reporter cassette but no TLR3; 2) HEK TLR3 low that couples a GFP reporter to TLR3 engagement, but TLR3 is only expressed

intracellularly, as is physiologically relevant; 3) HEK TLR3 high that contains the GFP reporter but with TLR3 overexpression to the point that it is also expressed on the cell surface. However, biotinylated T3N1.2, T3N3.2, and T3N4.3 failed to bind TLR3 low or TLR3 high cells over control HEK background (**Fig. 6.3b**). We noticed that T3N.1.2 and T3N.4.2 both exhibited signal above secondary only background, suggesting that there may be some nonspecific binding propensity to these clones.

Using a biotinylated polyspecificity reagent prepared from HEK surface proteins, we assessed non-specific binding of our three clones at different stages of affinity maturation and found that both T3N.1 and T3N.4 increased their non-specificity during affinity maturation, although non-specificity was only apparent at pH 5.5, not in neutral conditions (**Fig. 6.3c**). This observation that non-specificity was driven by slightly acidic conditions was replicated on the cell surface, as T3N.1.1, T3N.3.1, and T3N.4.2 expressed as TTR fusions all bound control HEK cells non-specifically at pH 5.5, but not at pH 7.4 (**Fig. 6.3d**). To try and find conditions where our T3N moieties could bind hTLR3 on the cell surface without the confounding variable of non-specific binding, we asked at what pH values hTLR3 could be bound (with T3N displayed on yeast, and hTLR3 in soluble form), but unfortunately found that all three clones exhibited optimal binding at pH 5.5, where non-specificity was also apparent (**Fig. 6.3e**). However, we also observed that biotinylated poly(IC), a commonly used TLR3 agonist, also exhibited some non-specific binding to control HEK cells relative to secondary only control (**Fig. 6.3b**), motivating us to move to attempt and demonstrate activation with our T3N binders, even if direct binding to cell-expressed hTLR3 could not be demonstrated.

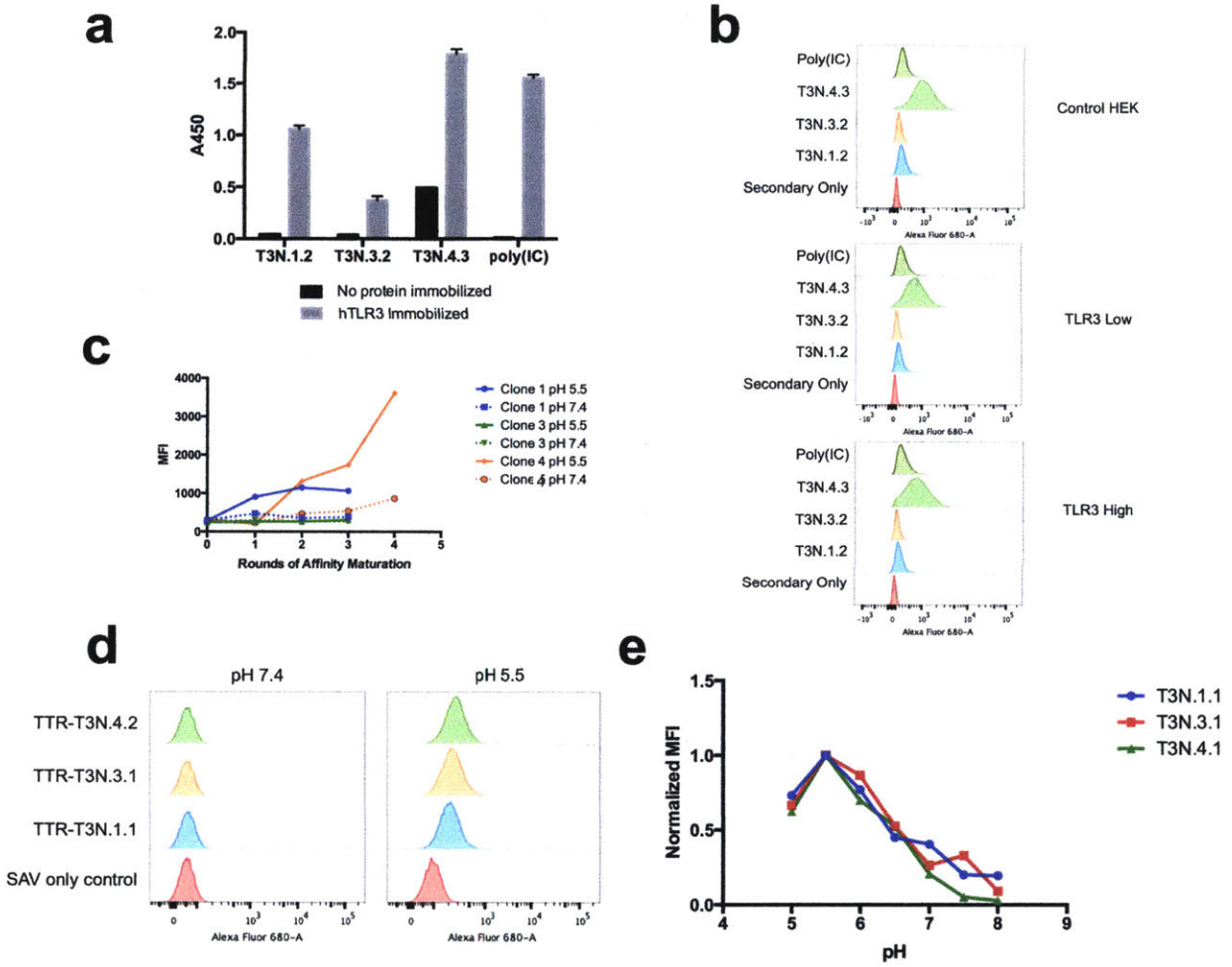

Figure 6.3. Selected clones bind recombinant but not surface-expressed TLR3

(**a**) The binding of the indicated biotinylated T3N clones (1 μM) or poly(IC) (1 μg/ml) to immobilized hTLR3 was measured via ELISA. (**b**) The indicated analytes were assessed for binding to the associated HEK cell lines by flow cytometry. (**c**) Shown are calculated MFIs of the indicated clone upon binding to biotinylated polyspecificty reagent and measured with flow cytometry. (**d**) Histograms depicting binding of the indicated analyte to control HEK cells that do not express hTLR3 on the cell surface. (**e**) T3N clones were displayed on yeast and binding to hTLR3 was assessed at the Kd at the indicated pH via flow cytometry.

Multimerization of binders and activation studies

Because TLR3 must be cross-linked to initiate downstream signaling, binders need to be multimerized to form agonists. We attempted several multimerization schemes including fusion: to TTR, a tetramer (**Fig. 6.4a**) either alone or along with 2.5F, an integrin-binding knottin that drives rapid internalization (**Fig. 6.4b**); fusion to the heavy and light chains of an irrelevant antibody (sm3e) (**Fig. 6.4c**) or the Fc region alone (**Fig. 6.4d**); directly stringing together three copies of binders without carrier protein (**Fig. 6.4e**); direct display on yeast (**Fig. 6.4f**); or display on avidin-coated beads (**Fig. 6.4g**). Unfortunately, however, none of these multimerization strategies proved effective at inducing activating hTLR3 on the HEK cell surface, as measured by GFP expression in reporter cell lines (**Fig. 6.5a-d**).

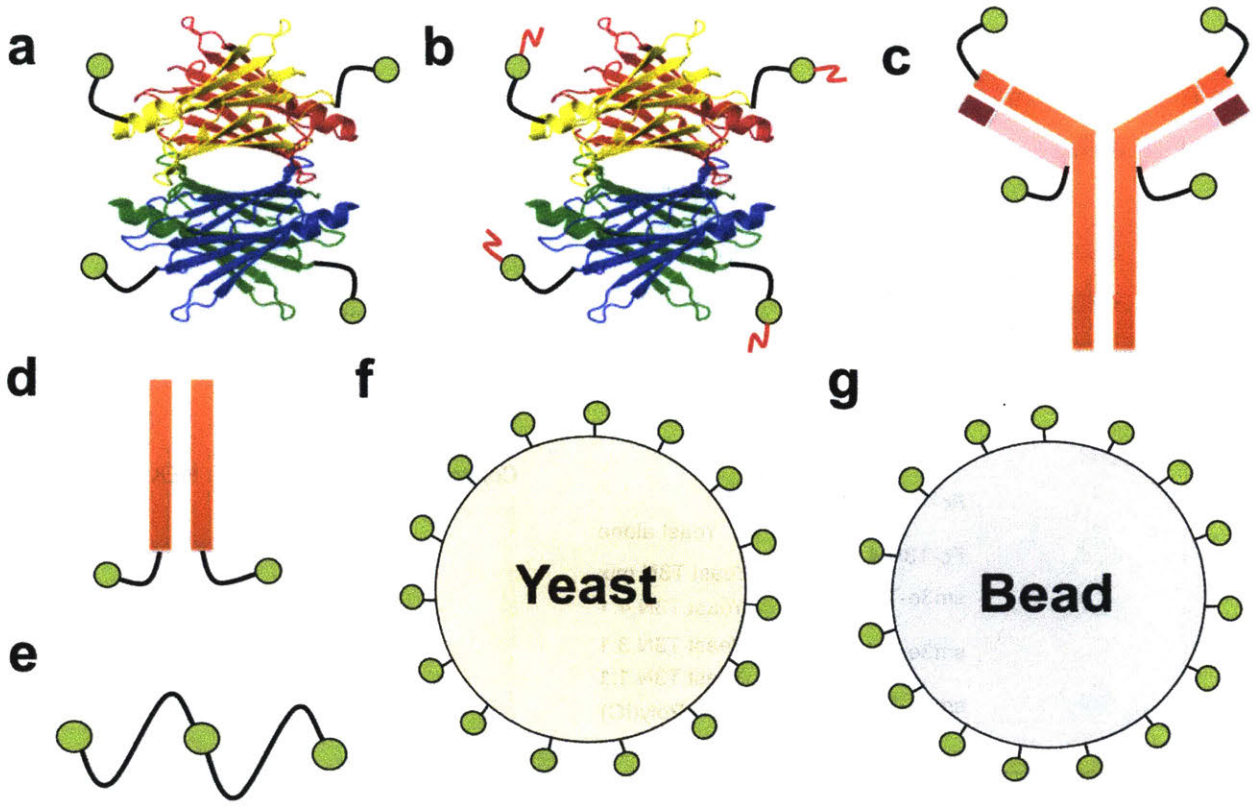

Figure 6.4. Schematics of the multimerization strategies attempted

(**a-b**) Fusion of T3N binders to the C-terminal end of tetramric TTR, either alone (**a**), or fused to 2.5F-Fc. In some iterations, plasmids encoding the different T3N clones were mixed to form a hetero-tetramer. (**c**) Fusion of T3N binders to sm3e via the N-terminus of the heavy chain and the C-terminus of the light chain. (**d**) Fusion to the C-terminus of the Fc fragment. (**e**) Three T3N binders attached via long flexible linkers. (**f**) T3N-expressing yeast clones following induction. (**g**) Biotinylated T3N binders attached to neutravidin-coated beads.

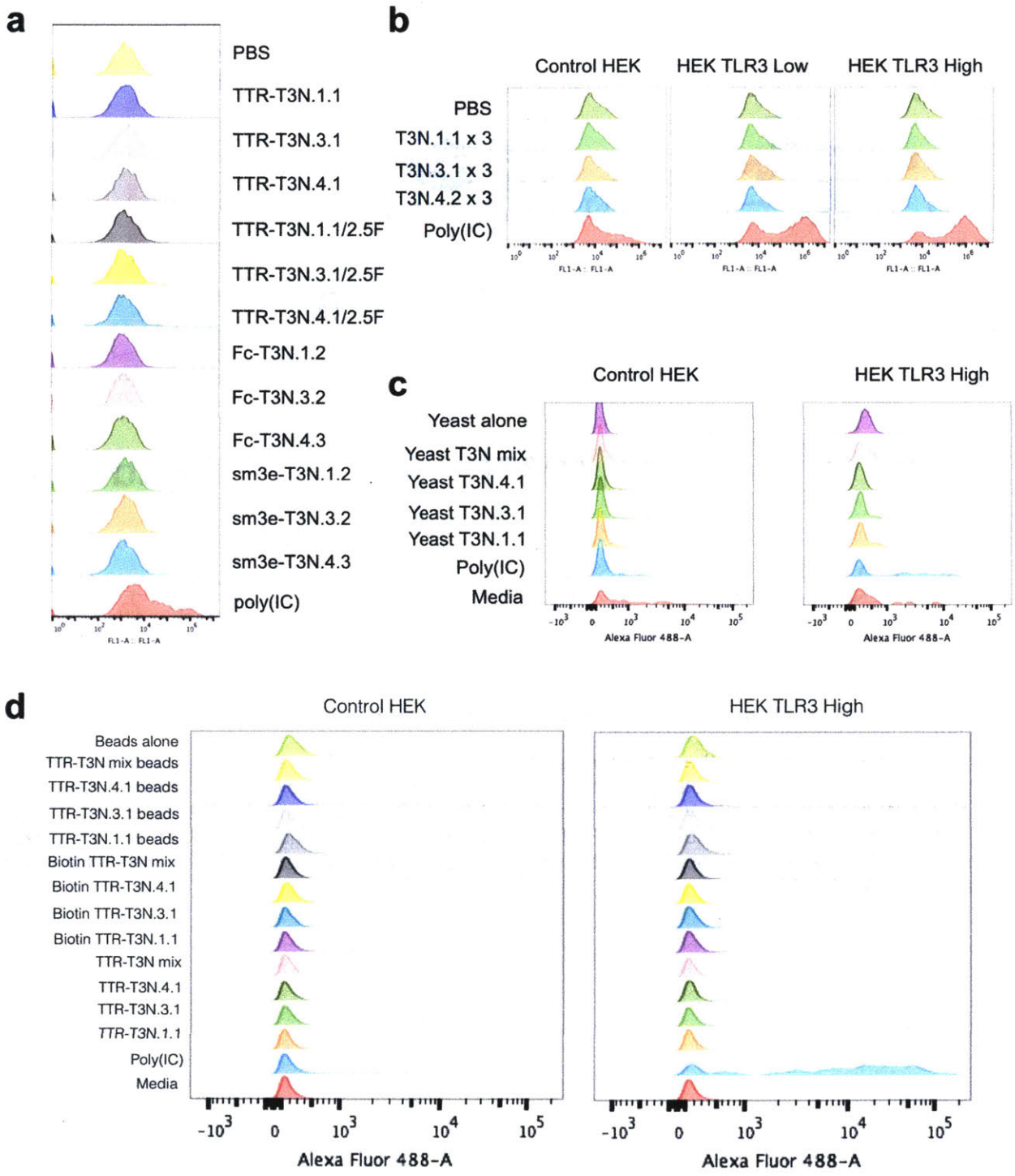

Figure 6.5. TLR3 activation studies

(**a-d**) Shown are representative histograms in the FL1/AF488 channel, measuring GFP expression in the indicated cell line (control HEK with no reporter, TLR3 low with endosomal TLR3 expression and NFκB-associated GFP expression, or TLR3 high with endosomal and surface TLR3 expression and NFκB-

associated GFP expression. In (**a**), TLR3 high cells are utilized. Poly(IC) is a positive control and media is a negative control.

6.3 Materials and Methods

Cells

HEK-FS cells (FreeStyle 293-F) were purchased from Thermo Fisher Scientific. Rosetta cells were purchased from Novagen. HEK 293 NEE cells (containing reporter only), HEK 293 NEE TLR3 Low (intracellular expression of TLR3 and reporter), and HEK 293 NEE TLR3 High (intracellular and extracellular expression of TLR3 and reporter) cells were kindly provided by Dr. Joshua N. Leonard. HEK-FS cells were cultured in FreeStyle 293 Expression Medium (Thermo Fisher Scientific) and passaged every two days to a density of 300k/ml. All mammalian cells were cultured at 37°C and 5% CO_2.

Protein production and characterization

Codon-optimized genes encoding desired proteins intended for mammalian expression were cloned into gWiz expression vectors (Genlantis) using the In-Fusion HD Cloning Kit (Clontech), prepared endotoxin free (Macherey-Nagel) and incubated with Opti-Pro (Thermo Fisher Scientific) and polyethylenimine (PEI) 25K (Polysciences) prior to drop-wise addition to HEK cell culture at 1 million cells/ml. 1 mg of DNA was mixed with 40 ml of Opti-Pro and 2 mg of PEI per 1 L of cell culture. One week after transfection, cell culture was spun down in endotoxin-free centrifuge tubes at 15000xg for 30 min, supernatant filtered, pH neutralized by addition of 10X PBS, and run through TALON metal affinity resin (Clontech) by gravity flow

per manufacturer instructions. Strings of sso7d proteins (Fig. 6.4e) were instead prepared as SUMO fusions. The associated gene was cloned into pE-SUMO using the In-Fusion HD Cloning Kit (Clontech). Plasmid was transformed into Rosetta cells and transformants were plated on LB plates plus kanamycin and chloramphenicol. Single clones were used for protein expression. At an OD600 = 2, culture was induced with 1mM IPTG and transferred to 20°C overnight. Following induction, cell culture was spun down at 15000xg for 30 min and resuspended in sonication buffer (300 mM NaCl, 50 mM sodium phosphate, 3% glycerol, 1% Triton X-100), with 30 ml of resuspension buffer per 100 ml original culture volume. On ice, resuspended pellets were sonicated 3x60s at 50% duty, output intensity of 5. Debris was subsequently spun out at 4000xg for 15 minutes, and supernatant filter sterilized. Supernatant was purified on TALON resin as described above. Product was analyzed via A280 to assess total protein yield, and 20 units of SUMO protease (Lucigen) was added per 50 mg protein product. Total eluate plus protease was added to a Slide-A-Lyzer Dialysis Device 3500 MWCO (Thermo Fisher Scientific) and stirred in 5L PBS overnight to remove imidazole, SUMO protease, and cleaved SUMO domain. Following purification, proteins were buffer exchanged into PBS with 30 kDa molecular weight cutoff Amicon Ultra-15 centrifugal filters (Millipore), filtered using Spin-X centrifuge tube filters (Corning) or 0.2 μm syringe filters (VWR), and flash-frozen in aliquots with liquid nitrogen, then stored at -80°C. After thaw, proteins were used within one month and stored at 4°C in sterile conditions.

Yeast display

Sso7d scaffolds were engineered as previously described[93] with some modifications. Selections were performed at pH 5.5 and with 20 μg/ml RNase A and 4 units/ml DNase I. Following selection of initial clones from naïve library, the cmyc tag was deleted from all clones due to potential steric hindrance with TLR3 binding. During affinity maturation, error prone PCR was performed as previously reported[160], but with 4 μM 8-oxo-dGTP and dPTP analogs instead of 2 μM, 19 cycles instead of 15 cycles, and with 6.65 pg/μl instead of 13.3 pg/μl template DNA. Primers: F: GGCTCTGGTGGAGGCGGTAGCGGAGGCGGAGGGTCGGCTAGC and R: TAATAGCTCGAGATCTGATAACAACAGTGTAGATGTAACAAAATC. During the second amplification run, two 100 μl PCR reactions were performed and used without purification along with 4 μg pCTCON2 digested backbone. Yeast displaying binders were assessed for non-specific binding as previously reported[161].

TLR3 activation studies

Binders in the indicated conformation were incubated with indicated HEK reporter cell lines at a concentration of 10X the K_d for 24 hrs at 37°C and 5% CO_2, with the exception of yeast incubation, which took place in an incubator without 5% CO_2. Reporter cells were plated at a density of 100,000 cells/well in 24 well plates. GFP expression was assessed using flow cytometry. To assess the efficacy of binder-decorated beads, biotinylated TTR-T3N clones were loaded onto neutravidin-coated polystyrene beads (Spherotech).

6.4 Conclusions

This project remains incomplete at the conclusion of the PhD. While yeast display was successfully utilized to find sso7d variants that bound to soluble TLR3, no identified clones were able to bind TLR3 when cell surface displayed. Confounding factors including stickiness at pH 5.5 and the inability to bind TLR3 at neutral pH complicated analysis. However, the fact that no multimerization strategy was able to turn any of the engineered binders into effective TLR3 agonists suggests that bound epitopes are possibly masked by the cellular membrane under physiological conditions. Alternatively, soluble TLR3 may have had a different structure than that of cell surface displayed TLR3. At the conclusion of these studies, other projects were prioritized, and this study never fully completed.

If this study were to be repeated, a number of changes may increase the chances of success. Perhaps more than one protein scaffold should be pursued in parallel, for example an scFv library in addition to the sso7d library. Additionally, it may be prudent to perform selections in neutral pH and use binding at mild acidic pH as a downstream funneling strategy, rather than performing all selections at pH 5.5 and possibly selecting for electrostatic interactions that are prone to enhancing non-specific associations. Yeast panning directly against cells expressing TLR3 versus a negative control would be the most direct strategy to find physiologically relevant TLR3 binders, although this approach would be technically challenging.

Although this project is left in an incomplete state, some important lessons in sso7d engineering have emerged from the work. Most importantly, because sso7d is derived from a DNA-binding protein, it has a strong propensity to bind nucleic acid contaminants during antigen preparation or during yeast manipulation. In this study, the problem was exacerbated by TLR3's natural affinity for RNA. The addition of DNase and RNase to selection buffer is a particularly effective way of fixing this problem and should be utilized if isolated clones are nucleic acid binders rather than protein binders, a phenomenon that is characterized by extremely cationic paratopes.

6.5 Acknowledgements

We kindly thank Dr. Joshua N. Leonard for helpful advice when planning out the sorting strategy and for providing the TLR3 reporter cells used in this chapter. Roma V. Pradhan, my UROP, also helped clone and produce many of the protein products in this study.

CHAPTER 7. PERSPECTIVES AND FUTURE DIRECTIONS

7.1 Contributions to vaccinology

Contributions in antigen engineering

In this thesis, we hope to have contributed a number of design principles to the field of antigen delivery. The first novel contribution is the finding that immunologically inert proteins can essentially serve as nanoparticle-like delivery vehicles to deliver antigen to draining lymph nodes following subcutaneous administration. In the past couple of decades, many different antigen delivery strategies have been developed[43,82,83,162,163], most premised on novel chemistry and/or biomaterial engineering. This work takes a step back and recognizes that if one of the primary design criteria of antigen delivery vehicles is simply molecular weight and hydrodynamic radius[80], whereby any injected component >40 kDa can appropriately access the draining lymphatics, then nature may have already provided us with delivery agents in the form of serum proteins, no additional engineering required.

While one could reasonably view the protein fusion approach as another "me too" method to increase the bioavailability of antigen in secondary lymphatics, we sought to explore new applications that would be impossible with alternative delivery strategies. By utilizing the central dogma to convert protein vaccines into DNA and RNA vaccines, we have developed an enabling technology that allows for the expression of antigenic payload pre-complexed with delivery vehicle, a strategy incompatible with delivery agents that cannot be genetically encoded. We also recognize that there are deficiencies in the utilization of this technology, as

the approach of encoding albumin-antigen fusions seems to enhance immunogenicity only in the case of single antigens, and not in the more clinically relevant case of multi-epitopic co-delivery. Nonetheless, we have demonstrated a unique use case for protein-antigen fusions that takes them beyond mere incremental advancement over the status quo.

But perhaps the most interesting and unexpected contribution of the work contained in this thesis is the dominant role played by pharmacokinetics in shaping the vaccine response. Minimizing k_{abs} to maximize bioavailability in the dLN and maximizing k_{clear} to minimize bioavailability in distal lymphoid organs is a principle that should hopefully contribute to higher potency vaccines in the future. The second principle, namely the avoidance of distal lymph nodes that fail to be inflamed by adjuvant, is a novel one to the best of our knowledge. While more work is needed to definitively weigh the role of pharmacokinetics against other popular strategies to improve immunogenicity, such as cellular targeting[84,85,164] and antigen/adjuvant co-delivery[165,166], in many ways modulating pharmacokinetics is relatively simple and requires little engineering to optimize properties. Particularly if protein fusions are utilized, the natural repertoire of proteins may contain the optimal set of parameters; we honed in on transthyretin as a fantastic protein carrier, but other endogenous serum proteins likely have similar or possibly even more desirable properties. Thus, we hope to have contributed not just knowledge to the field of vaccinology, but also a simple toolkit that can aid design in a manner orthogonal to current approaches.

Contributions in adjuvant engineering

While our primary effort at engineering a novel TLR-based adjuvant was ultimately unsuccessful, we were able to contribute to the field of adjuvant engineering primarily in our understanding of lipo-CpG's mechanism of action. As one of the most potent adjuvants we have ever worked with in the Irvine lab, lipo-CpG represents a case study to better understand the principles of adjuvant design, which should ultimately translate into tools for future design. Surprisingly, the discovered mechanism of action does not cleanly line up with the dogma that antigen and adjuvant should be co-delivered to the same cell at the same time[167]. In this case, we found that lipo-CpG primarily acts in trans; both CpG and lipo-CpG mature the antigen presenting dendritic cell similarly, but lipo-CpG is especially effective at targeting monocytes, triggering an IL-12 mediated cascade of inflammatory signals that ultimately induces a highly proliferative T cell response. This work builds upon previous knowledge of CpG biology[140], but more specifically describes how trans signaling can dramatically improve adjuvant potency.

7.2 Future Directions

Clinical translation

While our work was exclusively preclinical in nature, it can be a useful exercise to hypothesize about how the principles outlined in this thesis may contribute to clinical therapeutics. In general, excitement in the field over cancer vaccines remains modest. While the potential for combination with checkpoint inhibitors remains encouraging[16–18], challenges in neoantigen prediction algorithms may continue to pose hurdles for clinical adoption[168,169].

Alternative strategies to invigorate the immune response within the tumor microenvironment are gaining traction, including the use of tumor necrosis factor (TNF) superfamily receptors[170] and agonists of stimulator of interferon genes (STING)[171]. Overall, the jury is still out regarding the future of vaccines in clinical oncology, yet a number of companies, including Neon Therapeutics, Gritstone Oncology, and BioNTech continue to make progress. Given the rapid influx of new and exciting modalities in immuno-oncology, as well as the potential for enlightening clinical data from cancer vaccines in the next few years, the role of vaccines in the future of oncology should become clearer relatively soon.

If cancer vaccines do indeed have a promising future, it remains unlikely that the exact protein fusions developed in this thesis will be the cheapest and fastest modality. The more lasting impact that we hope to have contributed is the set of kinetic principles that dominate the immune response. On this front, it would be fascinating to get a better sense of how the timescales of lymphatic drainage differ between small and large animals. While the 40 kDa cutoff to access the lymphatics have proven informative in test mouse and sheep models, whether the concept holds up in patients is another question. Larger carriers that slow down k_{abs} still further may be necessary if average accumulation times from the site of injection to the dLN are significantly longer in human patients, although clinical modification of the injection site could potentially alleviate these concerns.

The clinical translation of CpG consistently runs into issues of differential TLR9 expression between mouse and human[153]. If the principles outlined in this thesis are to have clinical ramifications, one of two future steps should be taken. First, we should assess whether

lipo-CpG preferentially accumulates in human monocytes the same way it does in mice, and whether human monocytes that take up lipo-CpG are triggered to produce IL-12. This study may be technically challenging, however, as we do not yet fully understand why lipo-CpG is so efficiently uptaken by mouse monocytes, and may be a downstream product of specific biodistribution in the node that would be challenging to replicate in *ex vivo* studies. Alternatively, to demonstrate the versatility of the "signaling in trans" mechanism utilized by lipo-CpG, adjuvants beyond CpG could be purposefully targeted to monocytes to assess whether they similarly enhance the vaccine response; if so, then the principles outlined here could be more broadly applied to TLRs whose human distribution is more faithfully recapitulated in mouse models.

Further opportunities for engineering

Particularly with regards to antigen delivery, there are several exciting opportunities for future engineering. While we found TTR to outperform MSA due to its faster k_{clear} rate, there may be proteins that perform even better in this regard. A more thorough screening of the major serum proteins is thus warranted. A complementary approach would be to engineer delivery strategies to minimize circulating half-life following systemic absorbance. The cleanest approach could be the utilization of serum proteases to digest the protein carrier once in blood, but there is a dearth of proteases that are truly serum-specific and not present in interstitial fluid. Fusing antigens to antibodies against the liver or the kidney could be an alternative way to reduce circulating half life by increasing excretion rates, potentially without affecting drainage rates from the site of injection to the dLN.

There is much room for improvement in the treatment of autoimmunity, especially because fusion of MOG_{35-55} to serum albumin was only effective in the prophylactic setting. We conjecture that because protein fusions can readily diffuse into tissue and drain to the local lymphatics, they may inadvertently induce a vaccine-like effect in patients already suffering from inflammatory diseases. Thus, testing fusions during instances of disease remission may be warranted, rather than during acute relapse. Additionally, testing combination therapies, such as alongside rapamycin, could be a viable strategy moving forward. Finally, the opportunity for specific receptor engagement with albumin fusions has not been fully realized. Albumin interacts with the neonatal Fc receptor (FcRn), which is expressed both in the gut[172] and in the placenta[173], theoretically allowing for oral vaccination and/or maternal vaccination with potential delivery precisely to organs considered tolerizing[174,175].

Conclusions

In this thesis, we utilized protein-antigen fusions to better deliver peptide epitopes to secondary lymphoid organs, and we learned that antigen carriers should 1) protect peptide cargo from proteolytic degradation, 2) be appropriately bulky to drain into the lymphatics, and 3) be rapidly cleared once in the blood to prevent tolerization at distal poorly inflamed organs. Because our protein-epitope fusion approach was fully recombinant in nature, we converted our protein vaccines into nucleic acid modalities and demonstrated their enhanced immunogenicity. We also applied our understanding of vaccine pharmacokinetics to purposefully induce tolerization in the treatment of autoimmunity and found that carrier proteins with circulating half-lives over twenty-four hours maximize the efficacy of tolerization.

On the adjuvant front, we conducted a detailed mechanistic study of lipo-CpG and uncovered a cascade of inflammatory signals originating from monocytes that facilitates the induction of high magnitude T cell responses, largely by acting in trans rather than directly on the antigen-presenting cell. Overall, we utilized protein-antigen fusions and lipo-CpG as case studies to engineer more potent vaccines in the treatment of cancer and autoimmunity.

REFERENCES

1. Barquet, N. Smallpox: The Triumph over the Most Terrible of the Ministers of Death. *Ann. Intern. Med.* **127**, 635 (1997).
2. Robbins, F. C. Poliomyelitis eradication: a continuing story. *FASEB J.* **8**, 665–666 (1994).
3. Wolfson, L. J. *et al.* Has the 2005 measles mortality reduction goal been achieved? A natural history modelling study. *The Lancet* **369**, 191–200 (2007).
4. Couzin-Frankel, J. Cancer Immunotherapy. *Science* **342**, 1432–1433 (2013).
5. Germain, R. N. Vaccines and the Future of Human Immunology. *Immunity* **33**, 441–450 (2010).
6. Lauring, A. S., Jones, J. O. & Andino, R. Rationalizing the development of live attenuated virus vaccines. *Nat. Biotechnol.* **28**, 573–579 (2010).
7. McCarthy, E. F. The Toxins of William B. Coley and the Treatment of Bone and Soft-tissue Sarcomas. 5
8. Lipson, E. J. & Drake, C. G. Ipilimumab: An Anti-CTLA-4 Antibody for Metastatic Melanoma. *Clin. Cancer Res.* **17**, 6958–6962 (2011).
9. Tang, J., Pearce, L., O'Donnell-Tormey, J. & Hubbard-Lucey, V. M. Trends in the global immuno-oncology landscape. *Nat. Rev. Drug Discov.* **17**, 783–784 (2018).
10. Carbone, D. P. *et al.* First-Line Nivolumab in Stage IV or Recurrent Non–Small-Cell Lung Cancer. *N. Engl. J. Med.* **376**, 2415–2426 (2017).
11. Le, D. T. *et al.* PD-1 Blockade in Tumors with Mismatch-Repair Deficiency. *N. Engl. J. Med.* **372**, 2509–2520 (2015).
12. Neelapu, S. S. *et al.* Axicabtagene Ciloleucel CAR T-Cell Therapy in Refractory Large B-Cell Lymphoma. *N. Engl. J. Med.* **377**, 2531–2544 (2017).
13. Maude, S. L. *et al.* Tisagenlecleucel in Children and Young Adults with B-Cell Lymphoblastic Leukemia. *N. Engl. J. Med.* **378**, 439–448 (2018).
14. Housman, G. *et al.* Drug Resistance in Cancer: An Overview. *Cancers* **6**, 1769–1792 (2014).
15. Ribas, A. *et al.* New Challenges in Endpoints for Drug Development in Advanced Melanoma. *Clin. Cancer Res.* **18**, 336–341 (2012).
16. Snyder, A. *et al.* Genetic Basis for Clinical Response to CTLA-4 Blockade in Melanoma. *N. Engl. J. Med.* **371**, 2189–2199 (2014).
17. Rizvi, N. A. *et al.* Mutational landscape determines sensitivity to PD-1 blockade in non–small cell lung cancer. *Science* **348**, 124–128 (2015).

18. Hodi, F. S. *et al.* Immunologic and clinical effects of antibody blockade of cytotoxic T lymphocyte-associated antigen 4 in previously vaccinated cancer patients. *Proc. Natl. Acad. Sci.* **105**, 3005–3010 (2008).

19. Kantoff, P. W. *et al.* Sipuleucel-T immunotherapy for castration-resistant prostate cancer. *N. Engl. J. Med.* **363**, 411–422 (2010).

20. Kawai, T. & Akira, S. The roles of TLRs, RLRs and NLRs in pathogen recognition. *Int. Immunol.* **21**, 317–337 (2009).

21. Burdette, D. L. *et al.* STING is a direct innate immune sensor of cyclic di-GMP. *Nature* **478**, 515–518 (2011).

22. Vacchelli, E. *et al.* Trial watch: IDO inhibitors in cancer therapy. *OncoImmunology* **3**, e957994 (2014).

23. Ghiringhelli, F. *et al.* Metronomic cyclophosphamide regimen selectively depletes CD4+CD25+ regulatory T cells and restores T and NK effector functions in end stage cancer patients. *Cancer Immunol. Immunother.* **56**, 641–648 (2007).

24. Sharma, P. & Allison, J. P. The future of immune checkpoint therapy. *Science* **348**, 56–61 (2015).

25. Vanneman, M. & Dranoff, G. Combining immunotherapy and targeted therapies in cancer treatment. *Nat. Rev. Cancer* **12**, 237–251 (2012).

26. Fritsch, E. F., Hacohen, N. & Wu, C. J. Personal neoantigen cancer vaccines: The momentum builds. *OncoImmunology* **3**, e29311 (2014).

27. Yadav, M. *et al.* Predicting immunogenic tumour mutations by combining mass spectrometry and exome sequencing. *Nature* **515**, 572–576 (2014).

28. Gubin, M. M. *et al.* Checkpoint blockade cancer immunotherapy targets tumour-specific mutant antigens. *Nature* **515**, 577–581 (2014).

29. Medzhitov, R., Preston-Hurlburt, P. & Janeway, C. A. A human homologue of the Drosophila Toll protein signals activation of adaptive immunity. *Nature* **388**, 394–397 (1997).

30. O'Hagan, D. T., Ott, G. S., Nest, G. V., Rappuoli, R. & Giudice, G. D. The history of MF59 ® adjuvant: a phoenix that arose from the ashes. *Expert Rev. Vaccines* **12**, 13–30 (2013).

31. Morefield, G. L. *et al.* Role of aluminum-containing adjuvants in antigen internalization by dendritic cells in vitro. *Vaccine* **23**, 1588–1595 (2005).

32. Blander, J. M. & Sander, L. E. Beyond pattern recognition: five immune checkpoints for scaling the microbial threat. *Nat. Rev. Immunol.* **12**, 215–225 (2012).

33. Schwendener, R. A. Liposomes as vaccine delivery systems: a review of the recent advances. *Ther. Adv. Vaccines* **2**, 159–182 (2014).

34. Nembrini, C. *et al.* Nanoparticle conjugation of antigen enhances cytotoxic T-cell responses in pulmonary vaccination. *Proc. Natl. Acad. Sci.* **108**, E989–E997 (2011).

35. Noad, R. & Roy, P. Virus-like particles as immunogens. *Trends Microbiol.* **11**, 438–444 (2003).

36. Irvine, D. J., Swartz, M. A. & Szeto, G. L. Engineering synthetic vaccines using cues from natural immunity. *Nat. Mater.* **12**, 978–990 (2013).

37. Buckland, B. C. The process development challenge for a new vaccine. *Nat. Med.* **11**, S16–S19 (2005).

38. Steinman, R. M. The dendritic cell system and its role in immunogenicity. *Annu. Rev. Immunol.* **9**, 271–296 (1991).

39. Bonifaz, L. *et al.* Efficient Targeting of Protein Antigen to the Dendritic Cell Receptor DEC-205 in the Steady State Leads to Antigen Presentation on Major Histocompatibility Complex Class I Products and Peripheral CD8+ T Cell Tolerance. *J. Exp. Med.* **196**, 1627–1638 (2002).

40. Bozzacco, L. *et al.* DEC-205 receptor on dendritic cells mediates presentation of HIV gag protein to CD8+ T cells in a spectrum of human MHC I haplotypes. *Proc. Natl. Acad. Sci.* **104**, 1289–1294 (2007).

41. Dubensky, T. W., Kanne, D. B. & Leong, M. L. Rationale, progress and development of vaccines utilizing STING-activating cyclic dinucleotide adjuvants. *Ther. Adv. Vaccines* 2051013613501988 (2013).

42. Wu, T. Y.-H. *et al.* Rational design of small molecules as vaccine adjuvants. *Sci. Transl. Med.* **6**, 263ra160–263ra160 (2014).

43. Liu, H. *et al.* Structure-based programming of lymph-node targeting in molecular vaccines. *Nature* **507**, 519–522 (2014).

44. Moynihan, K. D. *et al.* Enhancement of peptide vaccine immunogenicity by increasing lymphatic drainage and boosting serum stability. *Cancer Immunol. Res.* canimm.0607.2017 (2018). doi:10.1158/2326-6066.CIR-17-0607

45. Curry, S., Mandelkow, H., Brick, P. & Franks, N. Crystal structure of human serum albumin complexed with fatty acid reveals an asymmetric distribution of binding sites. *Nat. Struct. Biol.* **5**, 827–835 (1998).

46. Fasano, M. *et al.* The extraordinary ligand binding properties of human serum albumin. *IUBMB Life Int. Union Biochem. Mol. Biol. Life* **57**, 787–796 (2005).

47. Chaudhury, C. *et al.* The Major Histocompatibility Complex-related Fc Receptor for IgG (FcRn) Binds Albumin and Prolongs Its Lifespan. *J. Exp. Med.* **197**, 315–322 (2003).

48. Murali-Krishna, K. *et al.* Counting Antigen-Specific CD8 T Cells: A Reevaluation of Bystander Activation during Viral Infection. *Immunity* **8**, 177–187 (1998).

49. The problem with neoantigen prediction. *Nat. Biotechnol.* **35**, 97–97 (2017).

50. Rosenblum, M. D., Gratz, I. K., Paw, J. S. & Abbas, A. K. Treating Human Autoimmunity: Current Practice and Future Prospects. *Sci. Transl. Med.* **4**, 125sr1-125sr1 (2012).

51. Goris, A. & Liston, A. The Immunogenetic Architecture of Autoimmune Disease. *Cold Spring Harb. Perspect. Biol.* **4**, a007260–a007260 (2012).

52. Klareskog, L., Rönnelid, J., Lundberg, K., Padyukov, L. & Alfredsson, L. Immunity to Citrullinated Proteins in Rheumatoid Arthritis. *Annu. Rev. Immunol.* **26**, 651–675 (2008).

53. Vossenaar, E. R. Expression and activity of citrullinating peptidylarginine deiminase enzymes in monocytes and macrophages. *Ann. Rheum. Dis.* **63**, 373–381 (2004).

54. Scally, S. W. *et al.* A molecular basis for the association of the HLA-DRB1 locus, citrullination, and rheumatoid arthritis. *J. Exp. Med.* **210**, 2569–2582 (2013).

55. Liu, G. Y. *et al.* Low avidity recognition of self-antigen by T cells permits escape from central tolerance. *Immunity* **3**, 407–415 (1995).

56. Lämmermann, T. & Sixt, M. The microanatomy of T-cell responses. *Immunol. Rev.* **221**, 26–43 (2008).

57. Mueller, D. L. Mechanisms maintaining peripheral tolerance. *Nat. Immunol.* **11**, 21 (2010).

58. Rothlin, C. V., Ghosh, S., Zuniga, E. I., Oldstone, M. B. A. & Lemke, G. TAM Receptors Are Pleiotropic Inhibitors of the Innate Immune Response. *Cell* **131**, 1124–1136 (2007).

59. Banchereau, J. & Steinman, R. M. Dendritic cells and the control of immunity. *Nature* **392**, 245–252 (1998).

60. Genovese, M. C., Luggen, M., Birbara, C., Nuamah, I. & Hagerty, D. T. Abatacept for Rheumatoid Arthritis Refractory to Tumor Necrosis Factor a Inhibition. *N. Engl. J. Med.* 10 (2005).

61. Lovell, D. J. *et al.* Adalimumab with or without Methotrexate in Juvenile Rheumatoid Arthritis. *N Engl J Med* 11 (2008).

62. Lee, E. B. *et al.* Tofacitinib versus Methotrexate in Rheumatoid Arthritis. *N. Engl. J. Med.* **370**, 2377–2386 (2014).

63. Genovese, M. C. *et al.* Interleukin-6 receptor inhibition with tocilizumab reduces disease activity in rheumatoid arthritis with inadequate response to disease-modifying antirheumatic drugs: The tocilizumab in combination with traditional disease-modifying antirheumatic drug therapy study. *Arthritis Rheum.* **58**, 2968–2980 (2008).

64. Ramanan, A. V. *et al.* Adalimumab plus Methotrexate for Uveitis in Juvenile Idiopathic Arthritis. *N. Engl. J. Med.* **376**, 1637–1646 (2017).

65. Carballido, J. M. & Santamaria, P. Taming autoimmunity: Translating antigen-specific approaches to induce immune tolerance. *J. Exp. Med.* jem.20182287 (2019). doi:10.1084/jem.20182287

66. Kontos, S., Kourtis, I. C., Dane, K. Y. & Hubbell, J. A. Engineering antigens for in situ erythrocyte binding induces T-cell deletion. *Proc. Natl. Acad. Sci.* **110**, E60–E68 (2013).

67. Grimm, A. J., Kontos, S., Diaceri, G., Quaglia-Thermes, X. & Hubbell, J. A. Memory of tolerance and induction of regulatory T cells by erythrocyte-targeted antigens. *Sci. Rep.* **5**, srep15907 (2015).

68. Pishesha, N. *et al.* Engineered erythrocytes covalently linked to antigenic peptides can protect against autoimmune disease. *Proc. Natl. Acad. Sci.* 201701746 (2017).

69. Hunter, Z. *et al.* A Biodegradable Nanoparticle Platform for the Induction of Antigen-Specific Immune Tolerance for Treatment of Autoimmune Disease. *ACS Nano* **8**, 2148–2160 (2014).

70. Jewell, C. M., Bustamante Lopez, S. C. & Irvine, D. J. In situ engineering of the lymph node microenvironment via intranodal injection of adjuvant-releasing polymer particles. *Proc. Natl. Acad. Sci.* **108**, 15745–15750 (2011).

71. Clemente-Casares, X. *et al.* Expanding antigen-specific regulatory networks to treat autoimmunity. *Nature* **530**, 434–440 (2016).

72. Moynihan, K. D. *et al.* Eradication of large established tumors in mice by combination immunotherapy that engages innate and adaptive immune responses. *Nat. Med.* **22**, 1402–1410 (2016).

73. Garon, E. B. *et al.* Pembrolizumab for the Treatment of Non–Small-Cell Lung Cancer. *N. Engl. J. Med.* **372**, 2018–2028 (2015).

74. Larkin, J. *et al.* Combined Nivolumab and Ipilimumab or Monotherapy in Untreated Melanoma. *N. Engl. J. Med.* **373**, 23–34 (2015).

75. Brahmer, J. R. *et al.* Safety and Activity of Anti–PD-L1 Antibody in Patients with Advanced Cancer. *N. Engl. J. Med.* **366**, 2455–2465 (2012).

76. Kantarjian, H. *et al.* Blinatumomab versus Chemotherapy for Advanced Acute Lymphoblastic Leukemia. *N. Engl. J. Med.* **376**, 836–847 (2017).

77. Andtbacka, R. H. I. *et al.* Talimogene Laherparepvec Improves Durable Response Rate in Patients With Advanced Melanoma. *J. Clin. Oncol.* **33**, 2780–2788 (2015).

78. Ott, P. A. *et al.* An immunogenic personal neoantigen vaccine for patients with melanoma. *Nature* **547**, 217–221 (2017).

79. Keskin, D. B. *et al.* Neoantigen vaccine generates intratumoral T cell responses in phase Ib glioblastoma trial. *Nature* **565**, 234 (2019).

80. McLennan, D. N., Porter, C. J. H. & Charman, S. A. Subcutaneous drug delivery and the role of the lymphatics. *Drug Discov. Today Technol.* **2**, 89–96 (2005).

81. Brinckerhoff, L. H. *et al.* Terminal modifications inhibit proteolytic degradation of an immunogenic mart-127–35 peptide: Implications for peptide vaccines. *Int. J. Cancer* **83**, 326–334 (1999).

82. Moon, J. J. *et al.* Interbilayer-crosslinked multilamellar vesicles as synthetic vaccines for potent humoral and cellular immune responses. *Nat. Mater.* **10**, 243–251 (2011).

83. Kuai, R., Ochyl, L. J., Bahjat, K. S., Schwendeman, A. & Moon, J. J. Designer vaccine nanodiscs for personalized cancer immunotherapy. *Nat. Mater.* **advance online publication**, (2016).

84. Bonifaz, L. C. *et al.* In Vivo Targeting of Antigens to Maturing Dendritic Cells via the DEC-205 Receptor Improves T Cell Vaccination. *J. Exp. Med.* **199**, 815–824 (2004).

85. Kretz-Rommel, A. *et al.* In Vivo Targeting of Antigens to Human Dendritic Cells Through DC-SIGN Elicits Stimulatory Immune Responses and Inhibits Tumor Growth in Grafted Mouse Models. *J. Immunother.* **30**, 715 (2007).

86. Johansen, P. *et al.* Direct intralymphatic injection of peptide vaccines enhances immunogenicity. *Eur. J. Immunol.* **35**, 568–574 (2005).

87. Feltkamp, M. C. W. *et al.* Vaccination with cytotoxic T lymphocyte epitope-containing peptide protects against a tumor induced by human papillomavirus type 16-transformed cells. *Eur. J. Immunol.* **23**, 2242–2249 (1993).

88. Hailemichael, Y. *et al.* Persistent antigen at vaccination sites induces tumor-specific CD8(+) T cell sequestration, dysfunction and deletion. *Nat. Med.* **19**, 465-+ (2013).

89. Unanue, E. R. Altered Peptide Ligands Make Their Entry. *J. Immunol.* **186**, 7–8 (2011).

90. Guevara-Patiño, J. A. *et al.* Optimization of a self antigen for presentation of multiple epitopes in cancer immunity. *J. Clin. Invest.* **116**, 1382–1390 (2006).

91. van Stipdonk, M. J. B. *et al.* Design of agonistic altered peptides for the robust induction of CTL directed towards H-2Db in complex with the melanoma-associated epitope gp100. *Cancer Res.* **69**, 7784–7792 (2009).

92. Gera, N., Hussain, M., Wright, R. C. & Rao, B. M. Highly Stable Binding Proteins Derived from the Hyperthermophilic Sso7d Scaffold. *J. Mol. Biol.* **409**, 601–616 (2011).

93. Traxlmayr, M. W. *et al.* Strong Enrichment of Aromatic Residues in Binding Sites from a Charge-Neutralized Hyperthermostable Sso7d Scaffold Library. *J. Biol. Chem.* jbc.M116.741314 (2016). doi:10.1074/jbc.M116.741314

94. Harris, J. R. & Markl, J. Keyhole limpet hemocyanin (KLH): a biomedical review. *Micron* **30**, 597–623 (1999).

95. Kim, S. K. *et al.* Comparison of the effect of different immunological adjuvants on the antibody and T-cell response to immunization with MUC1-KLH and GD3-KLH conjugate cancer vaccines. *Vaccine* **18**, 597–603 (1999).

96. Han, S., Asoyan, A., Rabenstein, H., Nakano, N. & Obst, R. Role of antigen persistence and dose for CD4+ T-cell exhaustion and recovery. *Proc. Natl. Acad. Sci.* **107**, 20453–20458 (2010).

97. Ramsdell, F. & Fowlkes, B. J. Maintenance of in Vivo Tolerance by Persistence of Antigen. *Science* **257**, 1130–1134 (1992).

98. Ehl, S. *et al.* Antigen persistence and time of T-cell tolerization determine the efficacy of tolerization protocols for prevention of skin graft rejection. *Nat. Med.* **4**, 1015–1019 (1998).

99. Ingenbleek, Y. & Young, V. Transthyretin (Prealbumin) in Health and Disease: Nutritional Implications. *Annu. Rev. Nutr.* **14**, 495–533 (1994).

100. Terje Andersen, J., Bekele Daba, M., Berntzen, G., Michaelsen, T. E. & Sandlie, I. Cross-species Binding Analyses of Mouse and Human Neonatal Fc Receptor Show Dramatic Differences in Immunoglobulin G and Albumin Binding. *J. Biol. Chem.* **285**, 4826–4836 (2010).

101. Colon, W. & Kelly, J. W. Partial denaturation of transthyretin is sufficient for amyloid fibril formation in vitro. *Biochemistry* **31**, 8654–8660 (1992).

102. Kelly, J. W. The alternative conformations of amyloidogenic proteins and their multi-step assembly pathways. *Curr. Opin. Struct. Biol.* **8**, 101–106 (1998).

103. McCutchen, S. L., Colon, W. & Kelly, J. W. Transthyretin mutation Leu-55-Pro significantly alters tetramer stability and increases amyloidogenicity. *Biochemistry* **32**, 12119–12127 (1993).

104. Prior, I. A., Lewis, P. D. & Mattos, C. A Comprehensive Survey of Ras Mutations in Cancer. *Cancer Res.* **72**, 2457–2467 (2012).

105. Waters, A. M. & Der, C. J. KRAS: The Critical Driver and Therapeutic Target for Pancreatic Cancer. *Cold Spring Harb. Perspect. Med.* **8**, a031435 (2018).

106. Bender, S. *et al.* Reduced H3K27me3 and DNA Hypomethylation Are Major Drivers of Gene Expression in K27M Mutant Pediatric High-Grade Gliomas. *Cancer Cell* **24**, 660–672 (2013).

107. Schwartzentruber, J. *et al.* Driver mutations in histone H3.3 and chromatin remodelling genes in paediatric glioblastoma. *Nature* **482**, 226–231 (2012).

108. Ochs, K. *et al.* K27M-mutant histone-3 as a novel target for glioma immunotherapy. *OncoImmunology* **6**, e1328340 (2017).

109. Wang, Q. J. *et al.* Identification of T-cell Receptors Targeting KRAS-mutated Human Tumors. *Cancer Immunol. Res.* **4**, 204–214 (2016).

110. Chheda, Z. S. *et al.* Novel and shared neoantigen derived from histone 3 variant H3.3K27M mutation for glioma T cell therapy. *J. Exp. Med.* **215**, 141–157 (2018).

111. Duperret, E. K. *et al.* A Synthetic DNA, Multi-Neoantigen Vaccine Drives Predominately MHC Class I CD8+ T-cell Responses, Impacting Tumor Challenge. *Cancer Immunol. Res.* (2019). doi:10.1158/2326-6066.CIR-18-0283

112. Walters, J. N. *et al.* A novel DNA vaccine platform enhances neo-antigen-like T-cell responses against WT1 to break tolerance and induce anti-tumor immunity. *Mol. Ther.* **0**, (2017).

113. Geall, A. J. *et al.* Nonviral delivery of self-amplifying RNA vaccines. *Proc. Natl. Acad. Sci.* **109**, 14604–14609 (2012).

114. Nomura, L. E., Walker, J. M. & Maecker, H. T. Optimization of whole blood antigen-specific cytokine assays for CD4+ T cells. *Cytometry* **40**, 60–68 (2000).

115. Chen, T. F., de Picciotto, S., Hackel, B. J. & Wittrup, K. D. Engineering Fibronectin-Based Binding Proteins by Yeast Surface Display. in *Methods in Enzymology* **523**, 303–326 (Elsevier, 2013).

116. Zom, G. G. *et al.* Efficient Induction of Antitumor Immunity by Synthetic Toll-like Receptor Ligand-Peptide Conjugates. *Cancer Immunol. Res.* **2**, 756–764 (2014).

117. Qiu, F. *et al.* Poly(propylacrylic acid)-peptide nanoplexes as a platform for enhancing the immunogenicity of neoantigen cancer vaccines. *Biomaterials* **182**, 82–91 (2018).

118. Deng, L. *et al.* Heterosubtypic influenza protection elicited by double-layered polypeptide nanoparticles in mice. *Proc. Natl. Acad. Sci.* **115**, E7758–E7767 (2018).

119. Lynn, G. M. *et al.* In vivo characterization of the physicochemical properties of polymer-linked TLR agonists that enhance vaccine immunogenicity. *Nat. Biotechnol.* (2015). doi:10.1038/nbt.3371

120. Sahin, U. & Türeci, Ö. Personalized vaccines for cancer immunotherapy. *Science* **359**, 1355–1360 (2018).

121. Porgador, A. *et al.* Predominant Role for Directly Transfected Dendritic Cells in Antigen Presentation to CD8+ T Cells after Gene Gun Immunization. *J. Exp. Med.* **188**, 1075–1082 (1998).

122. Sardesai, N. Y. & Weiner, D. B. Electroporation delivery of DNA vaccines: prospects for success. *Curr. Opin. Immunol.* **23**, 421–429 (2011).

123. Diebold, S. S. *et al.* Role of TLR3 in the immunogenicity of replicon plasmid-based vaccines. *Gene Ther.* **16**, 359–366 (2008).

124. Lazzaro, S. *et al.* CD8 T-cell priming upon mRNA vaccination is restricted to bone-marrow-derived antigen-presenting cells and may involve antigen transfer from myocytes. *Immunology* **146**, 312–326 (2015).

125. Fu, T.-M. *et al.* Priming of cytotoxic T lymphocytes by DNA vaccines: requirement for professional antigen presenting cells and evidence for antigen transfer from myocytes. *Mol. Med.* **3**, 362 (1997).

126. Dupuis, M. *et al.* Distribution of DNA Vaccines Determines Their Immunogenicity After Intramuscular Injection in Mice. *J. Immunol.* **165**, 2850–2858 (2000).

127. Kim, D. *et al.* Generation and characterization of a preventive and therapeutic HPV DNA vaccine. *Vaccine* **26**, 351–360 (2008).

128. Bagarazzi, M. L. *et al.* Immunotherapy against HPV16/18 generates potent TH1 and cytotoxic cellular immune responses. *Sci. Transl. Med.* **4**, 155ra138–155ra138 (2012).

129. Wagner, T. E. *et al.* Small-molecule-based regulation of RNA-delivered circuits in mammalian cells. *Nat. Chem. Biol.* **14**, 1043–1050 (2018).

130. Wherry, E. J. *et al.* Molecular Signature of CD8+ T Cell Exhaustion during Chronic Viral Infection. *Immunity* **27**, 670–684 (2007).

131. Tsai, S. *et al.* Reversal of Autoimmunity by Boosting Memory-like Autoregulatory T Cells. *Immunity* **32**, 568–580 (2010).

132. Baekkeskov, S., Hubbell, J. A. & Phelps, E. A. Bioengineering strategies for inducing tolerance in autoimmune diabetes. *Adv. Drug Deliv. Rev.* **114**, 256–265 (2017).

133. Carambia, A. *et al.* Nanoparticle-based autoantigen delivery to Treg-inducing liver sinusoidal endothelial cells enables control of autoimmunity in mice. *J. Hepatol.* **62**, 1349–1356 (2015).

134. Mondino, A., Khoruts, A. & Jenkins, M. K. The anatomy of T-cell activation and tolerance. *Proc. Natl. Acad. Sci.* **93**, 2245–2252 (1996).

135. Angel, C. E. *et al.* Distinctive localization of antigen-presenting cells in human lymph nodes. *Blood* **113**, 1257–1267 (2009).

136. Antas, P. R. *et al.* Kinetics of T cell-activation molecules in response to Mycobacterium tuberculosis antigens. *Mem. Inst. Oswaldo Cruz* **97**, 1097–1099 (2002).

137. Shiow, L. R. *et al.* CD69 acts downstream of interferon-α/β to inhibit S1P1 and lymphocyte egress from lymphoid organs. *Nature* **440**, 540–544 (2006).

138. Miller, S. D. & Karpus, W. J. Experimental Autoimmune Encephalomyelitis in the Mouse. in *Current Protocols in Immunology* (eds. Coligan, J. E., Bierer, B. E., Margulies, D. H., Shevach, E. M. & Strober, W.) im1501s77 (John Wiley & Sons, Inc., 2007). doi:10.1002/0471142735.im1501s77

139. Gutcher, I. & Becher, B. APC-derived cytokines and T cell polarization in autoimmune inflammation. *J. Clin. Invest.* **117**, 1119–1127 (2007).

140. Pham, N.-L. L., Badovinac, V. P. & Harty, J. T. A Default Pathway of Memory CD8 T Cell Differentiation after Dendritic Cell Immunization Is Deflected by Encounter with Inflammatory Cytokines during Antigen-Driven Proliferation. *J. Immunol.* **183**, 2337–2348 (2009).

141. Joshi, N. S. *et al.* Inflammation Directs Memory Precursor and Short-Lived Effector CD8+ T Cell Fates via the Graded Expression of T-bet Transcription Factor. *Immunity* **27**, 281–295 (2007).

142. De Koker, S. *et al.* Inflammatory monocytes regulate Th1 oriented immunity to CpG adjuvanted protein vaccines through production of IL-12. *Sci. Rep.* **7**, (2017).

143. Takeshita, S., Takeshita, F., Haddad, D. E., Ishii, K. J. & Klinman, D. M. CpG Oligodeoxynucleotides Induce Murine Macrophages to Up-Regulate Chemokine mRNA Expression. *Cell. Immunol.* **206**, 101–106 (2000).

144. Volpi, C. *et al.* High doses of CpG oligodeoxynucleotides stimulate a tolerogenic TLR9–TRIF pathway. *Nat. Commun.* **4**, 1852 (2013).

145. Wingender, G. *et al.* Systemic application of CpG-rich DNA suppresses adaptive T cell immunity via induction of IDO. *Eur. J. Immunol.* **36**, 12–20 (2006).

146. Casanova, J.-L. & Abel, L. The human model: a genetic dissection of immunity to infection in natural conditions. *Nat. Rev. Immunol.* **4**, 55–66 (2004).

147. Parihar, R., Dierksheide, J., Hu, Y. & Carson, W. E. IL-12 enhances the natural killer cell cytokine response to Ab-coated tumor cells. *J. Clin. Invest.* **110**, 983–992 (2002).

148. Nguyen, H. N. *et al.* Autocrine Loop Involving IL-6 Family Member LIF, LIF Receptor, and STAT4 Drives Sustained Fibroblast Production of Inflammatory Mediators. *Immunity* **46**, 220–232 (2017).

149. Torvinen, M., Campwala, H. & Kilty, I. The role of IFN-γ in regulation of IFN-γ-inducible protein 10 (IP-10) expression in lung epithelial cell and peripheral blood mononuclear cell co-cultures. *Respir. Res.* **8**, 80 (2007).

150. McLoughlin, R. M. *et al.* Interplay between IFN-γ and IL-6 signaling governs neutrophil trafficking and apoptosis during acute inflammation. *J. Clin. Invest.* **112**, 598–607 (2003).

151. Joshi, N. S. *et al.* Inflammation Directs Memory Precursor and Short-Lived Effector CD8+ T Cell Fates via the Graded Expression of T-bet Transcription Factor. *Immunity* **27**, 281–295 (2007).

152. O'Hagan, D. T. & Fox, C. B. Are we entering a new age for human vaccine adjuvants? *Expert Rev. Vaccines* **14**, 909–911 (2015).

153. Mestas, J. & Hughes, C. C. W. Of Mice and Not Men: Differences between Mouse and Human Immunology. *J. Immunol.* **172**, 2731–2738 (2004).

154. Datta, S. K. *et al.* A Subset of Toll-Like Receptor Ligands Induces Cross-presentation by Bone Marrow-Derived Dendritic Cells. *J. Immunol.* **170**, 4102–4110 (2003).

155. Park, H. *et al.* Polyinosinic-Polycytidylic Acid Is the Most Effective TLR Adjuvant for SIV Gag Protein-Induced T Cell Responses In Nonhuman Primates. *J. Immunol.* **190**, 4103–4115 (2013).

156. Choe, J., Kelker, M. S. & Wilson, I. A. Crystal Structure of Human Toll-Like Receptor 3 (TLR3) Ectodomain. *Science* **309**, 581–585 (2005).

157. Liu, L. *et al.* Structural Basis of Toll-Like Receptor 3 Signaling with Double-Stranded RNA. *Science* **320**, 379–381 (2008).

158. Leonard, J. N. *et al.* The TLR3 signaling complex forms by cooperative receptor dimerization. *Proc. Natl. Acad. Sci.* **105**, 258–263 (2008).

159. Boder, E. T. & Wittrup, K. D. Yeast surface display for screening combinatorial polypeptide libraries. *Nat Biotech* **15**, 553–557 (1997).

160. Chao, G. *et al.* Isolating and engineering human antibodies using yeast surface display. *Nat. Protoc.* **1**, 755–768 (2006).

161. Kelly, R. L., Le, D., Zhao, J. & Wittrup, K. D. Reduction of Nonspecificity Motifs in Synthetic Antibody Libraries. *J. Mol. Biol.* **430**, 119–130 (2018).

162. Reddy, S. T. *et al.* Exploiting lymphatic transport and complement activation in nanoparticle vaccines. *Nat. Biotechnol.* **25**, 1159–1164 (2007).

163. Reddy, S. T., Rehor, A., Schmoekel, H. G., Hubbell, J. A. & Swartz, M. A. In vivo targeting of dendritic cells in lymph nodes with poly(propylene sulfide) nanoparticles. *J. Controlled Release* **112**, 26–34 (2006).

164. Fossum, E. *et al.* Vaccine molecules targeting Xcr1 on cross-presenting DCs induce protective CD8+ T-cell responses against influenza virus. *Eur. J. Immunol.* **45**, 624–635 (2015).

165. Stano, A. *et al.* PPS nanoparticles as versatile delivery system to induce systemic and broad mucosal immunity after intranasal administration. *Vaccine* **29**, 804–812 (2011).

166. Steers, N. J., Peachman, K. K., McClain, S., Alving, C. R. & Rao, M. Liposome-encapsulated HIV-1 Gag p24 containing lipid A induces effector CD4+ T-cells, memory CD8+ T-cells, and pro-inflammatory cytokines. *Vaccine* **27**, 6939–6949 (2009).

167. Moyer, T. J., Zmolek, A. C. & Irvine, D. J. Beyond antigens and adjuvants: formulating future vaccines. *J. Clin. Invest.* **126**, 799–808 (2016).

168. Castle, J. C. *et al.* Exploiting the Mutanome for Tumor Vaccination. *Cancer Res.* **72**, 1081–1091 (2012).

169. Abelin, J. G. *et al.* Mass Spectrometry Profiling of HLA-Associated Peptidomes in Mono-allelic Cells Enables More Accurate Epitope Prediction. *Immunity* **46**, 315–326 (2017).

170. Sagiv-Barfi, I. *et al.* Eradication of spontaneous malignancy by local immunotherapy. *Sci. Transl. Med.* **10**, eaan4488 (2018).

171. Barber, G. N. STING: infection, inflammation and cancer. *Nat. Rev. Immunol.* **15**, 760–770 (2015).

172. Israel, E. J. *et al.* Expression of the neonatal Fc receptor, FcRn, on human intestinal epithelial cells. *Immunology* **92**, 69–74 (1997).

173. Simister, N. E., Story, C. M., Chen, H.-L. & Hunt, J. S. An IgG-transporting Fc receptor expressed in the syncytiotrophoblast of human placenta. *Eur. J. Immunol.* **26**, 1527–1531 (1996).

174. Mowat, A. McI. Anatomical basis of tolerance and immunity to intestinal antigens. *Nat. Rev. Immunol.* **3**, 331–341 (2003).

175. Burt, T. D. Fetal Regulatory T Cells and Peripheral Immune Tolerance *In Utero*: Implications for Development and Disease. *Am. J. Reprod. Immunol.* **69**, 346–358 (2013).